

RHYOLITES OF THE TEMAGAMI GREENSTONE BELT, ONTARIO

**PETROLOGY AND GEOCHEMISTRY OF FELSIC VOLCANICLASTIC
ROCKS ALONG THE SHERMAN MINE ROAD, TEMAGAMI GREENSTONE
BELT, STRATHY TOWNSHIP, ONTARIO.**

By

TIMOTHY CHARLES SCHWARTZ, B.Sc. (Hons)

A Thesis

Submitted to the School of Graduate Studies

in Partial Fulfilment of the Requirements

for the Degree

Master of Science

McMaster University

(c) Copyright by Timothy Charles Schwartz, March 1995

MASTER OF SCIENCE (1995)
(Geology)

McMASTER UNIVERSITY
Hamilton, Ontario

TITLE: Petrology and Geochemistry of Felsic Volcaniclastic Rocks
along the Sherman Mine Road, Temagami Greenstone Belt,
Strathy Township, Ontario

AUTHOR: Timothy Charles Schwartz,
B.Sc. (Honours) (University of Manitoba)
B.Sc. (University of Winnipeg)

SUPERVISOR: Dr. J.H. Crocket

NUMBER OF PAGES xiii, 180

ABSTRACT

Felsic volcanoclastic rocks and intrusions along the Sherman Mine road, Temagami greenstone belt, were studied to determine if the petrological and chemical characteristics of these rocks indicate they are favourable hosts for volcanogenic massive sulphide deposits. Mapping of these felsic rocks was done at a scale of 1:5000 utilizing a 100m spaced cut grid and pace and compass. Since outcrop is scarce and exposures are poor in this area, most correlation of the felsic horizons was done on the basis of trace and rare-earth element geochemistry.

On the basis of the chemistry of the rocks, three distinct felsic horizons were defined. The quartz feldspar porphyries are FI type calc-alkaline felsic intrusives with $[La/Yb]_n$ ratio from 16 to 29 and no Eu anomaly. The Link Lake and Sherman Gate horizons are a FII type calc-alkaline volcanoclastic horizon with $[La/Yb]_n$ ratio from 5 to 7 and weak negative to positive Eu anomalies. The Upper and Lower Felsic horizons are FIIIa type tholeiitic rhyolite lava flows and volcanoclastics. These horizons have $[La/Yb]_n$ ratios from 1 to 3 and strong negative Eu anomalies from 0.16 to 0.42.

Petrology and net transfer of material calculations indicate the Upper and Lower Felsic Horizons have been silicified, resulting in a net addition of Si and Al to these rocks. There is no distinct pattern of chemical changes which would indicate proximity to a single volcanogenic massive sulphide alteration pipe, however, an enrichment of the light rare-earth elements in the eastern section of the thesis area suggests this area maybe more proximal to an alteration pipe, and thus a vent. Lithological characteristics of the eastern

section of the thesis area also suggests it is more proximal to a vent than the western section.

Pyrite clasts are present in several of the volcanoclastic units. While the presence of sulphide rich clasts can be an indicator of proximity to a volcanogenic massive sulphide deposit, the textural and chemical characteristics of these clasts indicate they originated from shale horizons in this area. For this reason, these clasts should not be used as an indicator of proximity to a volcanogenic massive sulphide deposit.

Trace and rare-earth element classifications indicate both the Link Lake and Sherman Gate horizons, and the Upper and Lower Felsic horizons are favourable host rocks for volcanogenic massive sulphide style mineralization while the quartz feldspar porphyries, such as the Milne vent and City Dump vent, are not. Although the felsic volcanic packages are relatively thin, potential exploration targets would be the upper contact of the Upper Felsic horizon and the Link Lake and Sherman Gate horizons.

Acknowledgements

I express my greatest thanks to Dr. J.H. Crocket for taking me on as a graduate student, and providing a basis for increasing my knowledge on the theories of the formation of VMS deposits, and the principle lithogeochemical techniques used to explore for them. Maybe next time we will actually find a mine.

My sincere thanks goes to Mark, Richard, Jodie, Cam, Dave and Trev for the coffee and constructive conversation breaks. To Steve Zymela, Lens Zwicker and Jack Whorwood, thanks for the computer programs, thin sections and photographic work respectively. Thanks to Dr. Geoff Orton for the help with the volcanology and Dr. Bob Bowins for the ICP analyses.

A special thanks to Kathy, for helping me with field work, for being so patient, for your encouragement and your acceptance of my proposal of marriage.

Finally I would like to acknowledge the financial support, given through Dr. J.H. Crocket, from the Natural Sciences and Engineering Research Council (NSERC) Research Grant.

TABLE OF CONTENTS

	Page
Abstract	iii
Acknowledgements	v
Table of Contents	vi
List of Figures	xi
List of Tables	xii
List of Photographic Plates	xii
CHAPTER 1: INTRODUCTION	1
1.1 Location and Accessibility	1
1.2 Historical Background	1
1.3 Previous Work	3
1.3.1 Government projects	3
1.3.2 Academic studies	3
1.3.3 Exploration activity	3
1.4 Objective and Thesis	4
CHAPTER 2: METHODOLOGY	5
2.1 Field Approach	5
2.2 Petrology	7
2.3 Geochemistry	7
2.3.1 Preparation	7
2.3.2 XRF	7
2.3.2.1 Major oxide analysis	8
2.3.2.2 Trace element analysis	9
2.3.2.3 Trace element analysis: McMaster University	10
2.3.3 INAA	10

	Page
CHAPTER 3: GENERAL GEOLOGY.....	14
3.1 Regional Setting.....	14
3.2 Regional Structures.....	16
3.3 Age of the Temagami Greenstone Belt.....	17
3.4 Local Geology.....	18
3.4.1 General geology.....	18
3.4.2 Local structure.....	17
3.4.3 Outcrop exposure.....	20
CHAPTER 4: PETROLOGY.....	23
4.1 Nomenclature.....	23
4.2 Mafic Metavolcanics.....	24
4.2.1 Tholeiitic flows: Unit 1.....	24
4.2.2 Calc-alkaline flows: Unit 2.....	25
4.3 Mafic To Ultramafic Intrusives.....	26
4.3.1 Gabbro, diorite: Unit 6.....	26
4.3.2 Diabase: Unit 10.....	27
4.4 Felsic Metavolcanics.....	28
4.4.1 Introduction.....	28
4.4.2 Lower Felsic horizon: Unit 3.....	28
4.4.2.1 Garbage Dump trench.....	29
4.4.2.2 Hydro Station trench.....	34
4.4.2.3 Fold Nose trench.....	39
4.4.3 Upper Felsic horizon: Unit 3.....	39
4.4.3.1 Mineralogy.....	45
4.4.4 Link Lake and Sherman Gate horizons: Unit 4.....	47
4.5 Quartz Feldspar Porphyry: Unit 4f.....	47
4.6 Alteration Mineralogy.....	49
CHAPTER 5: GEOCHEMISTRY.....	51
5.1 Introduction.....	51
5.2 Alteration Processes and Their Effects on Whole Rock and Trace Element Geochemistry.....	52
5.2.1 Major element mobility.....	52
5.2.2 Trace element mobility.....	53
5.3 Test for the Mobility of the Elements.....	55

	Page
5.4	General Chemistry of the Major and Trace Elements..... 59
5.4.1	Upper and Lower Felsic horizons..... 59
5.4.2	Quartz feldspar porphyry 59
5.5	Classification Schemes..... 61
5.5.1	Rock type..... 61
5.5.2	Magmatic affinity..... 61
5.6	Rare Earth Element Chemistry..... 67
5.6.1	Upper and Lower Felsic horizons..... 67
5.6.2	Quartz feldspar porphyry 72
5.6.3	Link Lake and Sherman Gate horizons..... 72
5.7	Rare Earth Element Classifications 72
5.7.1	Upper and Lower Felsic horizons..... 75
5.7.2	Quartz feldspar porphyry 78
5.7.3	Link Lake, Sherman Gate and South Temagami..... 78
5.8	Effects of Alteration on the Immobile Element Classification Scheme ... 78
5.8.1	Net transfer of material..... 80
5.8.2	Explanation for the observed mass changes..... 88
5.8.2.1	Felsic horizons..... 88
5.8.2.2	Quartz feldspar porphyries 91
	 CHAPTER 6: PYRITE CLASTS 93
6.1	Introduction 93
6.2	Description..... 93
6.3	Petrography of the Sulphide Clasts 95
6.3.1	Mineralogy 95
6.3.2	Textures 97
6.3.2.1	Spherical pyrites 99
6.3.2.2	Concentric banding 99
6.3.2.3	Radiating crystals..... 99
6.3.2.4	Lattice pyrite 102
6.3.2.5	Secondary pyrite..... 102
6.3.2.6	Destruction of a pyrite sphere 102
6.4	Textures of Pyrite from the Carbonaceous Shales 103
6.5	Ag, Cu, Zn, Co and Ni in Pyrite from the Temagami Area 105
6.5.1	Sample preparation and analytical methods 105

	Page
6.5.2	Results 106
6.5.2.1	Silver 106
6.5.2.2	Copper 106
6.5.2.3	Zinc 108
6.5.2.4	Cobalt and nickel 108
6.5.3	Shale- and vein-hosted Temagami pyrites..... 111
6.5.3.1	Vein pyrite..... 111
6.5.3.2	Shale pyrite..... 113
6.6	Origin of the Pyrite Clasts..... 114
6.6.1	Chemistry 114
6.6.2	Incorporation of molybdenite into the pyrite 114
6.6.3	Textures 115
6.7	Source of Pyrite 118
	CHAPTER 7: VOLCANOLOGICAL DISCUSSION 120
7.1	Petrology 120
7.1.1	Definition of volcanoclastic..... 120
7.1.2	Pumice 121
7.1.3	Proximity to a vent 121
7.2	Chemistry 123
7.3	Geologic Reconstruction of the Thesis Area Rocks..... 126
7.3.1	Depositional history..... 126
7.3.2	Silicification of the Upper and Lower Felsic horizons..... 129
7.4	Comparison to other Archean and Modern Volcanism 130
7.5	Summary..... 133
	CHAPTER 8: VOLCANOGENIC MASSIVE SULPHIDE
	EXPLORATION..... 134
8.1	Introduction 134
8.2	Definition and Origin of a VMS Deposit..... 134
8.2.1	Precambrian VMS deposits..... 135
8.3	VMS Potential of Temagami Rocks..... 137
8.3.1	REE rhyolite classifications..... 137
8.3.2	Rock alteration characteristics 140
8.3.2.1	Major elements 140
8.3.2.2	Trace elements..... 141
8.3.3	Lithological characteristics..... 142

		Page
8.4	Comparison of the Temagami Thesis Area Rocks to Other VMS Host Rocks	144
8.5	Conclusions.....	145
REFERENCES CITED		147
APPENDIX A	Sample Descriptions, Locations and Geochemical Classifications	160
APPENDIX B	Major and Trace Element Data for all Samples.....	166
APPENDIX C	Precision and Accuracy of XRF and INAA Analyses.....	173
MAP POCKET.....		Field map Sample location map

LIST OF FIGURES

Figure		Page
1-1	Location map of Temagami, Ontario	2
2-1	Location of thesis area	6
3-1	Simplified geology of the Temagami greenstone belt.....	15
3-2	Map of fold in outcrop at L6W 0+75N	21
4-1	Map of Garbage Dump trench	30
4-2	Map of Hydro Station trench.....	35
4-3	Composite cross section of the Upper Felsic horizon	42
5-1	Depiction of mobility of trace elements beneath a VMS deposit	54
5-2	Depiction of the effects of alteration on the initial ratios of two immobile elements	56
5-3	Major and trace element rock classification schemes	62,63
5-4	Major element magmatic affinity classification schemes.....	64
5-5	Y/Zr trace element magmatic affinity classification scheme	66
5-6	Chondrite normalized REE patterns for the Upper and Lower Felsic horizons	68
5-7	Combined chondrite normalized REE patterns for the Upper and Lower Felsic horizons.....	69
5-8	Chondrite normalized REE patterns for the QFP, Link Lake and Sherman Gate horizons.....	73
5-9	Zr/Y vs Y, Zr/10-Ti/100-Y and $[La/Yb]_n$ vs $[Yb]_n$ rhyolite classification scheme for the Upper and Lower Felsic horizons, and the quartz feldspar porphyry	76,77
5-10	Zr/Y vs Y, Zr/10-Ti/100-Y and $[La/Yb]_n$ vs $[Yb]_n$ rhyolite classification scheme for the south Temagami, Link Lake and Sherman Gate horizons.....	79
5-11	Calculated mass change of the major elements of the Upper and Lower Felsic horizons as compared to sample 119.....	83,84
5-12	Calculated mass change of the major elements of the Upper and Lower Felsic horizons as compared to the Don rhyolite	86,87
5-13	Calculated mass change of the major elements for the quartz feldspar porphyries as compared to sample 16	92
6-1	Co/Ni ratios for the pyrite samples from the study area	112

Figure	Page
7-1	REE comparison of the south Temagami samples to the QFP 125
7-2	Geologic map of the thesis area indicating present stratigraphic position of the main horizons. 127
8-1	Idealized cross section of a VMS deposit..... 135

LIST OF TABLES

Table	Page
2-1	Schedule of irradiation for INAA..... 12,13
5-1	Element/Lu ratios for selected horizons as an indication of element mobility 58
5-2	Average compositions of the major felsic horizons 60
5-3	Rhyolite classification data..... 70,71
5-4	Zr/Hf ratios for the Temagami samples 90
6-1	Trace element contents in pyrite from the Temagami area 107
6-2	Summary of Co and Ni contents in pyrite as defined by their origins 109

LIST OF PHOTOGRAPHIC PLATES

Plate	Page
3-1	Shearing along the Link Lake deformation zone..... 18
3-2	Examples of folding within the thesis area..... 22
4-1	Lower debris flow at the Garbage Dump trench..... 31
4-2	Rhyolitic lava flow at the Garbage Dump trench 31
4-3	Black rhyolitic hyaloclastic at the Garbage Dump trench..... 33
4-4	Large clast debris flow at the Hydro Station trench..... 33
4-5	Perlitic texture in quartz feldspar intrusive at the Hydro Station trench . 38
4-6	Folded flow bands in massive rhyolite at the Hydro Station trench 40
4-7	Example of a bedded tuff and volcanic breccia of the Upper Felsic horizon..... 43

Plate		Page
4-8	Example of basal shear in the Upper Felsic horizon.....	43
4-9	Example of changes in grading in the Upper Felsic horizon.....	44
4-10	Example of poorly graded tuff in the Upper Felsic horizon.....	44
4-11	Examples of mineralogy and textures in the Upper and Lower Felsic horizons.....	46
4-12	Examples of mineralogy and textures in the quartz feldspar porphyry....	49
6-1	Examples of some of the largest pyrite clasts	94
6-2	Examples of hand sample textures from the pyrite clasts	97
6-3	Examples of the sulphides found in the pyrite clasts	99
6-4	Photomicrographs of textures in the pyrite clasts	100,101
6-5	Examples of shapes and textures of pyrite spheres in the carbonaceous shales	104

CHAPTER 1

INTRODUCTION

1.1 Location and Accessibility

The Temagami greenstone belt is an Archean greenstone belt in the Superior province of the Canadian shield. The townsite of Temagami, located on highway 11, about 97 km north of North Bay, Ontario, lies at the southern edge of the Temagami greenstone belt (Figure 1-1). The study area is located entirely within the Strathy Township, three kilometres north of Temagami, between 79° 47' and 79° 51' west longitude, and 47° 04' and 47° 05' north latitude. Access to the study area is along the Sherman Mine road, the new town garbage dump road and the old town garbage dump road.

1.2 Historical Background

At present, there are no operational mines within the belt, although there have been several small scale mining operations as well as the large Sherman iron mine (Bennett 1978). Various mineral deposits and showings located in this area include: iron (Sherman Mine); gold and silver (Big Dan, Milne showing, Arsenic Lake and others); molybdenum (Net Lake occurrence); copper and nickel (Ajax Minerals limited deposit, and Temagami Island diorite showing). Descriptions of these deposits can be found in Bennett (1978).

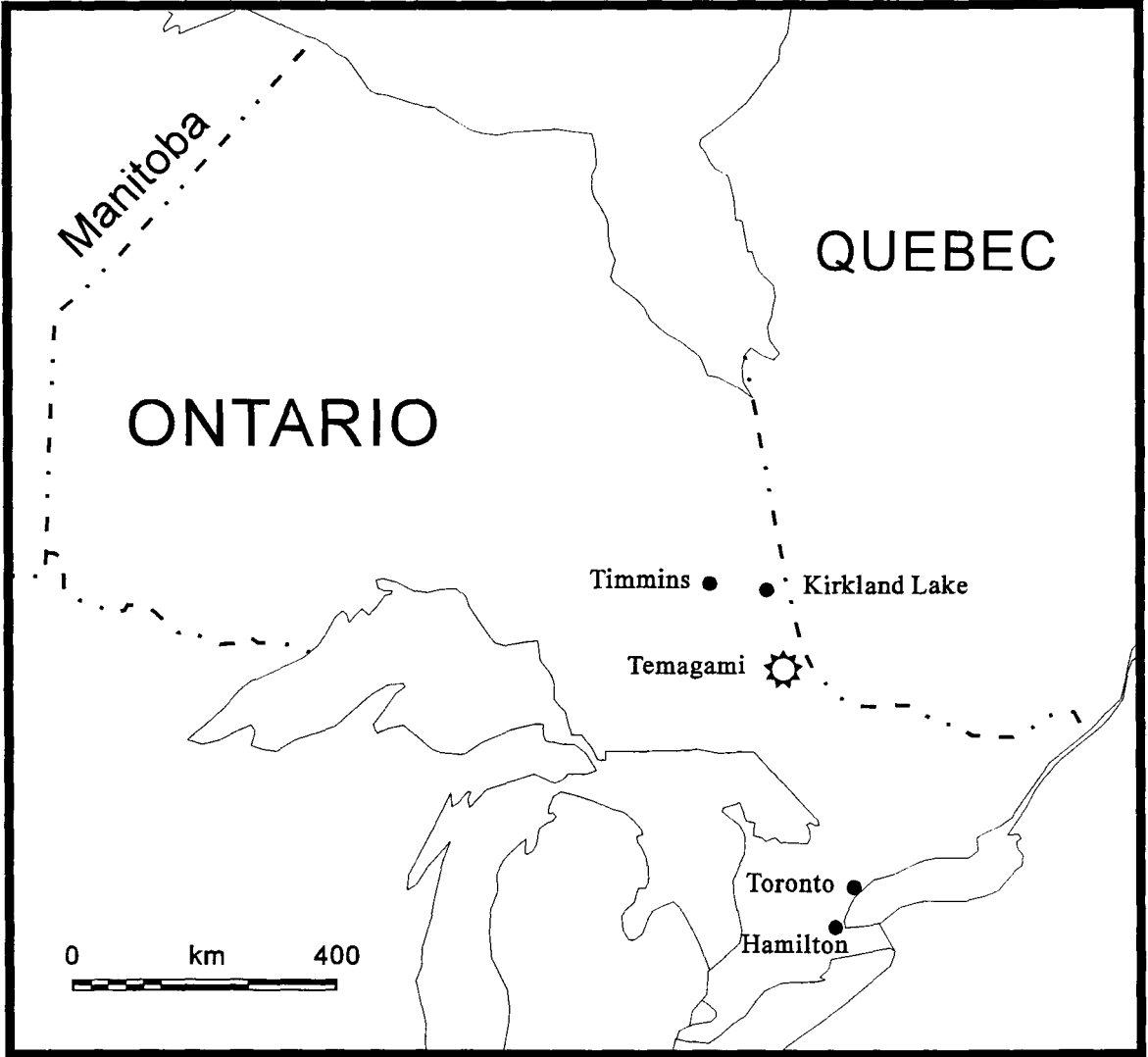


Figure 1-1: Location of Temagami, Ontario.

1.3 Previous Work

1.3.1 Government projects

Early work was carried out in the Temagami area by Barlow (1907) and Moorehouse (1942), and a more comprehensive study of the area was completed by Bennett (1978). A preliminary stratigraphic analysis and mineral occurrence study was conducted by Fyon and Crocket (1986), and subsequent follow-up work by Fyon and O'Donnell (1987), Fyon *et al.* (1988) and Fyon and Cole (1989) have produced a more defined synthesis of the geology of the Temagami greenstone belt.

1.3.2 Academic studies

Several projects have been conducted within the Temagami area by various students (e.g. Soucie 1979; Hurley 1985; Blum 1986; Bowins 1989; Brons 1989; Baknes 1990), but no studies have been conducted exclusively on the volcanics within the study area. The study by Hurley (1985), conducted on the volcanic rocks underlying the northern iron formation of the Sherman Mine, is the closest relevant study, but does not geographically overlap the present study area.

1.3.3 Exploration activity

Work previous to 1978 has been outlined in Bennett (1978). Since the re-opening for staking of the Strathy township in 1992, exploration activity within this township has been intense (Ireland *et al.* 1993). Falconbridge Exploration Limited has conducted deep electromagnetic surveys, reconnaissance and detailed mapping, compilation work and geochemical studies within the study area (Ireland *et al.* 1993). As well, new drill hole sites were observed on the Falconbridge property in 1994.

1.4 Objective and Thesis

Since the early 1980's, several studies using major and trace element analyses, in particular rare earth element (REE) analyses, have been conducted on felsic volcanic rocks associated with Cu-Zn massive sulphide mineralization (eg. Sopuck *et al.* 1980; Campbell *et al.* 1981b; Campbell *et al.* 1982a; Campbell *et al.* 1982b; Lesher *et al.* 1986). Of particular interest is the work by Lesher *et al.* (1986) which summarizes the work of others and provides a classification scheme, based on REE patterns, for both barren and ore-bearing felsic volcanic units which are Archean in age.

It was reported by Fyon and Crocket (1986) and Fyon and Cole (1989) that felsic subaqueous pyroclastic flows along the Sherman Mine road have a rare earth element pattern which, according to the work of Lesher *et al.* (1986), is typical of the host rocks for Archean volcanic associated massive sulphide mineralization. On the basis of this information, field and laboratory work were directed to confirm the existence of this pattern, the aerial extent, and the magmatic affinity of the felsic volcanics which host the favourable rare earth element pattern. This was accomplished by regional and detailed mapping of the study area, petrologic study, and geochemical analyses techniques including x-ray fluorescence (XRF) and instrumental neutron activation analysis (INAA).

During preliminary field work, it was noted that pyrite rich clasts are often associated with the subaqueous volcanoclastic flows. Since pyrite is associated with volcanogenic massive sulphide (VMS) deposits, field work, petrological study, and inductively coupled plasma - mass spectrometry (ICP-MS) analysis were conducted to determine the origin of the sulphide clasts.

CHAPTER 2

METHODOLOGY

2.1 Field Approach

As a follow up to field work by Fyon and Crocket (1986) a mapping and lithogeochemical sampling project was initiated along the Sherman Mine road, north of Temagami (Figure 2-1). This was done to confirm outcrop placement as recorded by Fyon and Crocket (1986), and lithology as described by Bennett (1978) and Fyon and Crocket (1986). It was determined early in this field work that meter scale structural information was not available in this area, and detailed 1:5000 mapping was initiated to gain a better understanding of the structural control on lithological placement (see field map back pocket). This map covers an area defined by the north shore of Link Lake, to approximately 600 meters north of the hydro transmission line, and extends from 100 m east of highway 11 to 4 km west of highway 11 (Figure 2-1).

Most of the 1:5000 mapping was conducted on a 100 meter spaced cut grid recently established in the area, and the rest was done by compass and pace at 100 meter intervals. Some additional mapping was carried out at a scale of 1:10000 using aerial photo control. Where warranted, detailed 1:100 scale mapping was conducted on a grid established using a compass and 30 meter tape measure.

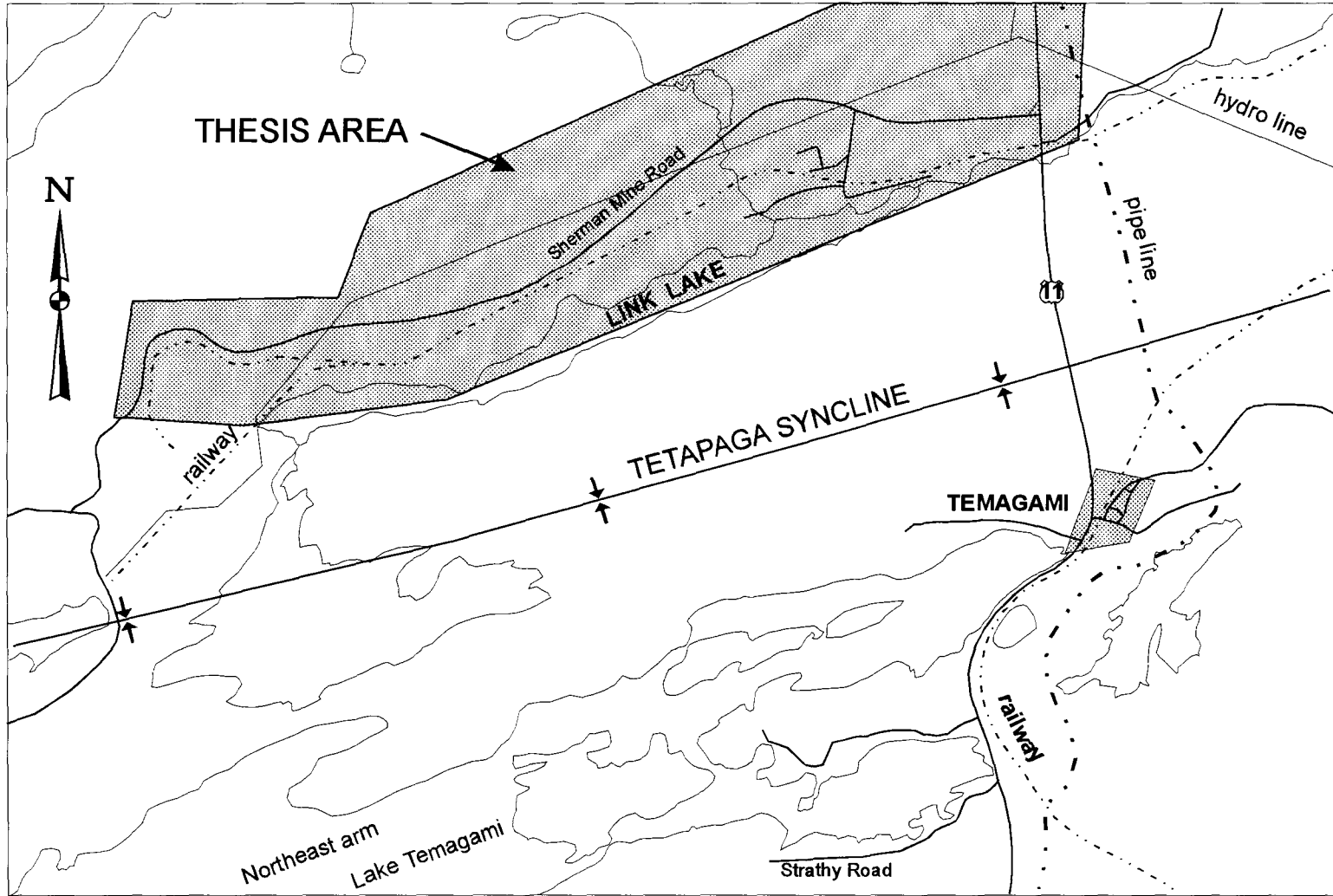
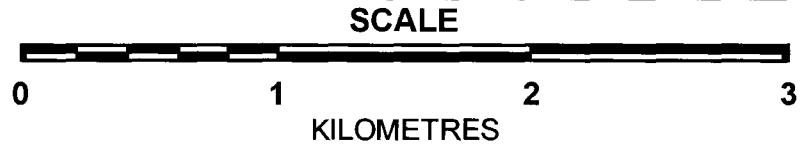


Figure 2-1: Location of thesis area.



From this mapping, stratigraphic control of the felsic horizons was gained, and samples were taken for further petrological and chemical studies. Reference to sample, trench and outcrop location throughout the thesis is given relative to the grid presented on the field map (back pocket). The coordinate system is a standard used by most exploration companies and is given as a east-west and north-south position.

2.2 Petrology

Many samples were collected during field work and subsequently several were made into either regular thin sections, polished thin sections or ore mounts. Description of the various rocks were made from both the hand samples and thin sections (see Appendix A). From this and other data, the petrography and origins of the rocks were determined.

2.3 Geochemistry

2.3.1 Preparation

All samples collected for geochemical analyses were cleaned of all weathered surfaces in preparation for crushing. Approximately 500g of each sample were sent to Activation Laboratories in Ancaster, Ontario, where they were crushed to <150 mesh powder using a low chromium mill.

2.3.2 XRF

XRF analysis was conducted by both the University of Western Ontario, London, Ontario, Canada, and McMaster University, Hamilton, Ontario. It was determined that, on the basis of a summation of $100 \pm 1\%$ wt for the major oxides plus LOI, the Western Ontario data would be used. Thus, the whole rock and LOI data for all samples, and the

trace element data on the 100 series samples were taken from the University of Western Ontario, sample analyses. Since trace element analysis was not conducted on samples 02 through 75 at the University of Western Ontario, this data was taken from the McMaster University analyses.

The methods used by Dr. Charles Wu (University of Western Ontario), and Jim McAndrew (McMaster University) for the determination of the various elements by XRF analysis, as outlined in a communications from them, are summarized below.

2.3.2.1 Major oxide analysis

Ten major elements expressed as oxides (SiO_2 , TiO_2 , Fe_2O_3 , MnO , MgO , CaO , K_2O , Na_2O , P_2O_5) were determined on fused disks prepared by the methods similar to that of Norrish and Hutton (1969). Approximately 1.00g of roasted powdered sample was mixed with 5.00g of the Norrish formula flux containing LaO as a heavy absorber. The mixture was then fused at about 1000°C for 20 minutes, and poured into a pre-heated mould and allowed to cool.

X-ray fluorescence spectrometry (XRF) analyses were carried out by a Philips PW-1450 automatic sequential spectrometer equipped with a side-window Rh-target X-ray tube using a 45 keV/ 50 mA tube voltage to excite the sample. All analytes were measured on spectra K-lines by a gas-flow proportional counter. Intensities of element peaks were collected and reduced on a PC using a series of in-house programs. Nominal oxide concentrations were calculated against a monitor (super-standard) which was prepared by Dr. K. Norrish. Inter-element and flux matrix effects were further corrected with iteration using coefficients provided by Norrish. Loss on ignition (LOI), expressed as wt.%, was determined from weight loss of a 1.000g powdered sample after roasting at 1000°C for 2 hours.

One Canadian Certified Reference Materials Project (CCRMP) standard (MRG-1) of CANAMET, and one Geological Survey of Japan standard (JB-1A) were run as unknowns to check the quality of data during routine analyses. In addition, duplicates of randomly selected samples from the suite were also made and analyzed to insure the quality of preparation procedures and instrument stability. Detection limits for the XRF analysis are 0.01 wt % for major oxides, and the precision error is 7% for P, <3% for Mn, K and Na, and <1% for Si, Ti, Al, Fe, Mg and Ca.

2.3.2.2 Trace element analysis

Trace elements (Nb, Zr, Y, Sr, Rb, Ba, Pb, Zn, Cu, Ni, Co, Cr, V) were determined on whole rock pressed powder pellets. Approximately 6.0g of powdered sample were mixed with 3 to 4 drops of a 2% polyvinyl alcohol solution, which serves as a binding agent. The mixture along with boric acid backing was then transferred into a loose-sleeve type briquetting device and pressed with 10 tons pressure for 5 minutes.

Trace elements were analyzed using both Rh- and W-target tubes with a tube voltage of 60 keV/ 40 mA. A scintillation detector combined with a flow proportional counter was used for measuring the spectral intensities. Mass absorption coefficients were derived from the RhK_{α} or WL_B Compton peak intensities as recommended by Willis (1989) and Nesbitt *et al.* (1976). Spectral interferences were corrected from pre-calculated interference factors.

A set of 24 international standards (eg. USGS, GIT-IWG, NIM, CCRMP) were used for concentration calibrations. In addition the two USGS standards G-2 and BHVO-1, one CCRMP standard MRG-1, and duplicates of randomly chosen samples from the suite are also run as unknowns to insure the accuracy and precision of the data during

analysis. Detection limits are 2 ppm for Nb, Zr, Y, Sr and Rb, and 5 ppm for Ba, V, Cr, Co, Ni, Cu, Zn, and Pb and precision error is <2% for all elements.

2.3.2.3 Trace element analysis: McMaster University

Trace elements (Nb, Zr, Y, Sr, Rb, Pb, Zn, Cu, Ni, Co, Cr, V) were determined on whole rock pressed powder pellets using a Philips PW-1480 automatic sequential spectrometer. Approximately 6.0g of powdered sample were mixed with 6 drops mowiol, which serves as a binding agent. The mixture was then pressed with 12 tonnes pressure for 5 minutes. All trace elements were analyzed using a Rh-target tube with a tube voltage of either 95 keV/ 30 mA for Rb, Sr, Y, Zr, Nb, or 60 keV/ 45 mA for V, Cr, Co, Pb, Cu, Zn, Ni. Scintillation detector and flow proportional counter combinations were used for measuring the spectral intensities. Mass absorption coefficients were derived from the RhK_{α} Compton peak intensities. Detection limits for the XRF trace element analysis is 1 ppm for all elements and precision error is <2% for all elements.

2.3.3 INAA

The techniques for Instrumental Neutron Activation Analysis outlined by Jacobs *et al.* (1977) were followed as a guide line to the proper analyses of the research samples. A more specific outline for the analyses of samples used in this thesis is outlined below.

Aliquots from each of the crushed samples, weighing approximately 500mg, were individually sealed in small polyethylene vials. These samples were then, along with two standards, bundled together in plastic petri dishes for irradiation in the McMaster reactor. Each sample was irradiated twice, with appropriate decay times and counting times between each irradiation. Irradiation times for the samples varied for the various elements being counted. The first irradiation, a 2 megawatt (2mw) epithermal irradiation,

allowed for the quantitative determination of the shorter lived isotopes As, La, Sb, and Sm. The second irradiation, a 7mw thermal irradiation, allowed for the quantitative determination of Au, Ba, Ce, Lu, Sc, Th, Yb, Eu, Hf, Tb, Ta and Cs. Samples were rotated during both of the irradiation events. A full schedule of irradiation times and the appropriate energy levels used is provided in Table 2-1.

Gamma-ray spectra were obtained from Aptec multichannel analyzers (MCA) coupled to an intrinsic coaxial germanium detector (Canberra Industries, Meriden, Connecticut) and an Aptec model 6300 spectroscopy amplifier. The detector geometry is a thin window closed ended coaxial with an active area facing window of 19.8cm^2 . The detector has a relative efficiency of 23%, resolution of 1.90keV (FWHM) at 1.33 MeV and a peak to Compton ratio of 47.1:1. Spectra from sample numbers 02 through 75 were taken in 4096 channels calibrated to approximately 0.4keV per channel, and all of the 100 series samples were taken in 16384 channels calibrated to approximately 0.1keV per channel. Counting dead times were kept to <5% for all samples, and <2% for most of the samples. All counting statistics were obtained using Aptec multichannel analyzer software version 5.3, release 4 for windows (copyright 1989-1994, Aptec engineering Ltd.).

Detection limits for the INAA analysis are 0.5 ppm for As, Ba, Ce, Eu, Hf, La, Lu, Sb, Sc, Sm, Ta, Tb, Th, Yb, and Cs, and 2 ppb for Au. Precision error is <4% for Ce, Cs, Eu, Hf, Lu, Sc, Ta, Th and Yb and <10% for Tb, La, Sm. Precision error is not available for As, Ba and Sb as analysed by INAA procedures.

Analysis of U and B were done on 0.5 gram samples at the Center for NAA at the McMaster Reactor, using delayed neutron activation analysis and prompt gamma respectively. The detection limit for U is approximately 0.5 ppm, and for B is approximately 1ppm. The precision and accuracy errors for all analyses is provided in Appendix C.

TABLE 2-1
Schedule of Irradiation for INAA

First irradiation (epithermal, 2mw)
Decay time following irradiation = 3 to 5 day
Count Time 3600 to 7200 seconds

Nuclide	Target Isotope	Product Isotope	Half-Life	Energy (keV)	Correcting Peak (keV)	Correction Factor
La	139 La	140 La	40.27 h	1596	-----	-----
La	139 La	140 La	40.27 h	487	-----	-----
Sm	152 Sm	153 Sm	47.1 h	69.6	-----	-----
Sm	152 Sm	153 Sm	47.1 h	103	312, 106	0.0119, 0.81
As	75 As	76 As	26.3 h	559	-----	-----
Sb	121 Sb	122 Sb	2.75 d	564	-----	-----

Second irradiation (thermal, 7mw)
Count one
14 days following epithermal irradiation
Decay time following irradiation = 7 to 10 days
Count Time 3600 to 7200 seconds

Nuclide	Target Isotope	Product Isotope	Half-Life	Energy (keV)	Correcting Peak (keV)	Correction Factor
Lu	176 Lu	177 Lu	6.75 d	208	106	0.128
Th	232 Th	233 Pa	27 d	312	-----	-----
Yb	174 Yb	175 Yb	4.19 d	396	312	0.0318
Ce	140 Ce	141 Ce	32.5 d	145	312	0.025
Au	197 Au	198 Au	2.7 d	412	-----	-----
Sc	45 Sc	46 Sc	83.9 d	889	-----	-----
Sc	45 Sc	46 Sc	83.9 d	1120	-----	-----
Ba	130 Ba	131 Ba	11.5 d	216	298	0.22

TABLE 2-1 (continued)
Schedule of Irradiation for INAA

Second irradiation (thermal, 7mw)

Count two

Decay time following irradiation = 50 to 60 days

Count Time 7200 to 14400 seconds

Nuclide	Target Isotope	Product Isotope	Half-Life	Energy (keV)	Correcting Peak (keV)	Correction Factor
Eu	151 Eu	152 Eu	12.2 y	1408	-----	-----
Eu	151 Eu	152 Eu	12.2 y	122	-----	-----
Hf	180 Hf	181 Hf	44.6 d	482	-----	-----
Tb	159 Tb	160 Tb	72.4 d	298	312	0.178
Ta	181 Ta	182 Ta	115 d	1221	-----	-----
Cs	133 Cs	134 Cs	2.05 y	604	-----	-----
Cs	133 Cs	134 Cs	2.05 y	796	-----	-----

h = hour

d = day

y = year

all reactions are n - gamma

The interference correction is made by the following calculation:

true counts = observed counts - (observed counts of the correction peak * correction factor).

CHAPTER 3

GENERAL GEOLOGY

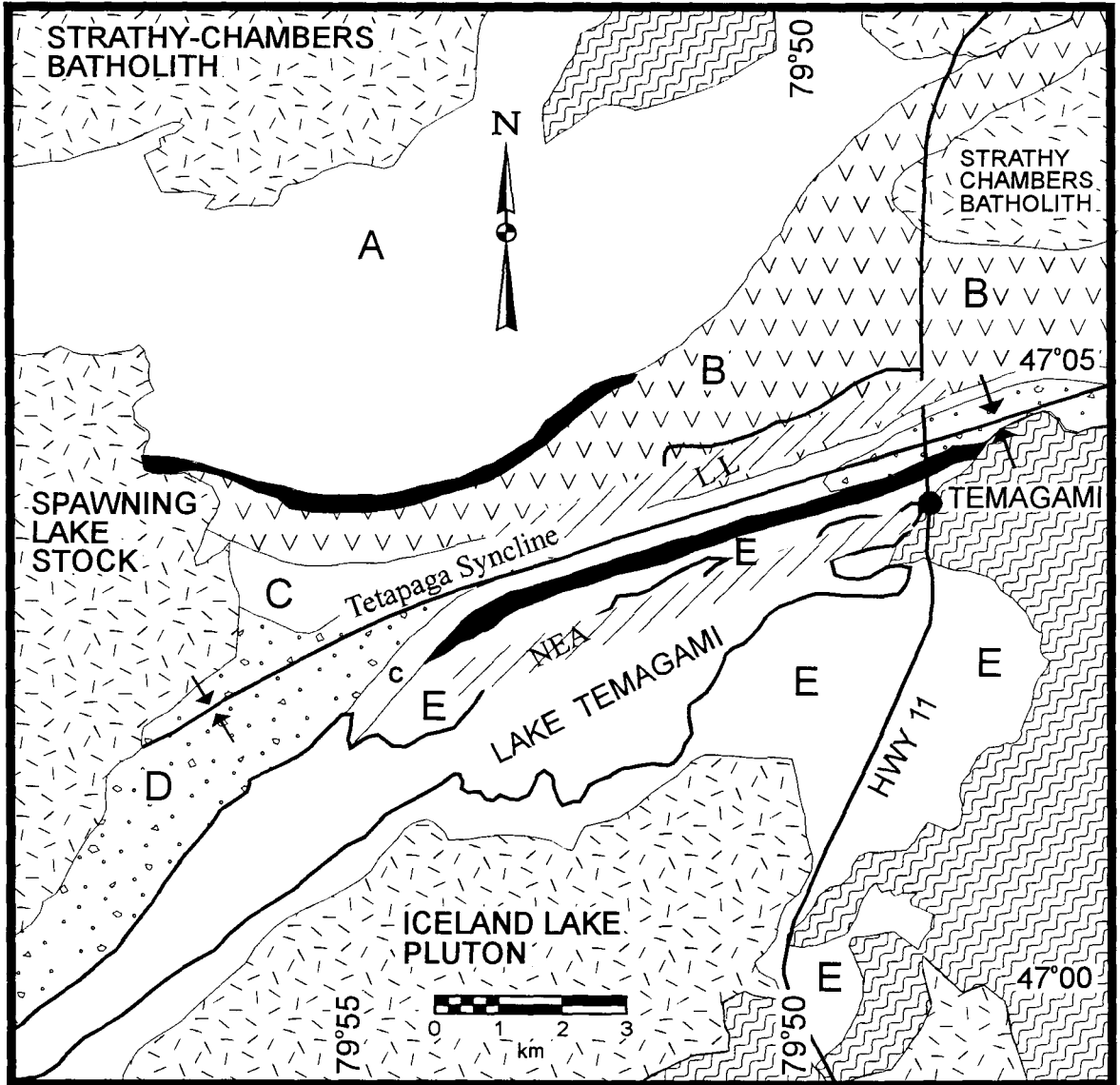
3.1 Regional Setting

The Temagami greenstone belt is a northeast trending metavolcanic-metasedimentary belt, consisting of tholeiitic and calc-alkalic metavolcanic rocks, and associated clastic and chemical metasedimentary rocks (Bennett 1978; Fyon and Cole 1989). For the sake of brevity, the prefix meta is implied for all lithologies, but is deleted from all of the following discussions. Greenschist facies metamorphic conditions prevail throughout the belt except adjacent to late granitoids where amphibolite conditions occur (Jackson and Fyon 1991).

From the work of Fyon and Crocket (1986), Fyon and O'Donnell (1987), and Fyon *et al.* (1988), a three fold lithostratigraphic subdivision of the volcanogenic-sedimentary rocks was developed and later refined by Fyon and Cole (1989). Fyon and Cole (1989) have subdivided the Temagami greenstone belt into five sequences defined as sequence A through E (Figure 3-1).

Sequence A consists of massive and pillowed, iron-rich, tholeiitic basalt flows, overlain by intermediate and felsic calc-alkalic flows and fragmentals. A thin oxide-facies iron formation caps the calc-alkalic unit, and is conformably overlain by fragmental ultramafics and clastic metasedimentary rocks.

Figure 3-1: Simplified geology of the Temagami greenstone belt in proximity to the thesis area. After Bennett (1978) and Fyon and Cole (1989).



PROTEROZOIC
Huronian Supergroup



Gowganda Formation



Zone of deformation
LL - Link Lake
NEA - Northeast arm

ARCHEAN



Granitoid intrusive rocks



Metavolcanic sequence



Metasedimentary sequence



Metavolcanic sequence



Banded iron formation



Metavolcanic sequences

Sequence B consists of iron-rich, tholeiitic basalt flows overlain by intermediate and felsic tholeiitic and calc-alkalic, effusive and fragmental metavolcanic rocks. The thesis study area is located within this sequence.

Sequence C consists of thinly bedded, turbiditic wacke-mudstone couplets and a matrix-supported conglomerate. Sequences A through C are all south facing.

Sequence D consists of massive and pillowed iron tholeiites with no consistent facing direction. These rocks occupy the core of the Tetapaga Syncline.

Sequence E consists of massive and pillowed iron tholeiites at the base, intermediate andesite and rhyolite effusive and fragmental flows in the middle, with a thin oxide-facies iron formation capping the top of the sequence.

On the basis of similar lithology and geochemistry, sequence A and E have been interpreted to be stratigraphically correlative by Fyon and Cole (1989).

Three late stage granitoid intrusions, the pre- to syntectonic Strathy-Chambers and Iceland lake trondhjemitic batholiths, and the posttectonic Spawning lake granite, have been emplaced into the greenstone belt. Fyon and Cole (1989) suggest that the Iceland Lake batholith and the trondhjemitic phase of the Strathy-Chambers batholith were comagmatic with the calc-alkalic metavolcanic sequences of A and E, and the dacitic and rhyolitic metavolcanic rocks of sequence B were comagmatic with the granitic phase of the Strathy-Chambers batholith. Further comparison of Sequence B and the Strathy-Chambers batholith will be made later.

3.2 Regional Structures

The Temagami greenstone belt has not been structurally deformed to any great extent. The major structure within the Archean terrain is an east-northeast syncline, the axis of which extends from 47° 02'N 79° 57'W to 47° 05'N 79° 46'W (Figure 3-1).

Three major zones of deformation have been recognized in this belt: the Link Lake deformation zone (LLDZ), the Northeast Arm (NEA) and the Net lake-Vermillion Lake Zones (Bennett, 1978; Fyon and Crocket, 1986). These deformation zones are marked by strong easterly trending foliations with vertical to subvertical dips, extension lineations and flattening.

The Link Lake and Northeast Arm deformation zones straddle the north and south sides of the Tetapaga syncline respectively (Figure 3-1), and represent zones of pure shear produced by the formation of the syncline (Fyon and O'Donnell, 1987). Steep westerly dipping drag folds on the extreme eastern end of Link Lake indicates a horizontal component of movement along this structure. Detailed petrography indicates rotation of clasts and therefore there is a component of simple shear in this deformation zone.

3.3 Age of the Temagami Greenstone Belt

U-Pb zircon dates have been reported for various sites in the Temagami greenstone belt. Bowins and Heaman (1991) have indicated that rhyolite flows from sequence E yield a U-Pb age of 2736 ± 3 Ma and a rhyolite porphyry dike cutting andesitic flows of sequence B has a U-Pb zircon date of 2687 ± 2 Ma. This infers that volcanic activity took place over ~ 50 Ma for the Temagami greenstone belt.

3.4 Local Geology

3.4.1 General geology

The thesis area has undergone a regional greenschist metamorphic event and lies solely within unit B as defined by Fyon and Cole (1989). The metavolcanics within this area consist of iron-rich tholeiitic basalts, (Fyon and Crocket 1986; Fyon and Cole 1989) tholeiitic rhyolites, calc-alkaline basalts, calc-alkaline rhyolites and quartz porphyries. All of these units have a facing direction of south, with a moderate to strong East-West trending steeply dipping foliation. While most of the rocks are strongly sheared within the Link Lake deformation zone (Plate 3-1), it is the volcanoclastic rocks that have the strongest foliation further away from the deformation zone .

The general succession of units from the base (north) to the top (south) are tholeiitic mafic volcanics, calc-alkaline mafic volcanics, tholeiitic felsic volcanics, calc-alkaline mafic volcanics interbedded with calc-alkaline mafic volcanics. A mafic to ultramafic sill with a pyroxenitic to dioritic composition (Fyon and Crocket 1986) intrudes the central part of the thesis area. The last intrusive event in the immediate area is marked by northwest-southeast trending diabase dykes.

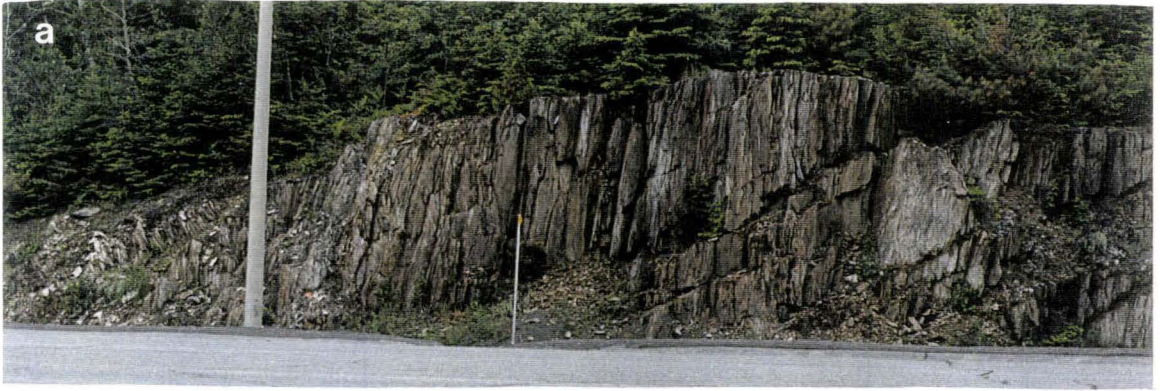
3.4.2 Local structure

On the basis of large lineaments and actual fault boundaries, several large fault structures have been defined. Of particular interest is the parallel set of 040° trending lineaments in the area of L14W to L24W and 2S to 4N (field map). Outcrops along the edges of these lineaments often contain fractures filled with pyrite and quartz. These lineaments dominantly show a sinistral offset pattern as indicated by the displacement of the felsic horizons. Other more northerly trending faults and lineaments also tend to show

Plate 3-1a: Shearing of calc-alkaline basalts and felsic tholeiitic volcanoclastics along the northern extent of the Link Lake deformation zone. The light pole is approximately 30cm wide.

Plate 3-1b: Shearing of felsic tholeiitic volcanoclastics along L20W and the Sherman Mine road. Note the iron staining caused by the weathering of sulphide clasts. Outcrop is approximately 2 meters high.

Plate 3-1c: Shearing of calc-alkaline pillow basalts along the Link Lake deformation zone. The diabasic dykes (black) are neither sheared nor faulted indicating they post date the LLDZ event. Hammer in center of photo for scale.



sinistral movement. All of these movements are apparent only. Where measurable these faults tend to be steep dipping towards the north west.

While most of the structural movement has not produced folds, small scale drag folds are present along the Link Lake deformation zone, and some small and large scale drag folds are present within the Lower Felsic horizon. The drag folds along the LLDZ have a steep ($>80^\circ$) westerly plunge. The folds in the Lower Felsic horizon demonstrate a dextral sense of movement and have a measured plunge of 75°W at the Fold Nose trench (Figure 3-2). The folds are most noticeable in the carbonaceous shale, however, they are distinguishable in the felsic units when sharp bedding contacts are present (Figure 4-1). The enhancement of folding within the carbonaceous shales indicates this unit is relatively incompetent and more ductile compared to the other units (Plate 3-2). Thus, the carbonaceous shales take up a lot of strain and act as the focus for tectonic movement.

3.4.3 Outcrop exposure

The last glacial event in this area has left thick deposits of glacial-fluvial material which tends to obscure most of the bedrock geology in the area. In addition large cedar swamps also tend to cover much of the area.

The best outcrop exposures are along the roads, railway and hydroline. Here mechanical stripping of the overburden during their construction has provided good two and three dimensional exposures. However, these areas are not being maintained and new moss, grasses and shrubs have started to obscure the exposures. Recent stripping by Falconbridge Ltd. has provided a few new areas of exposure, which has helped in the correlation of the felsic units. In all, outcrop is scarce and exposures are poor so that correlation of units tends to be difficult and problematic.

Figure 3-2: Map of fold in outcrop at the Fold Nose trench, L6W 0+75N. Deformation of the outcrop indicates shear is dextral and the fold is plunging to the west. Stratigraphic top is to the south. Points A and B are references to points A and B on Plate3-2a.

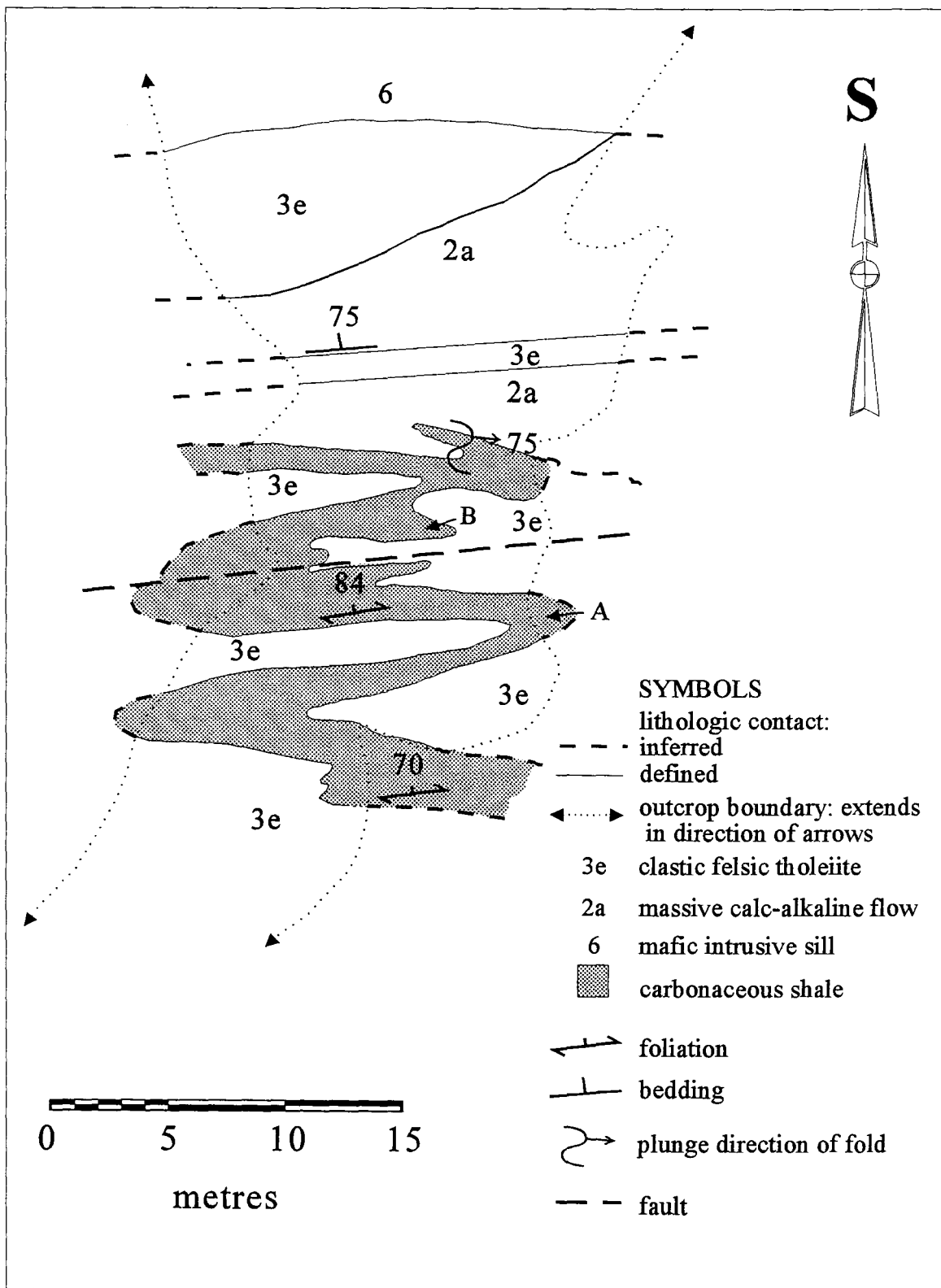


Plate 3-2a: Folded graphitic schist and felsic tholeiitic volcanoclastics in the Lower Felsic horizon as indicated in Figure 3-2. The sharp contrast between the two rock types makes the fold stand out. Points A and B are references to points A and B on Figure 3-2. South is to the right in this photo.

Plate 3-2b: Smaller folds in the greywacke at the Garbage Dump trench (Lower Felsic horizon). Apparent movement is also dextral here. South is to the top of the card.



CHAPTER 4

PETROLOGY

4.1 Nomenclature

As mentioned earlier, the study area was mapped in detail (1:4800) by Fyon and Crocket (1986). Units were subdivided both on the basis of petrology and chemistry, producing 10 major stratigraphic subdivisions within the Temagami area (see Fyon and Crocket 1986, map 3 legend). In the present study, with the exclusion of the diabase and mafic to ultramafic intrusive rocks, the mafic and felsic horizons were subdivided on the basis of chemistry and chemical classifications using immobile elements (see Chapter 5 for further discussion). As a result, the area was divided into the following 6 major stratigraphic subdivisions:

- 1) Mafic tholeiitic metavolcanics
 - a) massive
 - b) pillowed
 - c) breccia

- 2) Mafic calc-alkaline metavolcanics
 - a) massive
 - b) pillowed
 - c) breccia

3) Felsic tholeiitic metavolcanics

- a) massive
- c) breccia
- e) clastic
- f) quartz feldspar porphyry

4) Felsic calc-alkaline metavolcanics

- a) massive
- c) breccia
- e) clastic
- f) quartz feldspar porphyry

6) Mafic to ultramafic intrusive rocks

10) Diabase

Units 1, 2, 6 and 10 of this study correspond to units 1, 2, 6 and 10 of Fyon and Crocket (1986) respectively. There is no direct correlation of units 3 and 4 to any of the units of Fyon and Crocket (1986); however, their units 3 and 7 belong to either unit 3 or 4 of this study. Unless otherwise noted, all nomenclature used in the following discussions is that of this study.

4.2 Mafic Metavolcanics

4.2.1 Tholeiitic flows: Unit 1

The tholeiitic basalts are present only in the extreme northern extent of the study area (field map thesis pocket). Within this area the basalts are made up of massive lavas, pillowed lavas, and brecciated flows. These rocks are very fine grained to aphanitic, and both the fresh and weathered surfaces have a dark green color. This property makes it difficult to differentiate between the tholeiites and overlying calc-alkaline basalts of unit 2. With the exception of sample 2, chemistry was not available for the tholeiitic basalts, and thus the boundaries of this unit was defined and delineated according to the mapping of Fyon and Crocket (1986).

In thin section these basalts still retain a diabasic texture, indicating regional deformation within this area is minimal. Plagioclase laths vary in size from 0.2 to 0.5mm, and extinction of twinning in cross polars indicates these plagioclases are dominantly oligoclase. Chlorite has replaced all of the former mafic minerals, and carbonate content, dominantly confined to fractures, is less than 3%.

Fyon and Crocket (1986) also report the presence of variolitic and coarse grained (2cm) feldspar-phyric flows within the tholeiitic horizon. While the variolitic flows were not observed in the tholeiite section of the study area, coarse grained feldspar-phyric flows were observed within the tholeiitic basalt section, as mapped by Fyon and Crocket (1986). Chemical classification of these rocks (sample 2, see chapter 5) confirms that these feldspar-phyric flows are tholeiites, and were misidentified as calc-alkaline on map 2 of Fyon and Crocket (1986). The difference in magmatic affinities as recorded on maps 2 and 3 of Fyon and Crocket (1986), may present difficulties in the interpretation of the volcanic history of the area because it is not clear whether the Lower Felsic horizon is lying on top of tholeiite or calc-alkaline basalts. Thus, inferences made about the timing of calc-alkaline volcanism to that of tholeiite volcanism may be incorrect.

4.2.2 Calc-alkaline flows: Unit 2

This basalt type is dominant throughout the study area. It consists of massive lavas, pillowed lavas, and brecciated flows and underlies the lower tholeiitic felsic horizon (defined in this study) as mapped by Fyon and Crocket (1986). North of the Sherman Mine road these basalts are usually very fine grained to aphanitic with the occasional feldspar-phyric flow, and weather a dark green to slightly beige-green.

The massive and pillowed flows tend to be 1 to 10 meters thick and are often capped with a flow top breccia or pillow breccia, but there does not appear to be any rhythmical alternation between the massive and pillowed flows. Pillow flattening in this area is minimal in a east-west direction. In the field, not only are the northerly calc-alkaline basalts hard to differentiate from the tholeiites, they are also difficult to differentiate from the mafic intrusions (unit 6) when breccias and pillow lavas are not present.

South of the Sherman Mine road and in proximity to the Link Lake deformation zone, the basalts tend to weather a dark brown. This discoloration is due to the weathering of Fe-Mg-carbonates from the rocks. Fresh surfaces are beige, and the rock is very fine grained with occasional patches of quartz with a maximum dimension of ~1cm. Pillows tend to be flattened and elongated in the east-west direction. In general the pillows in the south tend to be smaller than those in the north, and massive flows are thinner and less common.

In thin section the basalts are strongly altered as indicated by the destruction of primary textures and the overprinting by Fe-Mg carbonates. Carbonate content ranges from 25% to 30% in the matrix. Chlorite, which is the metamorphic replacement of the original primary mafic minerals, is still dominant in thin section.

4.3 Mafic to Ultramafic Intrusives

4.3.1 Gabbro, diorite: Unit 6

This unit parallels the bedding planes of the surrounding rock and is referred to as the Sill. It extends the length of the study area, and can be up to 250 meters thick. Textually this Sill can vary from aphanitic at its peripheries to medium grained in the center, and it weathers a dark green to a slight orange-brown. Compositionally it consists

of chlorite replacement of original mafic minerals, quartz and plagioclase, with leucoxene as the primary accessory mineral. The modal variability of quartz and plagioclase leads to classification of the rock as a gabbro through diorite. Chemical classifications (Chapter 5) identify this Sill as having a calc-alkaline magmatic affinity.

Subhedral crystals of Mg-carbonate is present in amounts ranging from 5-15%, and crystal sizes between 0.5mm and 5mm. The carbonate content increases in proximity to the LLDZ indicating it is related to the deformation event. In proximity to the LLDZ, a moderately strong foliation is imparted on the Sill indicating it predates the LLDZ event.

4.3.2 Diabase: Unit 10

Two northwest trending diabase dykes are present in the central part of the map area (see field map). These dykes are coarse grained, up to 50 meters wide, and weather a rusty brown. Fresh surfaces are white and green, consisting of plagioclase laths, pyroxenes, olivines and biotite. Bennett (1978) refers to these as late Precambrian Sudbury-Type diabase dykes.

Several small very fine grained, black northwest trending dykes are also present in the area. Most of these dykes are too small to be noted on the map, and while they were referred to as fine grained diabase dykes, they may in fact be older lamprophyre dykes as noted by Bennett (1978) and Hurley (1985).

4.4 Felsic Metavolcanics

4.4.1 Introduction

The felsic metavolcanics, in particular those of tholeiitic magmatic affinity, make up the bulk of the thesis study, and considerable attention will be given to them. Two horizons of felsic tholeiites are present in the study area; the northern horizon, referred to as the Lower Felsic horizon, contains both massive lava flows and volcanoclastic rocks; the southern horizon, referred to as the Upper Felsic horizon, is made up entirely of volcanoclastic rocks. This distinct lithological difference and the physical separation of the units of up to 300m, warrants separate discussions of the two horizons. All abundances of minerals and clasts are given as estimates of modal proportions.

4.4.2 Lower Felsic horizon: Unit 3

The Lower Felsic horizon extends across most of the map area, from L3E BL0 to L30W 2+00N. A gap of 1.2km exists between lines 7W 0+50N and 19W 1+00N where the Lower Felsic horizon cannot be traced. This area is dominantly covered by swamps, glacial overburden and a small lake, which suggests that if the unit is continuous over the length of this area, then it may be hidden below the ground cover here.

Several good exposures exist along the length of the horizon, including the Temagami town Garbage Dump at L 25+50W, the Fold Nose trench on line L6W, Hydro Station at L 1+25W, and exposures along the Trans Canada pipe line at L2E (field map thesis pocket). Within these exposures several major lithologies exist including debris flows, massive flow banded rhyolites, rhyolite hyaloclastites, carbonaceous shales, thinly bedded greywacke, and lapilli tuffs. While the lithologies are similar across the area, two cross sectional areas, the Garbage Dump trench and Hydro Station trench, are described

to demonstrate the similarities and differences along the strike of the Lower Felsic horizon.

4.4.2.1 Garbage Dump trench

The Garbage Dump trench consists of six major lithologies all overlying massive to brecciated calc-alkaline basalts (unit 2, Figure 4-1). From base to top they are: lower debris flow, massive rhyolite, hyaloclastite, carbonaceous shale, greywacke, upper debris flow.

The lower debris flow is characterized by poorly developed normal grading ~12m thick. The unit consists of angular clasts of non vesicular basalt (~35%) and siliceous rhyolite (~10%), ranging in size from 10 x 10cm at the base to 2 x 2cm near the top (Plate 4-1). There is also up to 1% subrounded cherty clasts with a maximum dimension of 1x1cm, and up to 1% round 0.5 x 0.5cm pyrite clasts concentrated towards the bottom of the flow. The matrix (~50%) is dominated by very small basaltic clasts. The debris flow is in sharp contact with the overlying massive rhyolite.

The massive flow banded rhyolite is 8m thick and comprised of 2% subhedral quartz crystals, 5-10% sericite, which defines the plane of the foliation, and 80-85% quartz groundmass. Flow banding is recognizable by the presence of thin darker colored lines parallel to the top and bottom of the flow. Vesicles, 2x2 mm circular in shape and locally concentrated up to 20%, are concentrated at the top of the flow (Plate 4-2). Carbonate patches up to 2x3 mm occur throughout the samples and are estimated to comprise 5-10% of the unit. The carbonate surrounds quartz and cross cuts the foliation indicating it is a secondary replacement and formed during or after the Link Lake Deformation (LLD) event. Geochemical samples 46 and 119 originate from this unit.

Figure 4-1: Map of outcrop at the Garbage Dump trench demonstrating stratigraphic position of the various units. Note how the main fault in the south has offset and rotated these units, in a clockwise direction. Several smaller faults are also present indicating shear has produced dextral movement in this area. Stratigraphic top is to the south.

SYMBOLS

- — faults
- ↔ fault strike/dip
- contacts; defined, inferred
- limit of outcrop
- ↙↘ foliation strike/dip
- ┌ bedding strike/dip

LEGEND

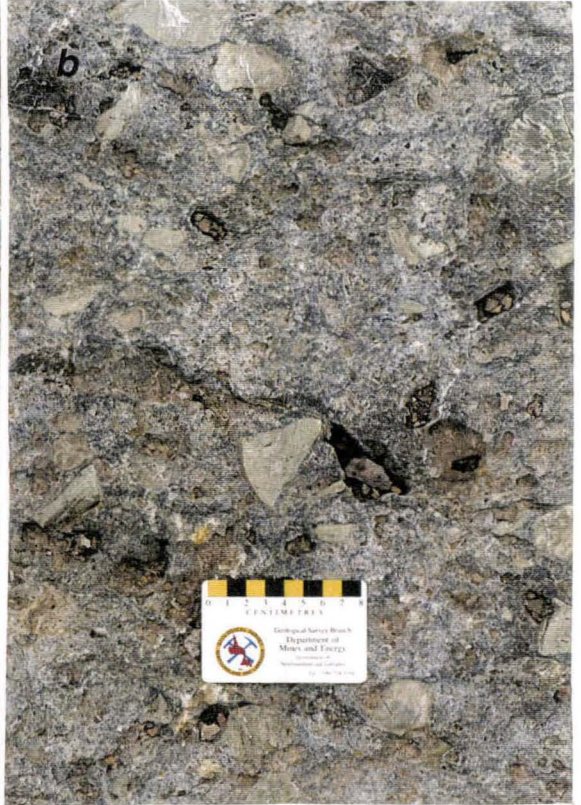
- | | | | |
|---|--------------------|---|--------|
|  | upper debris flow | } | unit 3 |
|  | greywacke | | |
|  | carbonaceous shale | | |
|  | black rhyolite | | |
|  | hyaloclastite | | |
|  | massive rhyolite | | |
|  | debris flow | | |
|  | massive basalt | | unit 2 |



Plate 4-1a: Base of the lower debris flow at the Garbage Dump trench (Lower Felsic horizon). South is to the top of the card, however, stratigraphic top is to the right of the card. Note the clasts have been rotated into the plane of the foliation (east-west).

Plate 4-1b: Near the top of the lower debris flow at the Garbage Dump trench. South and stratigraphic top are both to the top of the card.

Plate 4-2: Massive rhyolite flow at the Garbage Dump trench. Vesicles are present just above the card. South is to the top of the card.



The hyaloclastite is ~4 m thick, weathers a waxy yellow and has an irregular but sharp contact with the massive rhyolite. The hyaloclasts are slightly round to dominantly blocky with a maximum size of 5x5 cm and no preferred orientation. This unit has a sharp to slightly gradational contact with the overlying black rhyolite, which is marked by a distinct color change.

The black rhyolite is ~8 m thick and has the occasional clast of carbonaceous shale, hyaloclasts and/or lithic fragments (Plate 4-3). Superficially these lithic fragments resemble the lower debris flow material. Mineralogically, the only difference between the hyaloclastite and black rhyolite is the presence of 5-10% chlorite throughout the unit and ~10% pyrite cubes within the uppermost 1-1.2 m of the black rhyolite. The top of the black rhyolite is denoted by a sharp contact with the carbonaceous shale. Many small quartz veins (1.5 cm x 10-30 cm length) extend from the topmost part of the black rhyolite into the base of the carbonaceous shale, penetrating not more than 5cm into this unit.

The carbonaceous shale has a maximum thickness of 1m and is distinguished by its jet black color, fissile nature and the presence of pyrite nodules (Plate 6-5). Very fine angular grains of quartz, <0.1mm across, and iron oxides are surrounded by a matrix of very fine grained black opaque material. XRD analysis of a black residue, left over after the dissolution of pyrite spheres from this location (see Chapter 6), indicates it has a high quartz content and some graphite. Graphite was also confirmed by Bowins and Crocket (1994) in black, cherty, pyrite nodule-bearing rocks from the Sherman Mine. The thickest occurrence of the shale immediately overlies the black rhyolite, and here a few lenses of greywacke with maximum dimensions of 1cm x 1m are present.

The boundary between the shale and wacke is sharp. The wacke is dominated by fine grained thinly bedded siliciclastics with occasional continuous (<5cm) beds of shale

Plate 4-3: Example of black rhyolitic hyaloclastite from the Garbage Dump trench (Lower Felsic horizon). Note the variable angularity of the fragments and dark color of the matrix. Some of these fragments superficially resemble fragments in the lower debris flow. South is to the right of the card.

Plate 4-4: Large clast debris flow at the Hydro Station (Lower Felsic horizon). Note the large size and angularity of the clasts. South is towards the top of the card.



(Plate 3-2b). The grey and white colored layers are due to compositional differences in quartz dominated (white), and phyllosilicate dominated (grey) layers.

This area is structurally distinguished by dextral offsets along fault planes which have rotated lithologies 90° clockwise on the south east side of the main fault. Faults strike in a northeast-southwest to east-west direction and dip towards the north-northwest. The faulting and rotation of the units has caused the area to be structurally thickened by an estimated three times the true thickness. Much of the structural movement has taken place within the shale and wacke units suggesting that the original bedding of these units provided ideal slip planes for movement.

The Garbage Dump outcrops have been structurally moved as much as 125m north from their interpreted place of origin along 2+50N (field map). Bennett (1978) originally interpreted this unit as a hypabyssal felsic intrusive, but considering that all of the rocks are extrusive or sedimentary in origin, this interpretation is incorrect.

4.4.2.2 Hydro Station trench

The map area (Figure 4-2) is made up of a large clast debris flow, small clast debris flow, rhyolitic lapilli tuff and quartz porphyry and basaltic intrusives. Massive rhyolites, considered part of the Hydro Station area, are present approximately 30 m to the west and 15 m stratigraphically above the area mapped in Figure 4-2, and physically overlie the lapilli tuff.

The large clast debris flow is polymictic consisting of three major rock types. Vesicular basaltic clast are up to 15x25cm, subrounded to angular with cusped edges. Vesicles can be as large as 5x10 mm and make up 10-40% of the clast. Some of the vesicles are elongated in the plane of the foliation. This rock type makes up 5% of the large clast debris flow.

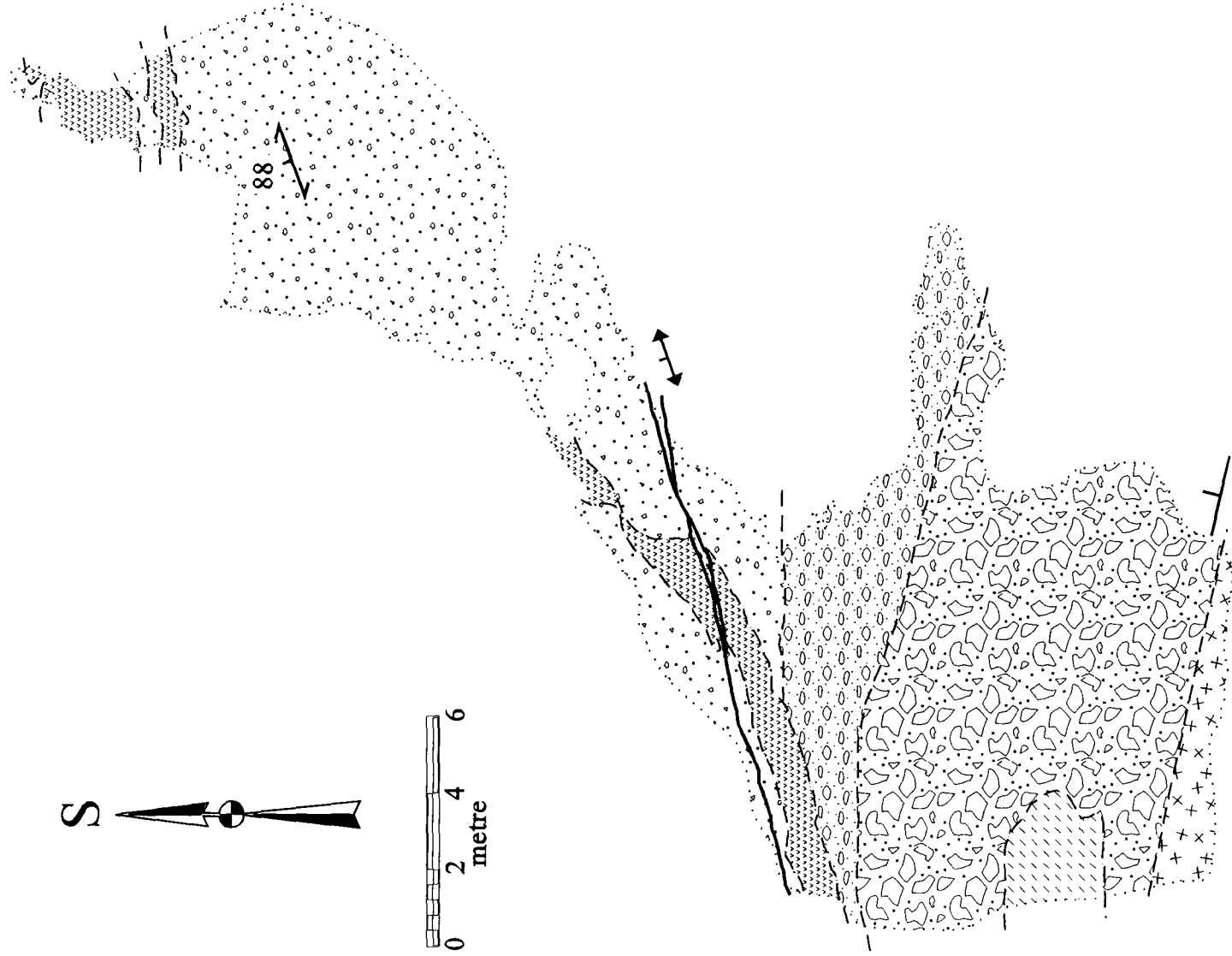
Figure 4-2: Map of Hydro Station trench L1+25W 0+50N demonstrating stratigraphic position of the various units. Stratigraphic top is to the south.

LEGEND

-  quartz feldspar porphyry intrusive
-  rhyolitic lapilli tuff
-  basaltic dyke
-  small clast debris flow
-  large clast debris flow
-  massive calc-alkaline basalt

SYMBOLS

-  foliation strike/dip
-  bedding strike/dip
-  fault strike/dip
-  fault
-  contact
-  limit of outcrop



Massive basaltic clasts are the largest clasts, ranging in size from 15x30 cm up to 25x100 cm, and make up to 60-70% of the flow. They are angular with cusped edges and those that have a distinct long axis are oriented in the plane of the foliation (Plate 4-4). Rhyolite clasts make up 5% of the large clast flow. They are angular and as large as 5x7 cm. Quartz phenocrysts make up as much as 3% of these clasts. This clast type is confined to the upper one third of the flow which suggests that the flow may represent more than one depositional episode. Large sulphide clasts make up a maximum of 2% of the flow. These clasts range in size from 10x15 cm to as large as 15x30 cm (Figure 6-1c), and are concentrated in the bottom 1/3 of the flow, and the bottom of the top 1/3 of the flow. These clasts are angular and tend to produce an iron stain on the surrounding rock. Approximately 25% of the flow is comprised of small (1x2 cm or smaller) angular clasts of basaltic material.

A sharp contact defines the boundary between the large and small clast debris flow. The small clast debris flow is dominated by 2x3 cm angular quartz-phyric rhyolite clasts. These clasts make up 40% of the flow. Approximately 30% of the flow is made up of 1x2cm angular basaltic clasts, and 10% is made up of round, <1x2 cm sulphide clasts. All of the clasts are elongate in the plane of the foliation. Approximately 20% of the sample is matrix consisting of very small rhyolite and basalt fragments. Together, the large and small clast flows make up the 10-12m thick hydro debris flow.

This unit was denoted in the work of Fyon and Crocket (1986) as a polymictic conglomerate. The debris flow ends abruptly 20 m west of the trench (ie. Figure 4-2), against massive to pillowed basalt, and can be traced 100 m to the east where it pinches out. The basalt at the terminus of the debris flow to the west does not appear to be fault bounded, but rather appears to mark a topographic high. This suggests the Hydro debris flow was deposited within a topographically low area.

Overlying the Hydro debris flow is a massive rhyolitic lapilli tuff up to 20 m thick. Due to the presence of sericite, the surface of the lapilli tuff has weathered yellow, and only ghostings of clasts are present within it. Even though the unit is monomictic, angular clast as large as 2x4 cm are identifiable.

A northeast trending carbonatized basaltic dyke and two basaltic sill-like bodies cross cut the small clast debris flow and lapilli tuff. These basaltic units have irregular shapes and appears to occur only in the presence of the lapilli tuff. As the dyke is in contact with the lapilli tuff to the east, and the debris flow to the west (Figure 4-2), it suggests the dyke may not be insitu. Had the dyke originally intruded into an unconsolidated lapilli tuff, it may have caused this lapilli tuff flow to avalanche down a slope only to be deposited at its present location. In the process, pieces of the dyke would be entrained in the flow and be deposited within the flow in a similar manner as described by Busby-Spera and White (1987), thus producing this apparently rootless dyke. Given the fact that the outcrop ends into overburden near the expected contact between the small clast debris flow and the lapilli tuff to the east of the dyke, it is conceivable that this dyke actually does cross-cut several units, and is insitu.

A small circular quartz porphyry intrusive is present within the lower section of the large clast debris flow. The presence of a chill margin along all edges of the body and perlitic texture (Plate 4-5), coupled with the fact that it is the only example of this lithologic type within the debris flow, indicates that it is an intrusive body and not a clast.

The massive flow banded rhyolites are present 15m above the lapilli tuff, and mark the upper most extent of the Lower Felsic horizon in this area. These flows are individually up to 3m thick, with a combined thickness of approximately 10m. At least one

Plate 4-5: Photomicrograph of the perlitic texture in the small circular quartz feldspar intrusive body at the Hydro Station trench (Lower Felsic horizon, sample 21). This texture has all but been destroyed by sericite alteration in the center of the photograph.

**Perlitic
texture**

**zone of intense
sericite alteration**

**Perlitic
texture**



1 cm

of the flows has been internally folded (Plate 4-6). The flow folding is complex, however, the overall folding pattern suggests a dextral sense of shear, which correlates to flow movement from east to west (Christiansen and Lipman 1966). Sample 23 was taken from these massive flows for geochemical analysis.

In comparison to the Garbage Dump sequence, there is no outcrop of the carbonaceous shale in the Hydro Station area. The nearest outcropping of the shale is on L2E BL0 along the Trans Canada pipeline (field map). Here, as was the case at the Garbage Dump, the shale overlies the massive rhyolites. If this is the case at the Hydro Station area then the shales would be in the low swampy area just above the massive lava flows.

4.4.2.3 Fold Nose trench

The Fold Nose trench is located on line 6W (Field map, Figure 3-2). Here the exposure of the felsic horizon is generally poor; however, monomictic volcanoclastic rhyolite and the carbonaceous shale are present. As at the Garbage Dump, the shale has taken up much of the strain, and the result is a large fold. Movement in the fold indicates dextral shear. Sample 113 was taken from the felsic horizon here for geochemical analyses.

4.4.3 Upper Felsic horizon: Unit 3

The Upper Felsic horizon extends over the majority of the length of the study area, but does not outcrop in the area between L12W 2S, and L6W 2S. In the same manner as indicated for the Lower Felsic horizon, this unit, if present, is probably covered.

In the western portion of the map area, the felsic horizon lies dominantly on top of the Sill (unit 6). Within this area, several small exposures demonstrate that the felsic

Plate 4-6: Complexly folded flow bands in massive rhyolite at the Hydro Station area. Overall folding pattern suggests a dextral sense of shear and flow movement from east to west. Top of card is south.



horizon immediately overlies both calc-alkaline basaltic pillow and massive lava flows. To the east the felsic horizon lies solely on top of similar type of lavas. This suggests that the Upper Felsic horizon was originally deposited on top of basalts overlying the Lower Felsic horizon, and that this contact relationship has been destroyed in the western map area by intrusion of the Sill.

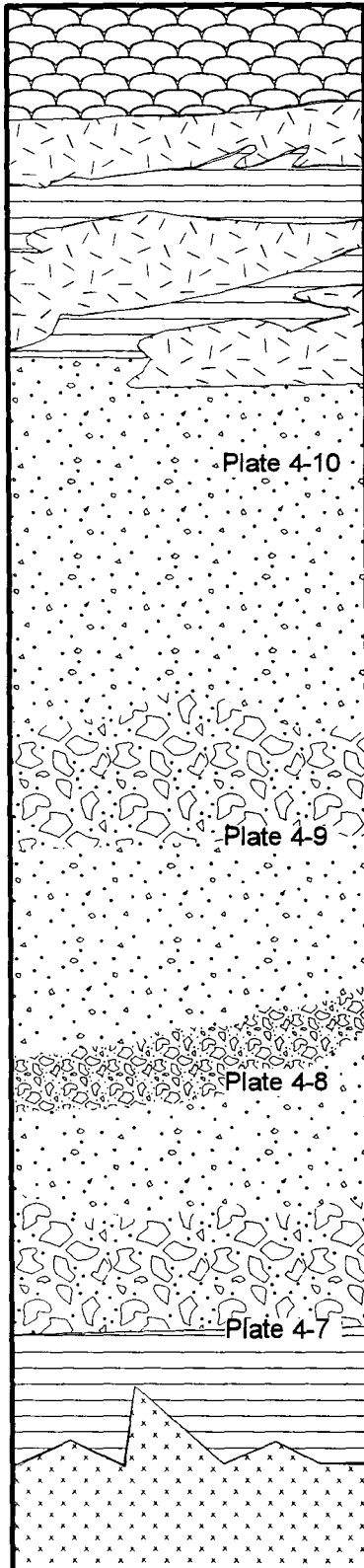
Unlike the Lower Felsic horizon, there are no known lava flows, shales or greywacke in the Upper Felsic horizon, but only volcanoclastic material. A few well exposed and complete sections, present in the area between L14W 2S and L20W 1S, allowed for a semi-quantitative analysis of the horizon.

In general, there are three different unit types; very fine grained thinly bedded tuffs (Plate 4-7), normally graded lapilli to lapilli tuffs, and nongraded to reversely graded block flows (Plate 4-9). At the top of the sequence there are a series of sill-like basaltic intrusions which come from the overlying basalt flows. Fingers of the basalt project into the volcanoclastics from the west to east indicating the basalt flowed from the west to the east and likely intruded into the volcanoclastic flows when they were still unconsolidated (Figure 4-3).

Figure 4-3 is a simplified cross section of the Upper Felsic horizon along L19W and L20W 1+00S with reference to Plates 4-7 to 4-10. Clast types are limited to a few including rhyolitic, shale, basaltic and pyrite. They are angular to subrounded, range in size from a maximum 20x35 cm to <1 cm in diameter and are often elongate in the plane of the foliation. Maximum contribution of clasts of various composition to the individual units are 20% shale ± pumice, 10% pyrite and 100% rhyolitic. Pyrite clasts tend to be concentrated in the basal part of individual flows, but can also be present throughout. Individual flows are usually <3 m thick with some flows measuring up to 7.5m thick.

Figure 4-3: Composite cross section of the Upper Felsic horizon, Unit 3, at L19 and 20W
~0+75S.

General Description



Basalt flows and pillow lavas. Fingers of the flow into the underlying sediment indicates flow movement was from west to east.

B Thinly bedded rhyolitic tuff. Unit has been intruded by basalt.



A' Monomictic rhyolitic lapilli; normal grading. Clasts are subround, 3x5 cm at base to <1cm in diameter at top.



A Polymictic volcanic breccia; consists of 70% angular rhyolitic, 20% shale and or pumice and 2% sulfide clasts. Largest clasts are 20x35 cm. Basal contact is sharp and defined by a change in clast size and composition.

A' Lapilli tuff; 95% of unit is rhyolite clasts, <5% pyrite clasts. Clasts are subrounded 5 cm diameter at the base to 1x2 cm at the top. Normally graded with a gradational lower contact.

A Polymictic volcanic breccia; <10% sulfide clasts. Clasts are subrounded 5 cm diameter. Contact at base is sharp and may show basal shear.

A' Rhyolitic volcanoclastic; massive to poor normal grading. Maximum clast size 2x3 cm. <1% pyrite clasts. Basal contact is marked by a change in clast types.

A Polymictic volcanic breccia with 75% rhyolitic, 20% shale and or pumice and 5% sulfide clasts. Maximum clast size is 4x26 cm. Sulfides do not exceed 1x2 cm. Basal contact is sharp.

B Thinly bedded tuff, highly siliceous. Weathers white to light grey.

Ultramafic sill, unit 6: Intrudes into lower bedded tuff.

Plate 4-7: Example of the lower bedded tuff in contact with a polymictic volcanic breccia, Upper Felsic horizon. South and stratigraphic top is to the top of the card.

Plate 4-8: Example of a sharp contact of a graded bed (lower) and unsorted bed (upper). Note the sharp contact caused by basal shearing during deposition of the upper unit. Stratigraphic top and south is to the top of the card.

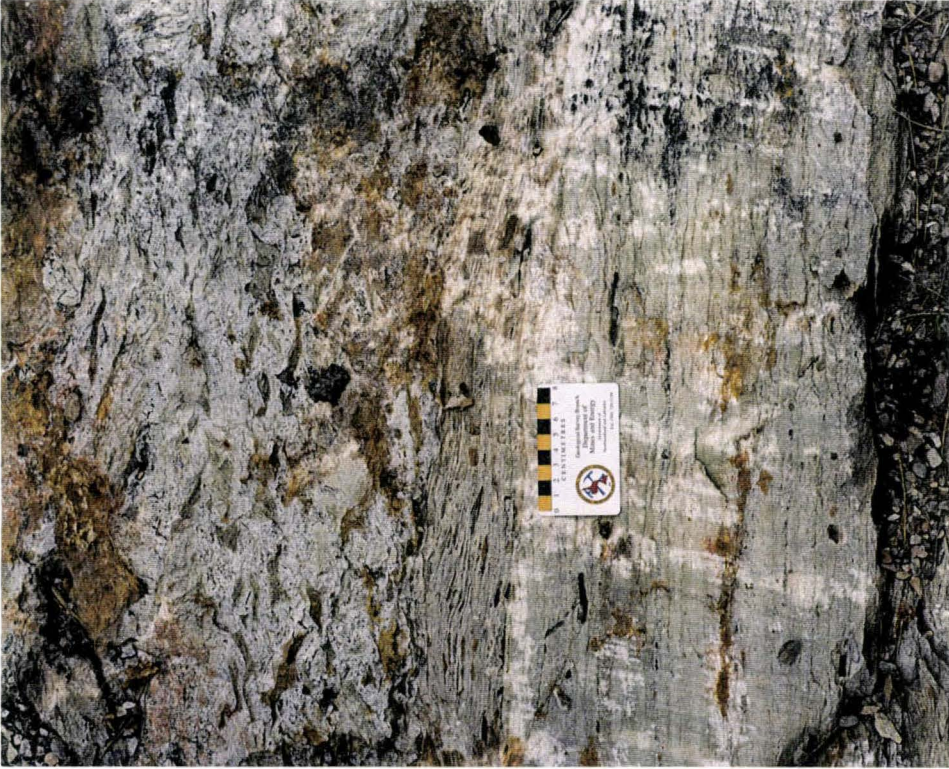


Plate 4-9: Example of the contacts between a graded unit (left), unsorted unit (middle) and another graded unit (right). Note the variability of clast sizes within the unsorted unit, and the presence of large black shale and or pumice clasts. South and stratigraphic top is to the top of the card.

Plate 4-10: Example of poor grading near the top of the unit. Note the uniform composition of the clasts. South and stratigraphic top is to the top of the card.



Individual flows are defined by sharp contacts which are often defined by basal shear (Plate 4-8).

Throughout this horizon there is a reoccurring depositional arrangement of an unsorted large clast dominated flow (A) with an overlying lapilli-tuff that is normally graded (A') and a final bedded tuff (B) (Figure 4-3). This succession (A-A') occurs at least three times in the area of L19 and 20W, and is similar in textural characteristics to that of a volcanoclastic debris or turbidity flow (Cas 1992). The individual pyrite rich horizons do not seem to be laterally continuous for more than 100 to 200m. The presence of the pyrite clasts, which have been derived from shale horizons (see Chapter 6), indicates these volcanoclastic flows must have cut through the shales during their emplacement.

4.4.4 Mineralogy

The Upper and Lower Felsic horizons are mineralogically simple, consisting of primary quartz and sanadine phenocrysts in a quartz matrix, along with the alteration minerals sericite, chlorite and carbonate (Plate 4-11). Quartz grains are very fine grained, subangular, and may make up as much as 20% of individual clasts. Quartz groundmass dominates the samples, and can be more than 80% of many rocks.

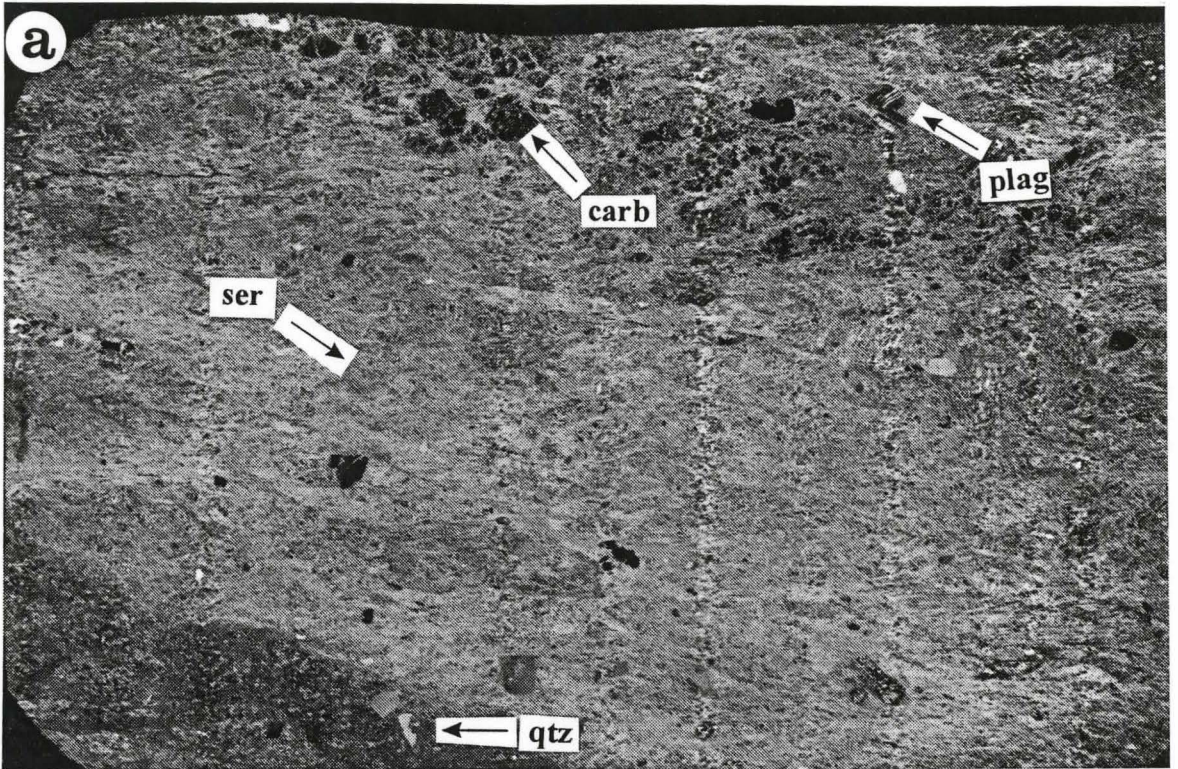
Thin sections of some black clasts from the Upper Felsic horizon, indicate they have been entirely replaced by chlorite, and their original textures are lost. This makes proper identification of their origin enigmatic. In the field, shale clasts can be identified if layering or sulphide spheres are present; however, separation of weathered and altered basalts from the shales (and pumice?) is almost impossible in the LLDZ.

Sericite is the second most abundant mineral, with modal proportions of up to 30%. It occurs as very fine grained wisps, or as large irregular shaped masses, and wraps around clasts and grains of quartz, indicating it is an alteration mineral.

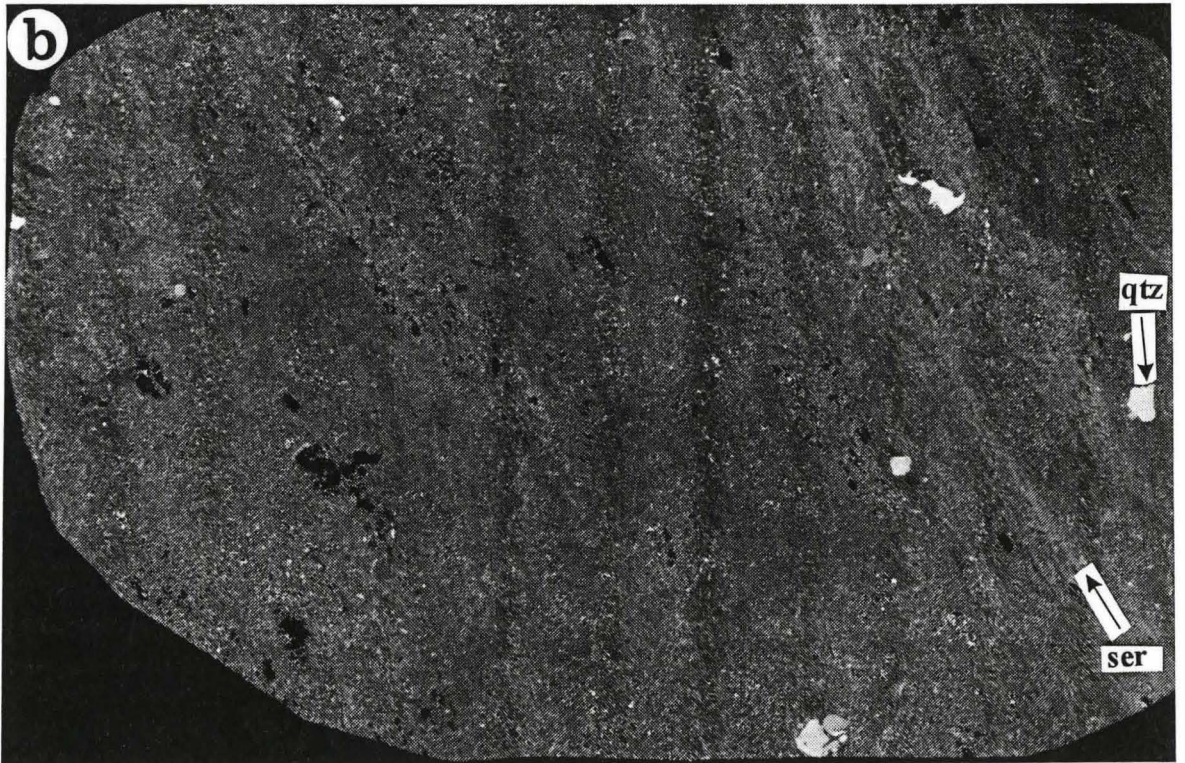
Plate 4-11: Photomicrographs of representative examples of Upper and Lower Felsic horizon mineralogy and textures.

a) Pervasive sericitization (ser) and carbonate (carb) replacement of a volcanoclastic (tuff?) (sample 110). Quartz (qtz) and plagioclase (plag) phenocrysts are identifiable as primary mineralogy. Sericite defines the foliation in all samples. Sample has been photographed in cross polarized light.

b) Sericitization of a massive rhyolite lava flow (sample 23). Sericitization is not as pervasive as in Plate 4-11a. As with the most samples, only quartz phenocrysts are identifiable as primary mineralogy. Sample has been photographed in cross polarized light.



1 cm



Carbonate, dominantly dolomite with occasional iron carbonate, cross cuts the foliation, and was the last mineral to have formed. It occurs as irregular masses up to 3 mm across, and as a fracture filling mineral. In some samples it constitutes >20% of the rock.

With the exception of the previously mentioned clasts, only minor quantities of chlorite and epidote are present throughout these horizons. This minor chlorite reflects the high silica and potassium, and low iron contents of the rocks.

4.4.5 Link Lake and Sherman Gate horizons: Unit 4

These units are generally very poorly exposed, and as a result, the true thickness and compositional changes are not known to any great extent (see field map). In general the horizon is dominated by felsic volcanoclastic material of calc-alkaline magmatic affinity. Several areas contain pyrite clasts of variable size, although the horizons that host the clasts are not laterally continuous over any great distance. In some areas basalts adjacent to or within these felsic horizons, are silicified. The LLDZ has, for the most part, destroyed primary textural features.

4.5 Quartz Feldspar Porphyry: Unit 4f

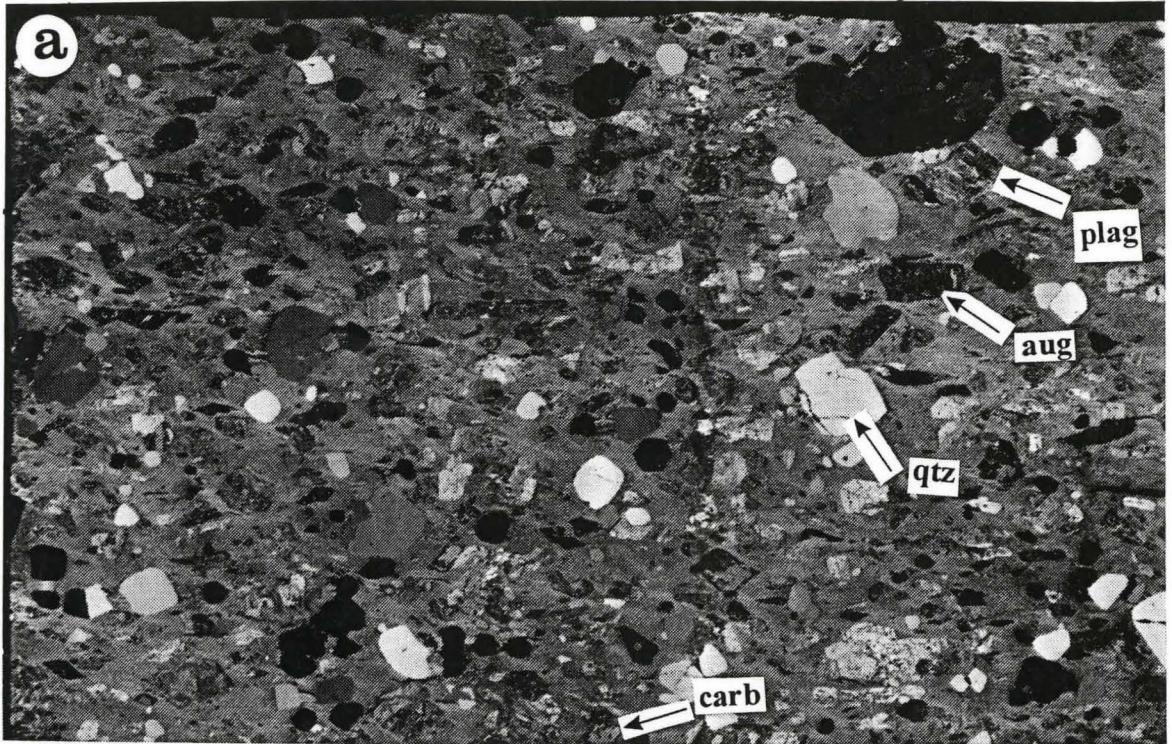
This unit was subdivided on the basis of chemistry, and as a result was found to have a calc-alkaline affinity. This rock type includes such horizons as the Milne and City Dump vents (Fyon and Crocket 1986) and several small dykes and sills. These rocks are dominated by quartz phenocrysts (10-40%) that are as large as 5mm in diameter, but average around 2-3 mm in diameter and often show resorption textures (Plate 4-12).

Plagioclase and potassic feldspar phenocrysts, present in abundances of up to 10%, have a maximum diameter of 3 mm. Maximum abundances of the feldspars are coincident

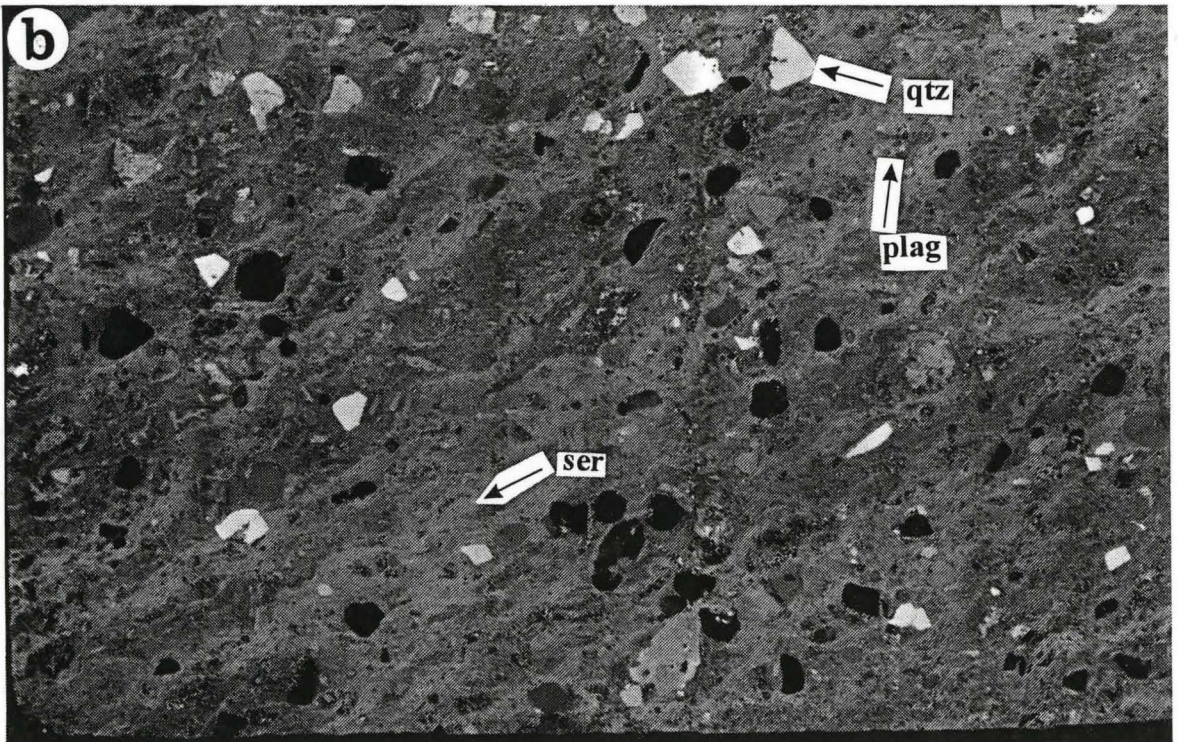
Plate 4-12: Photomicrographs of representative examples of the mineralogy and textures of the quartz feldspar porphyry.

a) This sample (sample 16) shows minor alteration of the minerals as compared to most of the QFP, and its chemistry was used as the least altered sample for the mass gain and losses calculations (Chapter 5). Identifiable minerals include quartz (qtz), chloritized augite (aug), plagioclase feldspar (plag) and carbonate (carb). Sericite (ser) alteration is relatively minor. Sample has been photographed in cross polarized light.

b) A more pervasive sericite alteration of the QFP (sample 13). Only quartz and remnants of plagioclase feldspar are identifiable as primary mineralogy. Sample has been photographed in cross polarized light.



1 cm



with maximum abundances of quartz phenocrysts. Most of the feldspar is corroded and altered to micaceous minerals. Some of the samples have 1-3% chloritized remnants of augite.

Other alteration minerals include sericite to a maximum of 50%, 5-10% disseminated chlorite with local concentrations of 25%, and 2-5% carbonate. As with the other samples, carbonate is the last mineral to have formed in the samples, and appears as a replacement mineral.

4.6 Alteration Mineralogy

This area of the Temagami greenstone belt is dominated by silicification, sericitization and carbonatization, with a relatively minor amount of chloritization. Silicification and sericitization, as indicated by the high modal abundances of quartz and mica, are pervasive throughout all of the felsic horizons. It was determined that matrix quartz can be present in abundances exceeding 60% (eg. samples 03, 13, 30, 33, 43, 46), while sericite can be present in excess of 20% (eg. samples 11, 23, 26, 27, 30, 43). Silicification of pillowed basalts is also evident within a 50 m radius of L24W BL0.

The pervasiveness and extensiveness of the silicification and sericitization suggests a large scale hydrothermal alteration event took place in the area. Since the alteration extends a significant distance away from the Link Lake deformation zone, this deformation event is likely not the source of the alteration. A more likely source is hydrothermal circulation associated with volcanic activity during the deposition of these units.

Chloritization throughout the felsic horizons is only extensive in the black rhyolite of the Garbage Dump area. As the chlorite alteration here is confined to the hyaloclastite, it likely formed during the deposition of the rhyolite lavas.

Carbonatization is extensive and present in all units regardless of their relative age. This indicates that the tectonic and/or hydrothermal event which produced the carbonatization occurred after the deposition of all of the units with the exclusion of the diabase dykes. Fyon *et al.* (1988) noted this intense alteration is associated with the various deformation zones which are in turn associated with late-forming gold mineralization. This suggests the hydrothermal event responsible for the introduction of the carbonate is not responsible for the sericite and silica alteration. More will be added on this subject in Chapter 7.

CHAPTER 5

GEOCHEMISTRY

5.1 Introduction

Many articles have been written with emphasis placed on the use of geochemical parameters as a tool for the determination of parentage, magmatic affinity and tectonic setting of packages of rocks ranging from intrusive and extrusive to sedimentary. The basic principle behind all of these methods is that the source (eg. a magma) of these rocks has a particular chemical signature which will be retained throughout its geologic history. By determining the 'parent' chemical signature we should then be able to determine the source of any rock type. However, as soon as there is any significant chemical alteration of the rocks, such as that produce by metasomatism and metamorphism, the 'parent' chemical signature can become sufficiently modified that it is not possible to determine with certainty the true parentage of the rocks.

What follows is a review of processes which can change the composition of rocks, and what methods are considered to best determine the parentage of a rock package which have sustained compositional changes subsequent to initial formation.

5.2 Alteration Processes and Their Effects on Whole Rock and Trace Element Geochemistry

In general, metasomatic processes are responsible for the change in chemistry of any rock. Whether the process was hydrothermal alteration associated with volcanism or fluid movements associated with tectonism, alteration of the surrounding rocks and ultimately the minerals thereof, requires a transfer of elements from one location to another. These processes ultimately require the presence of fluids whose physical (eg. temperature, volume, pressure) and chemical (eg. Eh, pH, composition) properties are in part responsible for the alteration assemblages. How easily one element can move from the fluid to the host rock or from the host rock to the fluid relative to another element, that is the mobility of an element, determines how much the chemistry will change within the rock.

5.2.1 Major element mobility

In general terms, the major elements tend to be readily affected by alteration processes. Condie (1976), summarizing the work of many authors, concluded that deep-sea alteration of mafic volcanic rocks can both enrich and deplete volcanic rocks of various elements. He found that as a result of seawater alteration, Fe and K are enriched in the rocks, while Si, Ca, Al and Mg tend to be depleted in the rocks. Thurston (1981) compared the work of several authors and concluded that during the formation of volcanogenic massive sulphide bodies, the host rocks tend to be enriched in Mg, Fe, Si, and K, and depleted in Na, Ca and rarely K. Clearly a variety of different alteration processes may cause major elements to become mobile, and at the same time, the relative enrichments and depletions of elements will also vary with the process.

5.2.2 Trace element mobility

Compared to the major elements, trace elements are generally considered to be immobile under conditions of slight to moderate degrees of alteration of various volcanic rocks (Cann 1970; Nicholls and Islam, 1971; Condie 1976). If during the alteration process it is assumed the rock volume does change, then Ti, Zr, Nb, and Y are considered to be immobile (MacLean and Kranidiotis 1987; Elliott-Meadows and Appleyard 1991). However, Osterberg *et al.* (1987) found Ti and Zr to be mobile and Finlow-Bates and Stumpfl (1981) found Y and Nb to be mobile under conditions of volume change.

From a study of the Phelps Dodge massive sulphide deposit, MacLean (1988) concluded that the light rare earth elements (LREE) will become mobile under conditions of extreme hydrothermal alteration associated with temperatures $>300^{\circ}\text{C}$. In this case, in the cooler areas away from the main alteration pipe, there is a net increase in the LREE as measured by La/Yb ratios with $\text{La}_{(n)}/\text{Yb}_{(n)}$ increasing from 1.9 to as much as 13 (Figure 5-1). The greatest effects are found in the quartz-chlorite alteration zone.

Campbell *et al.* (1984) and MacLean (1990) demonstrated that in the most intense area of alteration of a volcanogenic massive sulphide deposit, namely the alteration pipe, rare earth elements (REE) can become mobile. In this case LREE tend to become depleted in the alteration pipe (the hottest area), and enriched away from this zone (cooler areas) until normal background levels are reached. Barrett and MacLean (1994) indicate that even under conditions of extreme alteration below VMS deposits, REE, Hf, Ta and Th will remain immobile. In a study of the massive sulphide deposit at Que river, Tasmania, Whitford *et al.* (1988) determined that only Eu was mobile in the alteration area, which resulted in a larger than normal negative anomaly. He also notes that under normal fractional crystallization of a rhyolite, the same large anomalies can form.

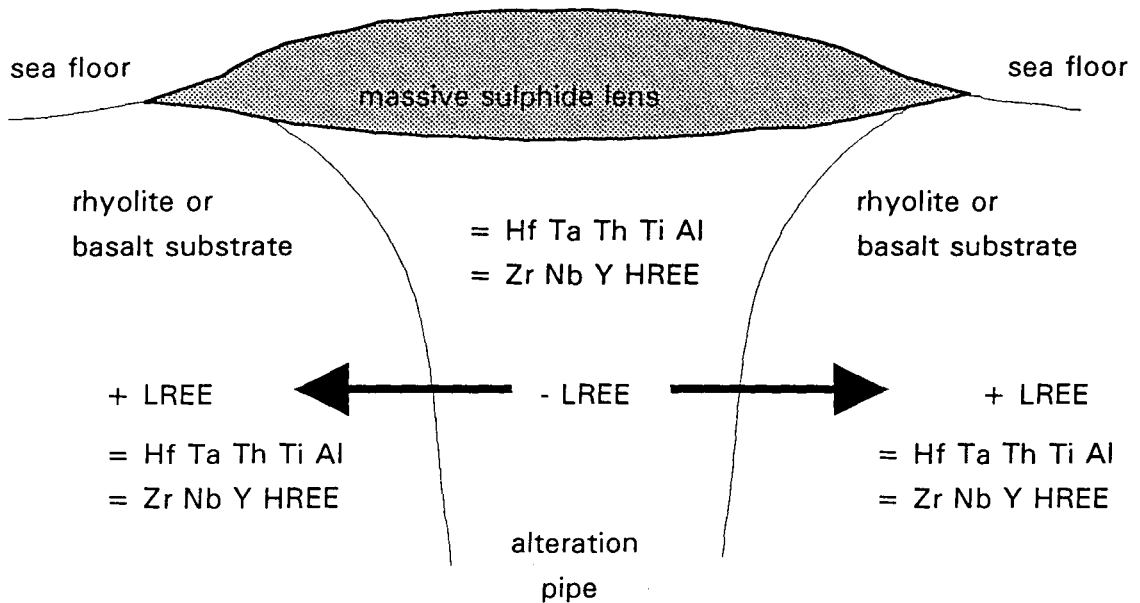


Figure 5-1: Diagram depicting the immobility of trace elements beneath a VMS deposit: + gains, - losses, = immobile. Arrows indicate movement of mobile elements away from the alteration pipe. Under conditions of extreme hydrothermal alteration the immobile elements can become mobile and migrate out of the alteration pipe.

Contrary to popular belief, Schandle *et al.* (1990), and Schandle and Gorton (1991) suggest that rare earth element mobilization does not occur during the deposition of VMS mineralization but rather some time after the hydrothermal system has died out. However, this mobility is still confined to the most intense zones of alteration.

Several other authors including Hellman *et al.* (1979), McLennan and Taylor (1979), Alderton *et al.* (1980), Dostal *et al.* (1980) and MacGeehan and MacLean (1980), have also demonstrated that under certain intense alteration conditions the REE and other trace elements can become mobile.

In summary, in areas of low to moderate grades of hydrothermal alteration Al, Zr, Ti, Y, Nb and the rare earth elements are considered to be immobile, and only in areas of extreme alteration do these elements become mobile. However, even in areas of low grades of alteration Si, Ca, Fe, Mg, K, and Na will become mobile. Whitford *et al.* (1989) and Barrett and MacLean (1994) suggest a test for immobility should be done on a homogenous rock body to determine which elements are immobile.

5.3 Test for the Mobility of the Elements

Barrett and MacLean (1994) indicate that elements that are immobile during alteration processes will retain their initial ratios (Al/Ti, Nb/Zr etc.). If there is a significant system size change (ie. large additions and/or subtractions of material) then for a group of samples the ratios of immobile elements will produce linear trends which will pass through both the precursor and the origin in a binary plot (ie positive correlation). If there has been no significant system size change, then the samples will plot as a cluster, but still show a high correlation for a line passing through the origin (Stanley and Madeisky 1994). For samples that show a fractionation trend, correlations produced by alteration will be poor as there will actually be more than one linear trend produced by the alteration of the samples (Figure 5-2).

In the thesis area the Upper and Lower Felsic horizon rhyolite units show a pervasive sericite alteration, with near equal modal proportions of this mineral. Also, many of the samples have been taken from clastic units which display some variability of clast types. Such is the case with sample 32 which has the highest Ti, and lowest Si contents and at least two identifiable clast types. The QFP's, while homogenous in bulk composition, are not correlateable over any distance, and may not be from one parent source.

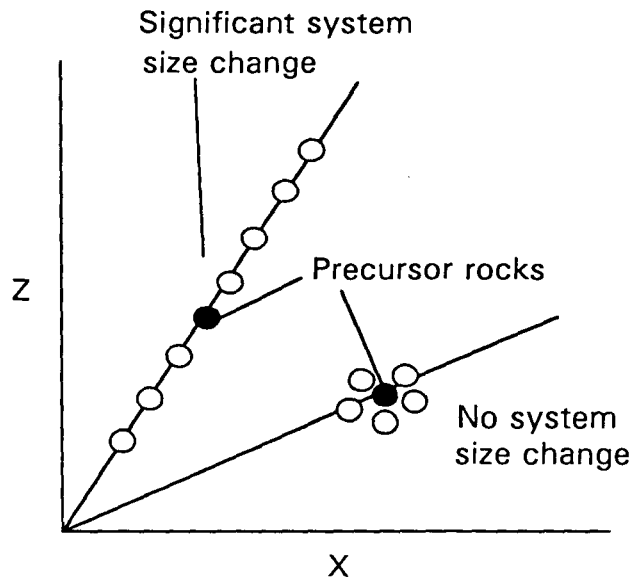


Figure 5-2: Diagram demonstrating the effects of alteration on the initial ratios of two immobile elements X and Y. If the rocks have not undergone a significant system size change then the samples plot as a cluster. If there is a significant system size change, then the samples will produce a linear trend.

Ratios of expected immobile and mobile elements divided by Lu, the least mobile REE (Maclean 1988), are presented in Table 5-1. This method of determining the relative mobility of elements has been used by Campbell *et al.* (1982a). Based on the assumption that these samples are all derived from a single parent, then major differences of the ratios represent element mobilization. In their example, they were able to trace a rock horizon from the outside to the inside of an alteration pipe, and suggested that if an element/La ratio changes significantly from the outside to the inside of the alteration pipe, then the element is considered to have been mobile. Their data indicates that outside of the alteration pipe the ratios could vary by a factor of two or more, but generally <2 , and inside the alteration pipe the ratios could vary by a factor >10 . They concluded that if the

ratios varied more inside the alteration pipe than outside, then the element was considered to have been mobile.

Since there are no areas which visually exhibit a greater degree of hydrothermal alteration (ie. no outcrop scale area with greater abundances of chlorite or sericite than for anywhere else) through which element ratio changes can be documented, the degree of ratio variability for the immobile elements is not known. By using the element/Lu ratio, and a cutoff ratio value of 2, any element whose ratio varies by a quotient factor >2 (where the quotient factor is equivalent to the maximum ratio value/minimum ratio value for the data set under consideration) is considered to be mobile. The greater the quotient factor, the more mobile the element is. Campbell *et al.* (1982a) have indicated that where individual volcanoclastic beds cannot be traced and sampled with confidence, then one can only expect to identify examples of very large element mobility.

The Temagami data (Table 5-1) indicates that most of the trace elements have remained relatively immobile. Generally Sr and Sc demonstrate the greatest degree of mobility, and Hf and Tb also exhibit some degree of mobility. Rb and Zr exhibit a small degree of mobility in the QFP, but are not mobile in the Upper and Lower Felsic horizons. Na exhibits the greatest degree of mobility with a factor >1000 in the QFP. Relative to Na, all of the other trace elements would be considered highly immobile.

Assuming Al_2O_3 remained immobile during alteration, Beswick and Soucie (1978) determined that volcanics from the Temagami greenstone belt indicate Na, K, Ca, Mg and Fe were mobilized to various extents throughout the belt. Their study implies that any classification of the rocks dependant on mobile elements is less likely to be accurate than classifications using immobile elements.

Table 5-1
Element/Lu ratios for selected horizons as an indication of element mobility

sample	Na ₂ O/Lu	Sr/Lu	Rb/Lu	Eu/Lu	Hf/Lu	Sc/Lu	Sm/Lu	Tb/Lu	Zr/Lu
quartz feldspar porphyry									
TS03	0.0	498	1643	5.3	37	18	32	2.8	1134
TS-12	28.9	958	698	7.8	48	51	29	1.9	2060
TS-13	41.5	3065	964	8.0	56	32	25	3.3	2388
TS-14	0.2	749	1070	6.9	46	47	27	2.6	2183
TS-15	24.3	674	908	8.0	47	51	30	3.2	2121
TS-16	52.7	1110	792	9.4	53	44	35	3.2	2303
TS-17	14.2	759	984	8.0	47	15	31	2.9	1969
TS102	13.2	1800	1012	8.7	46	16	38	3.4	1029
factor*	5.3E+06	6.2	2.4	1.8	1.5	3.5	1.5	1.8	2.3
Upper Felsic horizon									
TS-11	0.771	110	111	0.9	5.8	5.2	8.9	2.1	174
TS-26	0.409	86.8	117	0.8	6.3	7.0	9.7	2.1	183
TS-27	0.002	67.6	112	0.8	6.0	5.6	7.4	1.9	179
TS-30	0.001	46.2	145	0.7	6.6	5.9	7.8	1.9	183
TS-32	0.212	154	108	0.8	5.9	12	10	1.9	229
TS-36	0.001	42.6	131	0.7	6.5	4.1	9.5	1.9	204
TS-43	0.001	31.1	111	0.5	6.4	4.2	8.8	1.8	179
TS106	0.256	44.9	101	0.8	5.3	4.1	6.9	1.6	122
TS109	0.222	62.2	97.8	0.6	5.6	4.4	5.8	1.5	126
TS114	0.114	13.9	82.3	0.6	2.6	3.0	5.5	0.9	127
factor	567	11.0	1.8	1.8	2.6	3.9	1.9	2.5	1.9
Lower Felsic horizon									
TS-23	0.002	24	229	0.8	11	3.3	9.4	1.9	327
TS-46	0.002	33	223	1.0	11	3.1	12	1.9	328
TS100	0.002	37	197	1.1	8.9	2.8	10	1.8	245
TS101	0.002	1.0	275	1.0	12	3.3	9.2	1.6	271
TS110	1.475	32	185	0.8	8.5	2.6	7.4	1.6	216
TS113	0.683	43	181	1.1	7.4	4.0	9.1	1.6	202
TS116	0.360	82	256	1.4	11	3.2	11	1.8	282
TS119	0.035	10	237	1.1	11	3.5	9.1	1.4	285
factor	945.5	82.0	1.5	1.8	1.6	1.5	1.7	1.3	1.6

Notes: * factor is the maximum ratio value/ minimum ratio value

5.4 General Chemistry of the Major and Trace Elements

5.4.1 Upper and Lower Felsic horizons

While there are petrographical differences between the Upper and Lower Felsic horizons (Chapter 4), there is very little difference in the chemistry of the two horizons. Average compositional differences of major and minor elements (Table 5-2) for these two horizons indicate that most differences in the chemistry can be explained as either experimental error (see Appendix C), or heterogeneity of the samples .

In general, with the exception of sample 32, these two horizons are marked by high Si contents (>78%), high Al (>10%) and moderate K (>2%) . The relative increase in Sr, Mg and Ca in the Upper Felsic horizon is coincident with higher loss on ignition (LOI) values and with the greater abundances of carbonates in these samples as compared to the Lower Felsic horizon. The increases in carbonate associated elements (Ca, Mg, Sr) in the Upper Felsic horizon, offsets the apparent depletions in the other major elements (K, P, Na) in this horizon. This indicates the two felsic horizons are chemically the same with respect to the major elements. The relative increase in Rb in the Lower Felsic horizon is coincident with the higher K values, reflecting a higher content of sericite.

5.4.2 Quartz feldspar porphyry

In comparison to the Upper and Lower Felsic horizons, the quartz feldspar porphyries (QFP) have the lowest average abundance of Si despite their abundant quartz phenocrysts. Their higher Al and Na contents reflect higher abundance of sodic feldspars relative to the Upper and Lower Felsic horizons. Fe content tends to be the highest in the QFP and reflects the higher chlorite content in the rock.

Table 5-2
Average compositions of the major felsic horizons

		Upper Felsic Horizon	Lower Felsic Horizon	QFP
	sample	average	average	average
%	SiO ₂	78.02	79.41	72.30
%	TiO ₂	0.07	0.04	0.20
%	Al ₂ O ₃	11.53	11.24	14.23
%	Fe ₂ O ₃	1.33	1.37	2.35
%	MnO	0.05	0.03	0.03
%	MgO	0.83	0.67	0.84
%	CaO	1.37	0.85	1.88
%	K ₂ O	2.89	3.35	2.69
%	P ₂ O ₅	0.01	0.02	0.05
%	Na ₂ O	0.15	0.22	1.67
%	LOI	3.38	2.22	2.93
ppm	Nb	14	18	9
ppm	Zr	117	154	153
ppm	Y	47	35	5
ppm	Sr	40	19	89
ppm	Rb	80	127	79
ppm	Ba	412	275	497
ppm	Pb	15	9	5.71
ppm	Zn	21	23	34
ppm	Cu	16	12	35
ppm	Ni	11	13	12
ppm	Co	6	5	5
ppm	Cr	6	9	13
ppm	V	4	4	12
ppm	As	6.2	2.7	1.2
ppm	Au	0.60	1.20	1.26
ppm	B	39.6	64.0	28.8
ppm	Ce	36	49	35
ppm	Cs	1.8	3.8	3.0
ppm	Eu	0.52	0.60	0.61
ppm	Hf	4.0	5.7	3.7
ppm	La	15.8	18.6	18.8
ppm	Lu	0.72	0.58	0.08
ppm	Sb	2.30	1.02	1.20
ppm	Sc	3.5	1.9	2.8
ppm	Sm	5.6	5.6	2.4
ppm	Ta	1.7	1.4	0.6
ppm	Tb	1.2	0.99	0.23
ppm	Th	12	11	4
ppm	U	3.8	2.8	1.1
ppm	Yb	5.0	4.0	0.6

5.5 Classification Schemes

5.5.1 Rock type

Several classification schemes have been developed in an attempt to use the chemistry of the rocks to help identify their original (pre-alteration) rock types, such as basalts or rhyolites. Three such classifications considered are those of Jensen (1976), Winchester and Floyd (1977) and Middlemost (1985). A comparison of these three classification schemes indicates the Upper and Lower Felsic horizons and the QFP's are rhyolites to dacites (Figure 5-3) and comendite-pantellerite to trachytes (Figure 5-3d). In comparison to the mineralogy, these classification schemes seem appropriate, indicating the Upper and Lower Felsic horizon samples are rhyolites.

5.5.2 Magmatic affinity

The work of Hurley (1985), Fyon and Crocket (1986) and Fyon and Cole (1989) make reference to the presence of mafic tholeiitic volcanic rocks in the Temagami greenstone belt, yet they do not make reference to the presence of any felsic tholeiitic volcanic rocks. It would seem atypical of an Archean greenstone belt to not have some felsic tholeiites, and so the question 'Where are the felsic tholeiites' arises. In light of this question the geochemical data will be used to determine the magmatic affinities of the felsic horizons in the study area.

Geochemical classification schemes have been devised to determine the magmatic affinity of bodies of rocks. Such schemes include those devised by Irvine and Baragar (1971), Miyashiro (1974), Jensen (1976), and Barrett and MacLean (1994). Figure 5-3b, and 5-4 a, b are more common schemes used to identify and differentiate calc-alkaline and

LEGEND FOR FIGURES 5-3, 5-4, 5-5, 5-9, 5-10

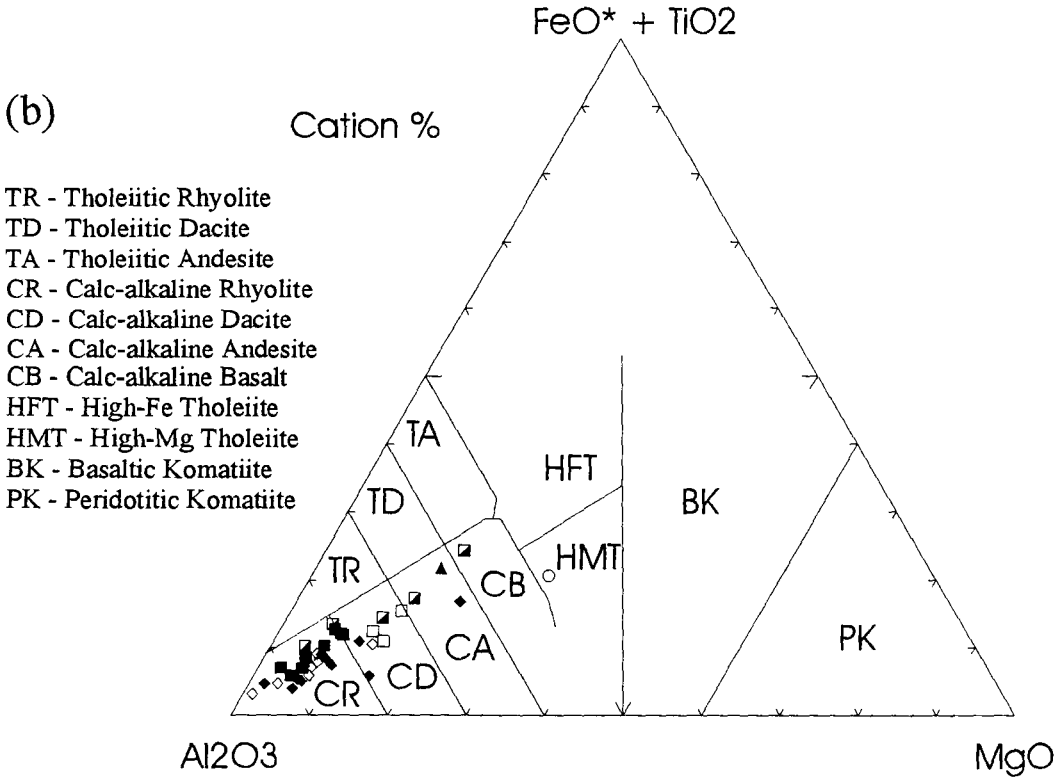
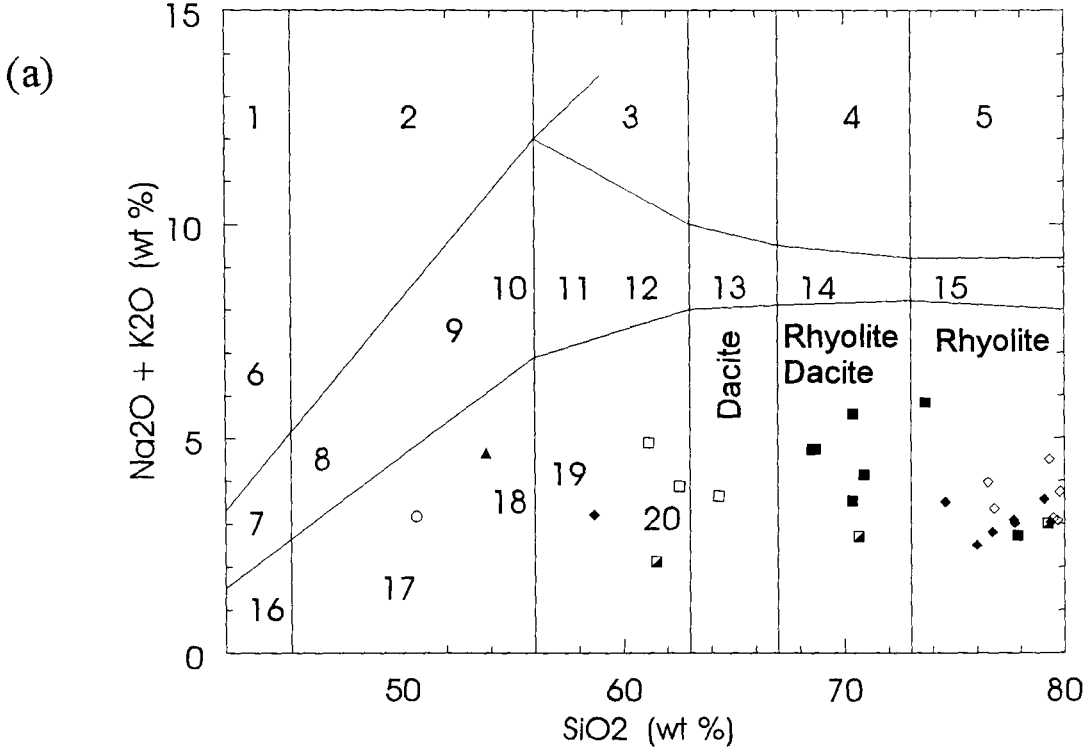
UPPER FELSIC HORIZON	LOWER FELSIC HORIZON	QUARTZ FELDSPAR PORPHYRY
◆ TS-11	◇ TS-23	■ TS-03
◆ TS-26	◇ TS-46	■ TS-12
◆ TS-27	◇ TS100	■ TS-13
◆ TS-30	◇ TS101	■ TS-14
◆ TS-32	◇ TS110	■ TS-15
◆ TS-36	◇ TS113	■ TS-16
◆ TS-43	◇ TS116	■ TS-17
◆ TS106	◇ TS119	■ TS102
◆ TS109		
◆ TS114		
 BASALT	 SOUTH TEMAGAMI	 LINK LAKE AND SHERMAN GATE HORIZONS
▲ TS-02	□ TS-41	▣ TS-45
 SILL	□ TS103	▣ TS108
○ TS-05	□ TS105	▣ TS117
		▣ TS120
		▣ TS121

Figure 5-3a: $\text{Na}_2\text{O} + \text{K}_2\text{O}$ vs SiO_2 rock classification scheme of Middlemost (1985, figure 3.3.3). Both the Upper and Lower Felsic horizons plot as rhyolites (except 32) and the quartz feldspar porphyries plot as dacites to rhyolites.

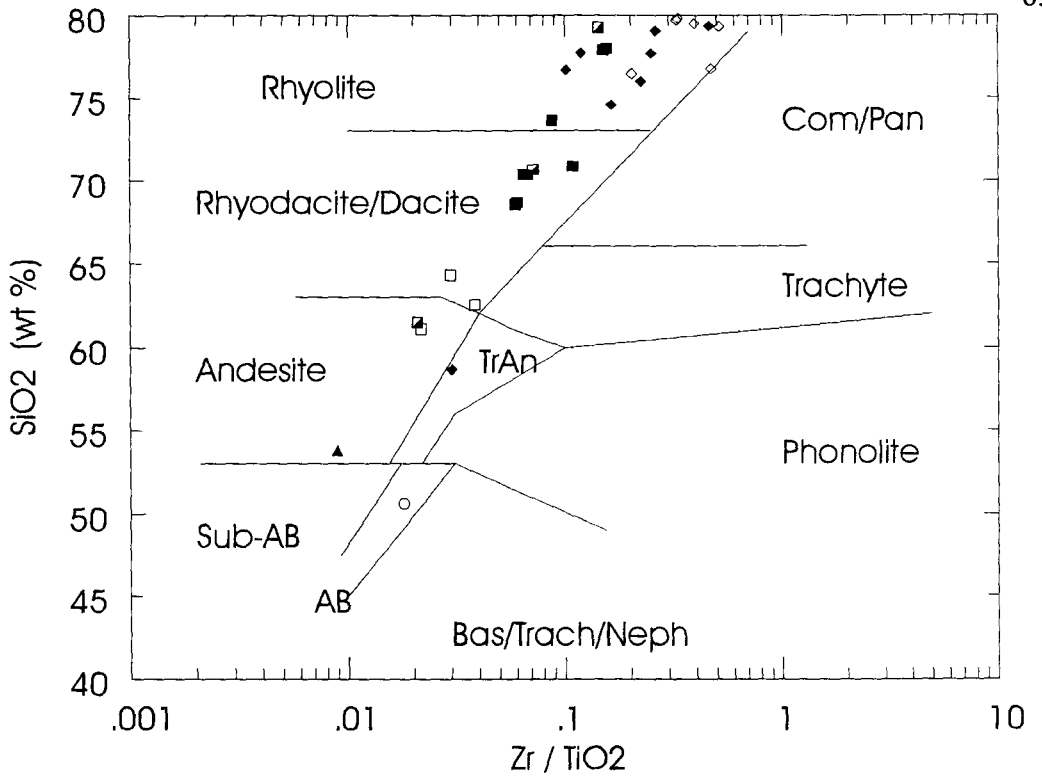
Figure 5-3b: Jensen cation plot of all of the samples indicates all of the samples are calc-alkaline. The Upper and Lower Felsic horizons and quartz feldspar porphyries plot as dacites to rhyolites. After Jensen (1976, figure 1).

Figure 5-3c: SiO_2 vs Zr/TiO_2 rock classification scheme of Winchester and Floyd (1977, figure 2). The Upper and Lower Felsic horizons and quartz feldspar porphyries plot as dacites to rhyolites.

Figure 5-3d: Zr/TiO_2 vs Nb/Y rock classification scheme of Winchester and Floyd (1977, figure 6). The Upper and Lower Felsic horizons dominantly plot as rhyolites, but the quartz feldspar porphyries are now classified as trachyandesites and trachytes.



(c)



(d)

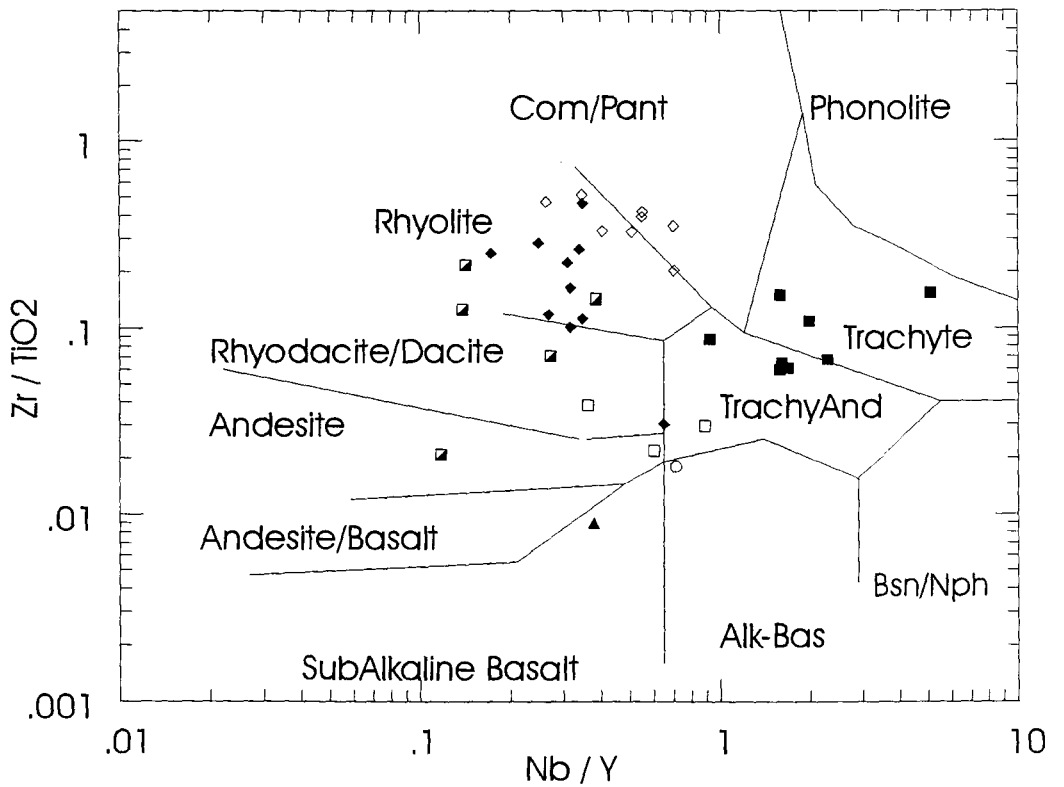
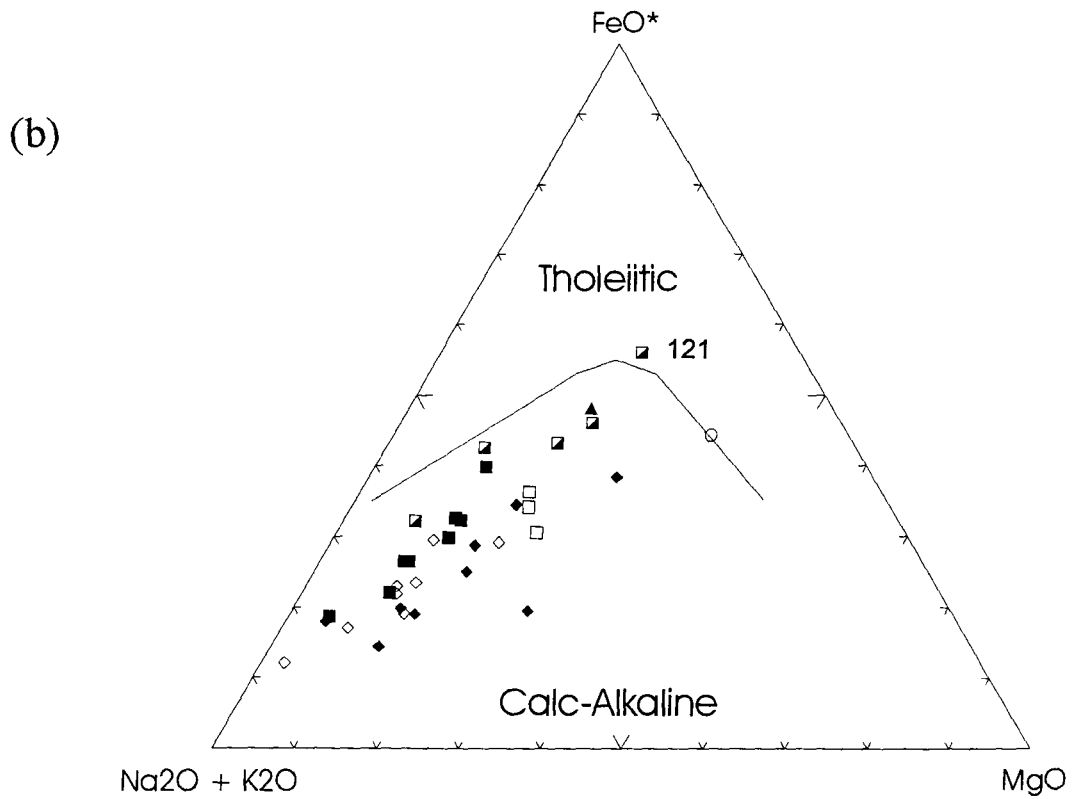
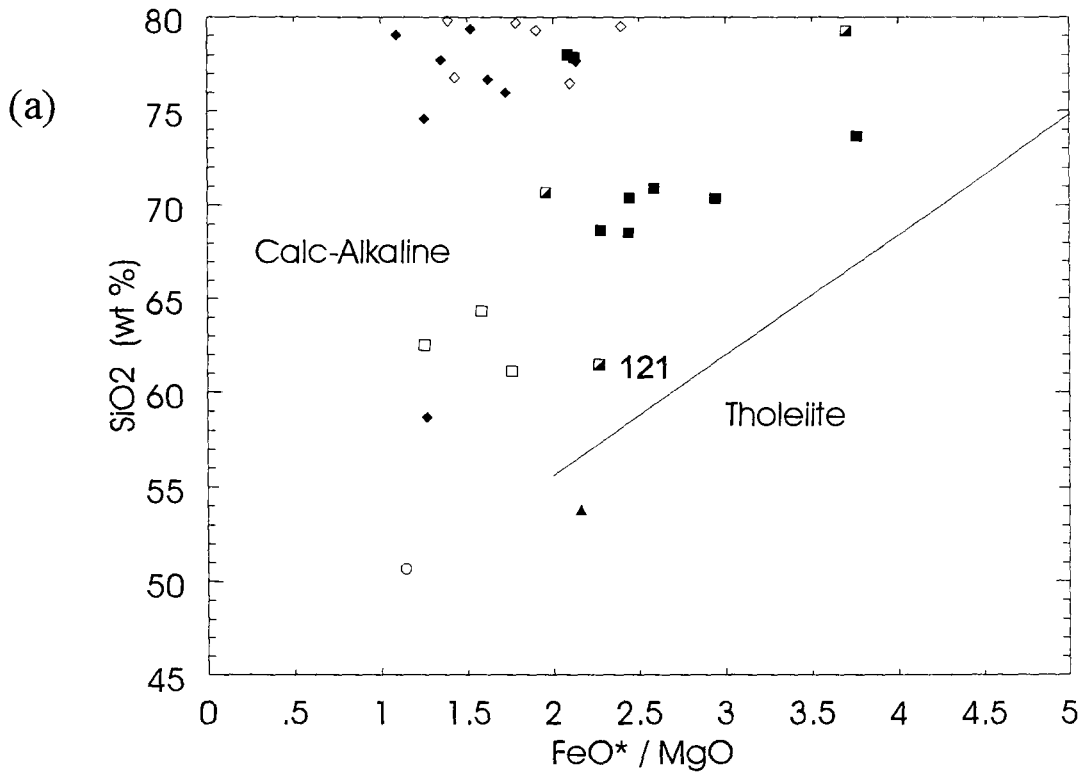


Figure 5-4a: Magmatic affinity classification of Miyashiro (1974, figure 1a). All felsic samples plot as calc-alkaline.

Figure 5-4b: $(\text{Na}_2\text{O} + \text{K}_2\text{O}) - \text{FeO} - \text{MgO}$ magmatic affinity classification of Irvine and Baragar (1971, figure 2) Except for sample 121, all felsic samples plot as calc-alkaline.



tholeiitic trends. These examples clearly indicate that on the basis of major element analyses, the felsic rocks are calc-alkaline.

Clearly, the lack of any mafic mineralogy will influence the position of the samples on the various plots. The various felsic horizons are dominated by a felsic mineralogy, and thus control the position of the samples on these binary and ternary plots. If the samples have been altered such that they are depleted in Fe, Mg, Mn, then in all cases the samples will be improperly identified as calc-alkaline, when in fact they could be tholeiitic. Such was the case documented by MacGeehan and MacLean (1980), in which iron-rich basalts and tholeiites were converted to rocks of apparent calc-alkaline affinity. In other cases the alteration has been so great that samples originally identified as rhyolites were in fact andesites (Gibson *et al.* 1983).

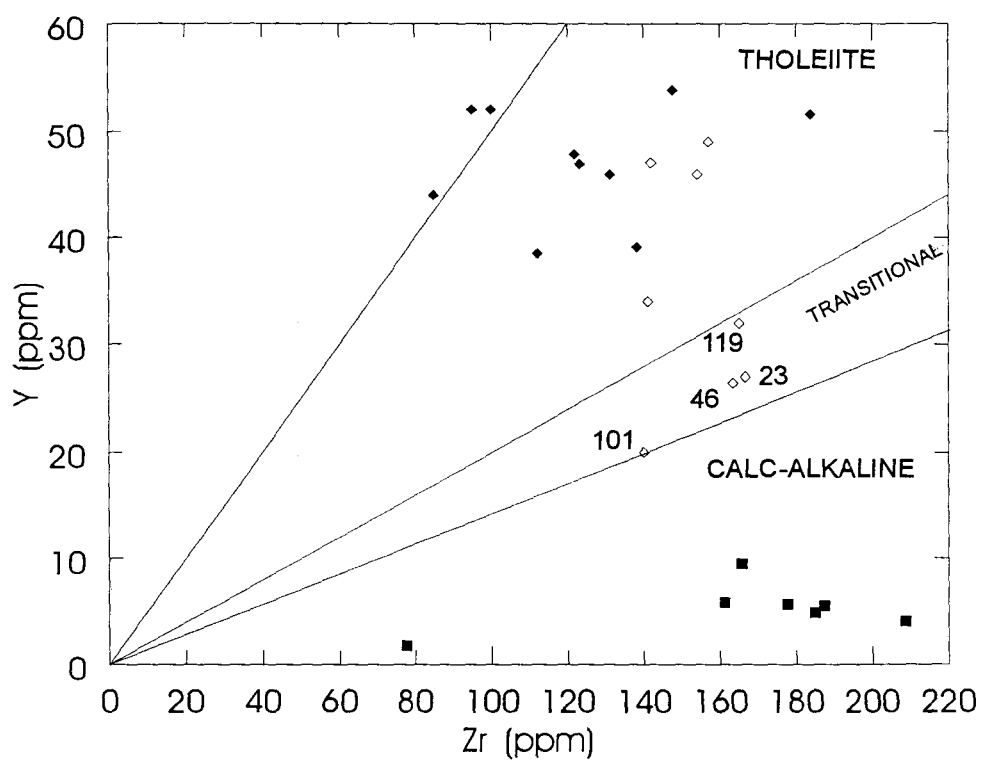
To check if this is the case for the Temagami rocks, immobile elements, in particular Y and Zr, as described by MacLean and Barrett (1993) have been used to determine magmatic affinity of the samples (Figure 5-5a, b). These plots indicate that both the Upper and Lower Felsic horizons are tholeiitic, with samples 101, 23, and 46 showing a transitional affinity, and the quartz feldspar porphyries are all calc-alkaline in origin (Figure 5-5a).

It is interesting to note that sample 2, mapped as tholeiitic basalt by Fyon and Crocket (1986) and classified as calc-alkaline on the plot of Irvine and Baragar (1971) (Figure 5-4b), is classified as a tholeiite in Figure 5-5b and Figure 5-4a. With the exception of samples 108 and 117, the Link Lake, Sherman Gate, Sill and South Temagami samples are calc-alkaline. It is only in the Y vs Zr plots of MacLean and Barrett (1993) that sample 108 has a tholeiite affinity. Thus depending on which classification method is used different magmatic affinities for the rocks can be correctly or improperly identified.

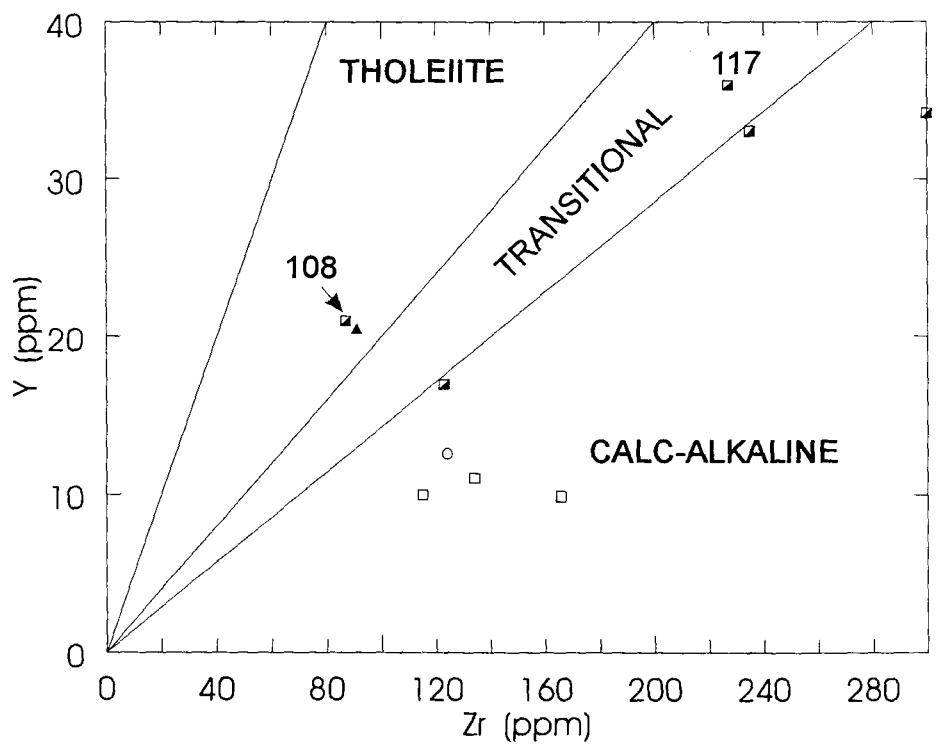
Figure 5-5a: Y vs Zr plot for magmatic affinity. The Upper and Lower Felsic horizons plot as a transitional to tholeiitic affinity, and the quartz feldspar porphyries plot as calc-alkaline. After MacLean and Barrett (1993).

Figure 5-5b: Y vs Zr plot for magmatic affinity for all of the other samples. The Link Lake and Sherman Gate samples, with the exception of 108, plot as transitional to calc-alkaline. All of the South Temagami samples and the Sill plot as calc-alkaline. After MacLean and Barrett (1993).

(a)



(b)



5.6 Rare Earth Element Chemistry

All samples were analysed for the rare earth elements, and these data are presented in Appendix B. Chondrite normalizing values used in this study are the recommended chondrite values of Boynton (1984). Chondrite values are as follows: La 0.31, Ce 0.808, Sm 0.195, Eu 0.0735, Tb 0.0474, Yb 0.209, Lu 0.0322. Eu anomalies were calculated by linear interpolation between chondrite-normalized Sm and Tb.

As with the major and trace element geochemistry, the rare earth element plots indicate the Upper and Lower Felsic horizons and the QFP's are distinctly different (see Figures 5-6 and 5-8), and will therefore be discussed separately.

5.6.1 Upper and Lower Felsic horizons

The Upper and Lower Felsic horizons have a flat REE pattern with a well defined negative Eu anomaly (Figure 5-6). LREE are enriched between 30 to 70 times chondritic values, and the heavy rare earth elements (HREE) are enriched from 10 to 25 times chondritic values. The $(La/Yb)_n$ values range from 1 to 3 with the exception of sample 113 which has a ratio of 6 (Table 5-3). Eu values range from 5 to 10 times chondritic values, and Eu/Eu^* values range from 0.16 to 0.42 defining strong negative anomalies.

While there are no large differences in REE concentrations or proportions between the Upper and Lower Felsic horizon, the Upper Felsic horizon is slightly more enriched in the HREE (Figure 5-7a), and also has a greater range in LREE values. Similar trends have been recognized by MacLean (1988) at the Phelps Dodge massive sulphide deposit. These variations suggest the LREE have been slightly mobilized in the Upper Felsic horizon.

Figure 5-6: Chondrite normalized REE patterns (rock/chondrite vs REE) for (a) Upper Felsic horizon; (b) Lower Felsic horizon. Chondrite normalizing values are those of the recommended chondrite, Boynton (1984).

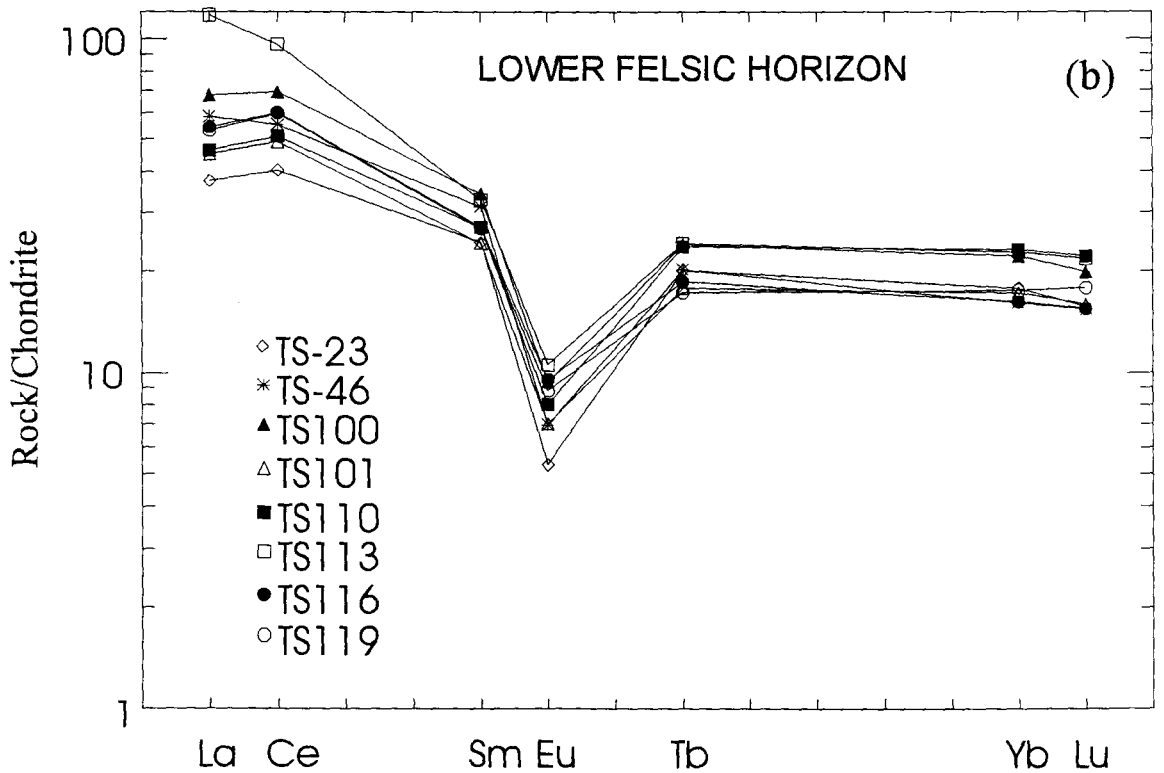
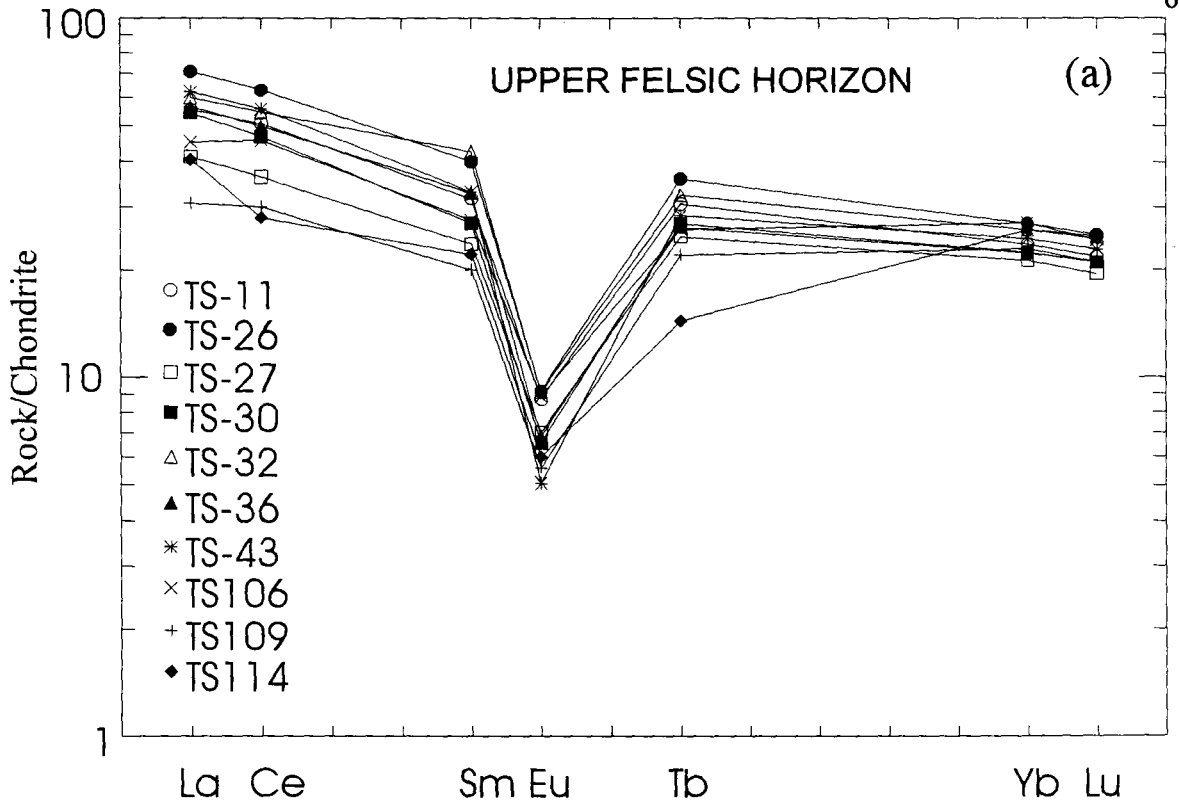


Figure 5-7a: Comparison of REE patterns for the Upper and Lower Felsic horizons indicate the similarity of the patterns. The Upper Felsic horizon **has a greater** range of LREE enrichment, and a greater enrichment of HREE compared to the Lower Felsic horizon. The Eu anomaly is nearly identical in both cases.

Figure 5-7b: Combined chondrite normalized REE patterns for the felsic horizons and the quartz feldspar porphyries. The distinct depletion of HREE and lack of an Eu anomaly for the quartz feldspar porphyries indicates different degrees of fractionation for the two rock types.

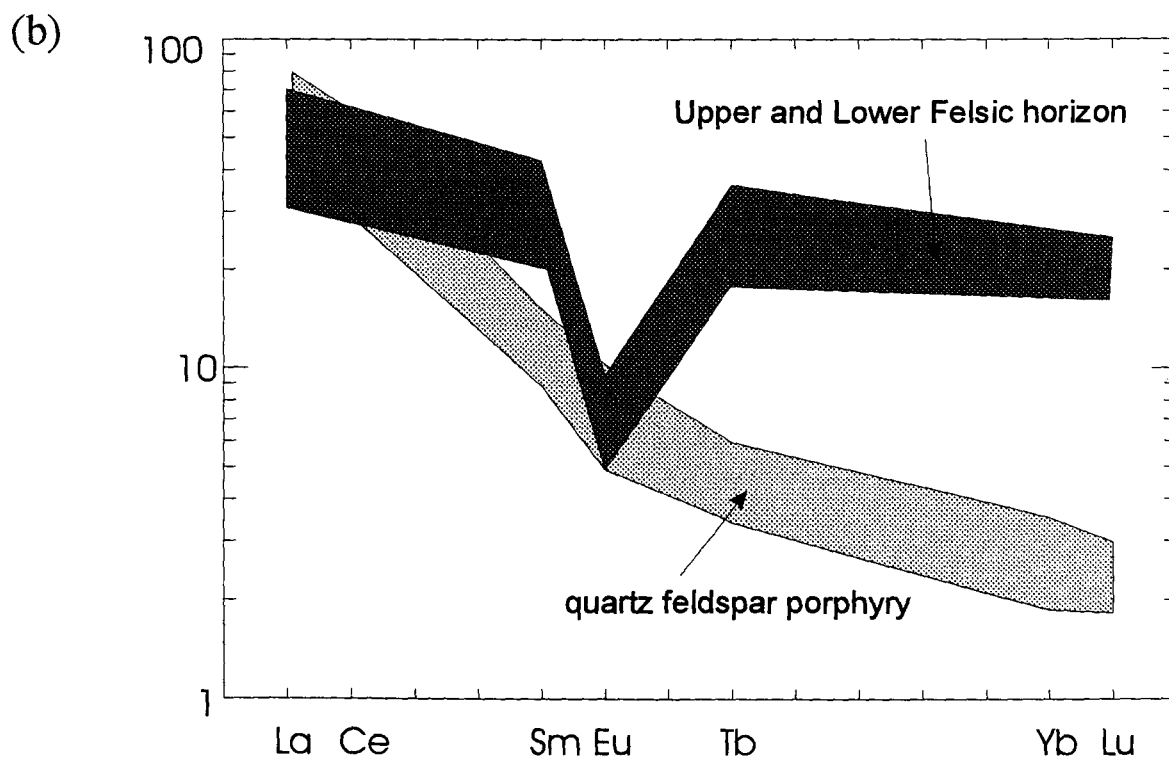
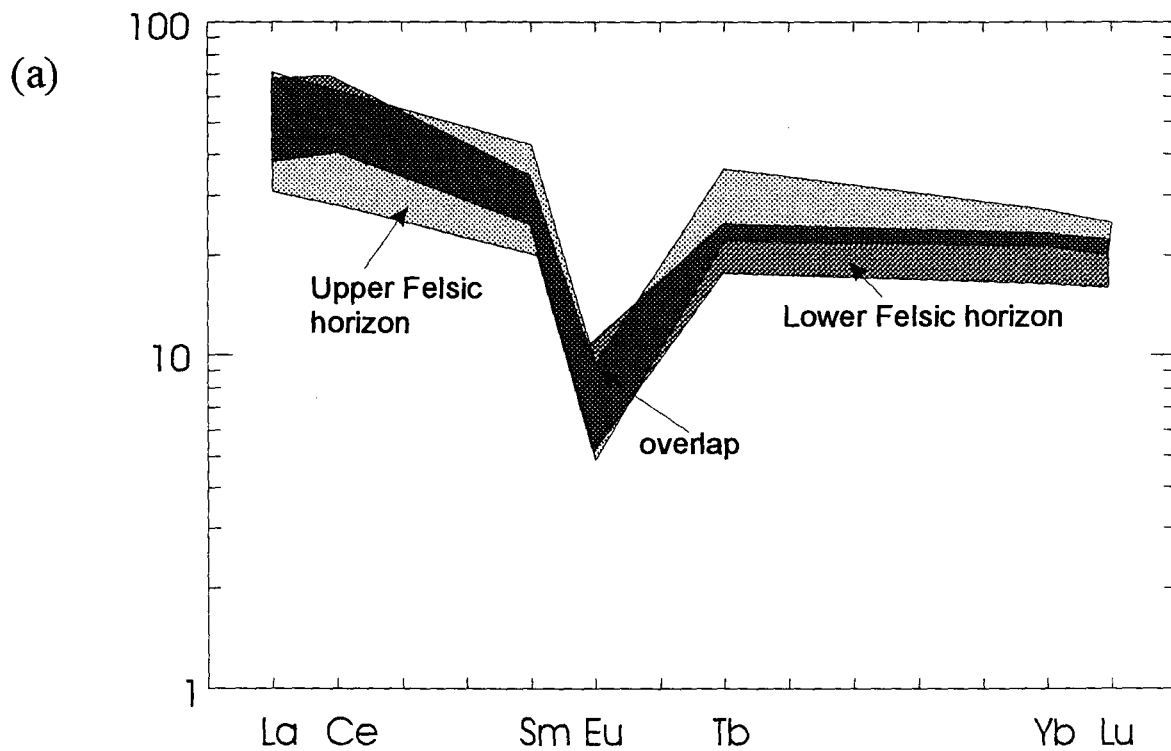


Table 5-3

Rhyolite classification with recommended chondrite values (after Lesher et al. 1986)

sample	TiO ₂ wt %	Zr PPM	Y PPM	Zr/Y	Sr PPM	Sc ppm	La(n)/Yb(n)	Eu/Eu*	Horizon
TS-03	0.05	78	2	44	34	1.3	24	0.65	Milne vent
TS-12	0.3	178	6	31	53	4.4	19	1.12	Milne vent ?
TS-16	0.25	161	6	28	78	3.1	27	1.04	Milne vent
TS-17	0.17	185	5	38	71	1.4	26	0.98	Milne vent
TS102	0.04	60	5	12	105	0.9	29	0.89	Milne vent?
TS-13	0.19	166	10	17	213	2.2	20	1.11	City Dump
TS-14	0.31	209	4	51	72	4.6	16	0.98	City Dump
TS-15	0.31	187	6	34	69	4.5	17	0.99	City Dump
TS-23	0.04	166	27	6	12	1.7	2	0.24	Lower Felsic
TS-46	0.05	163	26	6	16	1.6	4	0.27	Lower Felsic
TS100	0.04	157	49	3	24	1.6	3	0.32	Lower Felsic
TS101	0.04	140	20	7	< 2	1.8	2	0.33	Lower Felsic
TS110	0.03	154	46	3	23	1.9	2	0.32	Lower Felsic
TS113	0.07	142	47	3	30	2.7	6	0.37	Lower Felsic
TS116	0.03	141	34	4	41	1.6	3	0.42	Lower Felsic
TS119	0.05	165	32	5	6	2.0	3	0.40	Lower Felsic
FI	0.15 to 0.65	90 to 275	3 to 30	9 to 31	100 to 620	1.5 to 21	6 to 34	0.87 to 2.0	
FII	0.15 to 0.65	95 to 430	7 to 55	6 to 11	45 to 265	4.5 to 25	2 to 6	0.35 to 1.4	
FIIIA	0.2 to 1.0	170 to 370	25 to 70	4 to 7	5 to 100	7 to 20	1 to 4	0.37 to 0.94	
FIIB	0.1 to 0.75	190 to 730	70 to 240	2 to 6	7 to 210	1.5 to 10	1 to 4	0.20 to 0.61	

Table 5-3
continued

Sample	TiO ₂ wt%	Zr ppm	Y ppm	Zr/Y	Sr ppm	Sc ppm	La(n)/Yb(n)	Eu/Eu*	Horizon
TS-11	0.12	122	48	3	77	3.7	2	0.28	Upper Felsic
TS-26	0.09	148	54	3	70	5.7	3	0.24	Upper Felsic
TS-27	0.05	112	38	3	42	3.5	2	0.29	Upper Felsic
TS-30	0.11	123	47	3	31	4.0	2	0.24	Upper Felsic
TS-32	0.61	184	52	4	124	9.3	2	0.24	Upper Felsic
TS-36	0.03	138	39	4	29	2.8	3	0.23	Upper Felsic
TS-43	0.05	131	46	3	23	3.1	3	0.15	Upper Felsic
TS106	0.08	95	52	2	35	3.3	1	0.33	Upper Felsic
TS109	0.03	85	44	2	42	3.1	1	0.27	Upper Felsic
TS114	0.04	100	52	2	11	3.3	1	0.33	Upper Felsic
TS108	0.04	87	21	4	23	2.1	5	0.53	Link Lake
TS117	0.18	227	36	6	72	5.0	5	1.02	Link Lake
TS120	0.33	238	33	7	48	7.4	7	0.90	Link Lake
TS121	0.59	123	17	7	70	12.2	11	1.17	Link Lake
TS-45	0.21	300	34	9	70	5.8	6	0.57	Sherman Gate
TS-41	0.56	166	10	17	213	9.3	17	1.09	south Temagami
TS103	0.35	134	11	12	260	5.1	24	1.50	south Temagami
TS105	0.63	116	10	12	178	9.1	9	1.36	south Temagami
FI	0.15 to 0.65	90 to 275	3 to 30	9 to 31	100 to 620	1.5 to 21	6 to 34	0.87 to 2.0	
FII	0.15 to 0.65	95 to 430	7 to 65	6 to 11	45 to 265	4.5 to 25	2 to 6	0.35 to 1.4	
FIIIA	0.2 to 1.0	170 to 370	25 to 70	4 to 7	5 to 100	7 to 20	1 to 4	0.37 to 0.94	
FIIB	0.1 to 0.75	190 to 730	70 to 240	2 to 6	7 to 210	1.5 to 19	1 to 4	0.20 to 0.61	

5.6.2 Quartz feldspar porphyry

The QFP's have very steep REE patterns defined by a La enrichment of up to 90 times chondrite, and no Eu anomalies (Figure 5-8a). The $(La/Yb)_n$ ratios are much larger than those of the felsic horizons, and vary from 16 to 29 (Table 5-3). Like the felsic horizons, Eu values range between 5 and 10 times chondritic values, but Eu/Eu^* values range between 0.65 to 1.12 indicating there are no significant Eu anomalies. Thus there are significant differences between the REE chemistry of the felsic horizons and QFP (Figure 5-7b) indicating they have different origins.

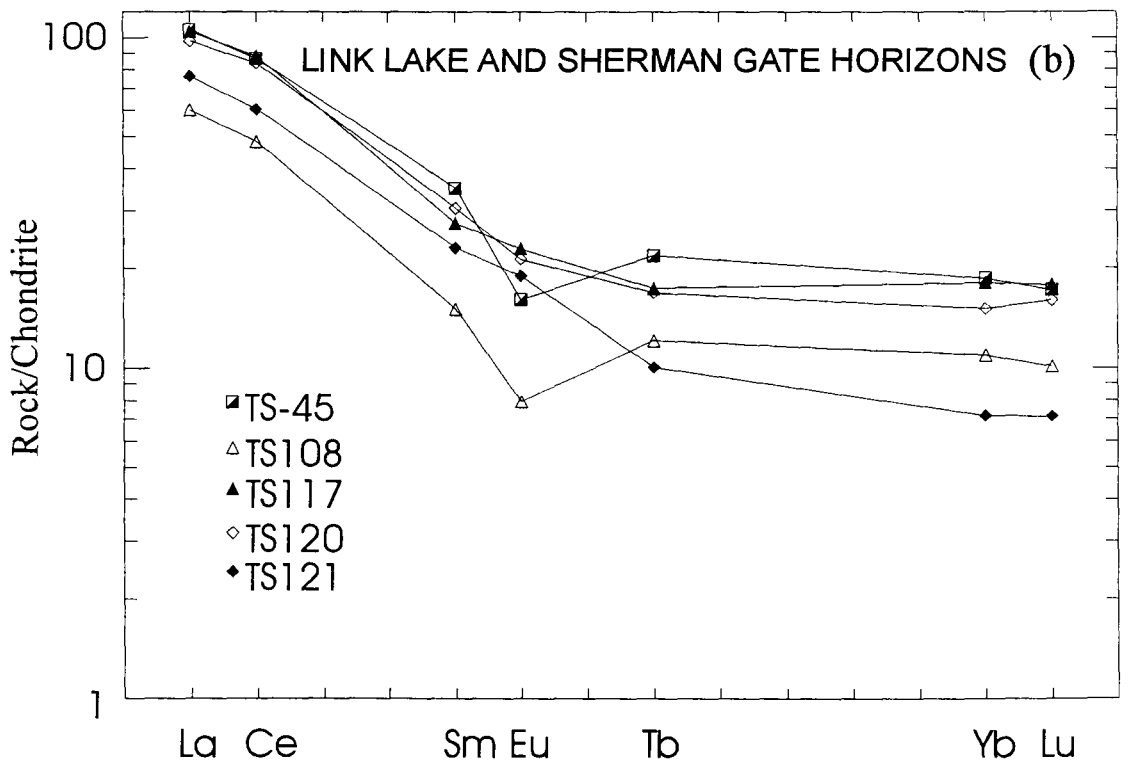
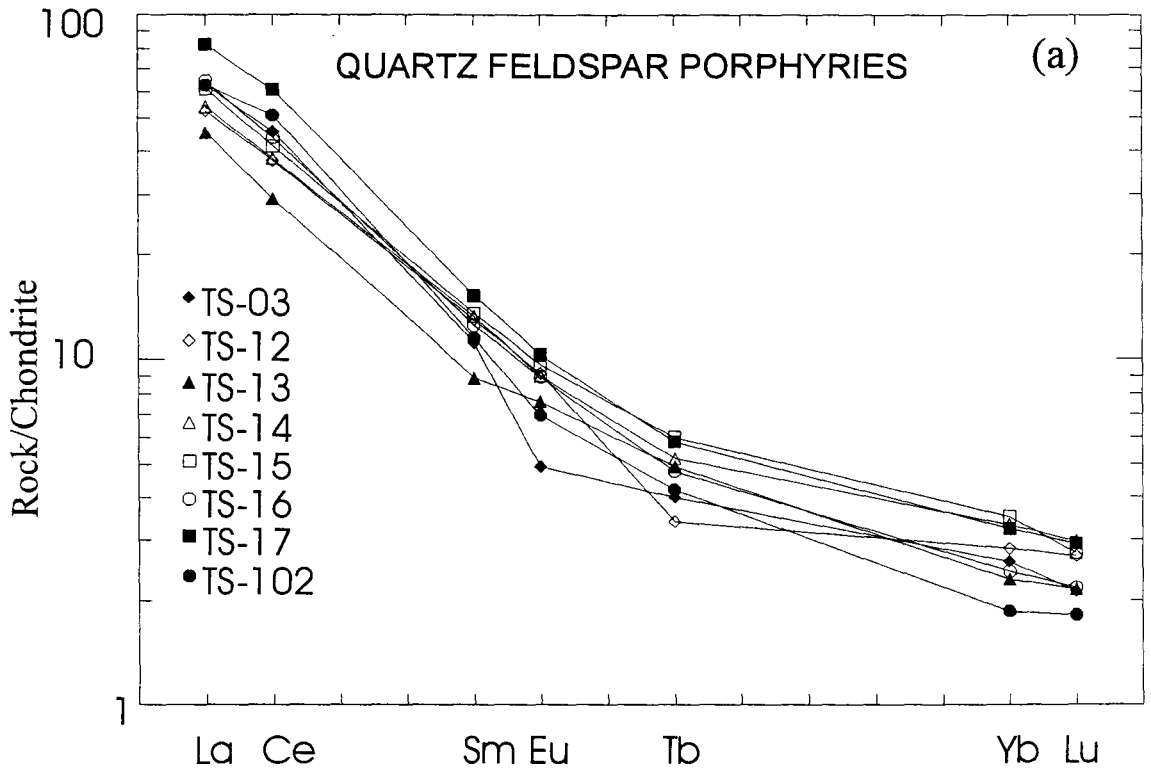
5.6.3 Link Lake and Sherman Gate horizons

As mentioned earlier, the Link Lake and Sherman Gate horizons consist of poorly exposed felsic to intermediate volcanoclastics of calc-alkaline magmatic affinity. The REE patterns for these horizons are moderately flat with very weak Eu anomalies (Figure 5-8b). The $(La/Yb)_n$ ratios are slightly greater than for the Upper and Lower Felsic horizons, ranging from 5 to 7, and Eu/Eu^* range from 0.57 to 1.17 (Table 5-3). These Eu anomalies are much smaller than those of the Upper and Lower Felsic horizons.

5.7 Rare Earth Element Classifications

It has been established that major elements are often mobile during metasomatic events, and classifications using major elements alone are often problematic. It was demonstrated that the immobile trace elements Zr and Y, classified the Upper and Lower Felsic horizons as tholeiitic to transitional, and the QFP, Link Lake and Sherman Gate horizons as transitional to calc-alkaline. In contrast, based on major elements alone (eg. Jensen cation plot Figure 5-3b) all of the felsic units are classified as calc-alkaline. Classifications using rare earth elements are also available to help identify magmatic

Figure 5-8: Chondrite normalized REE patterns for (a) quartz feldspar porphyries; (b) Link Lake and Sherman Gate horizons.



affinity of felsic rocks. The classification of Leshner *et al.* (1986) based on the work of Condie (1976, 1981) has been used extensively to define the origins of Archean felsic volcanics.

Leshner *et al.* (1986) and Condie (1976, 1981) recognized three major groups of Archean felsic metavolcanic rocks based on trace element geochemistry which they termed FI, FII, and FIII. The chondritic normalizing values used by Leshner *et al.* (1986) are that of the Leedy chondrite/1.2 which is nearly identical to those values of the recommended chondrite (Boynnton 1984). The following is a summary of the characteristics of these felsic rock types from Leshner *et al.* (1986) (see also Table 5-3).

FI felsic metavolcanic rocks are dacites and rhyodacites characterized by steep chondrite - normalized REE distribution patterns, with weakly negative to moderately positive Eu anomalies, high Zr/Y ratios, low abundances of high field strength (HFS) elements, and high abundances of Sr.

FII felsic metavolcanic rocks are rhyodacites and rhyolites characterized by gently sloping REE patterns, with variable Eu anomalies, moderate Zr/Y ratios, and intermediate abundances of HFS elements and Sr.

FIII felsic metavolcanic rocks are rhyolites and high silica rhyolites characterized by relatively flat REE patterns. This type of felsic rock has been subdivided into two subcategories. The FIIIa type exhibits moderately negative Eu anomalies, low Zr/Y ratios, high abundances of Sc, and intermediate abundances of HFS elements. The FIIIb type exhibits pronounced negative Eu anomalies, low Zr/Y ratios, high abundances of HFS elements, and low abundances of Sc and Sr.

Types FI and FII are comparable to calc-alkaline volcanics (Condie, 1981) and FIII are comparable to tholeiites (Leshner 1986).

A summary of the trace element characteristics of these felsic volcanic types, along with a comparison to the Temagami data are given in Table 5-3. The parameters defined by Lesher *et al.* (1986) do overlap from one category to the next, so that several parameters need to be considered to put the rocks into a specific category.

5.7.1 Upper and Lower Felsic horizons

These rocks with their the flat REE profiles, large negative Eu anomalies, low Zr/Y ratios and low Sc values are classified as FIII rhyolites. However, their Sr, Zr and Ti values dominantly fall within the range of FI and FII types.

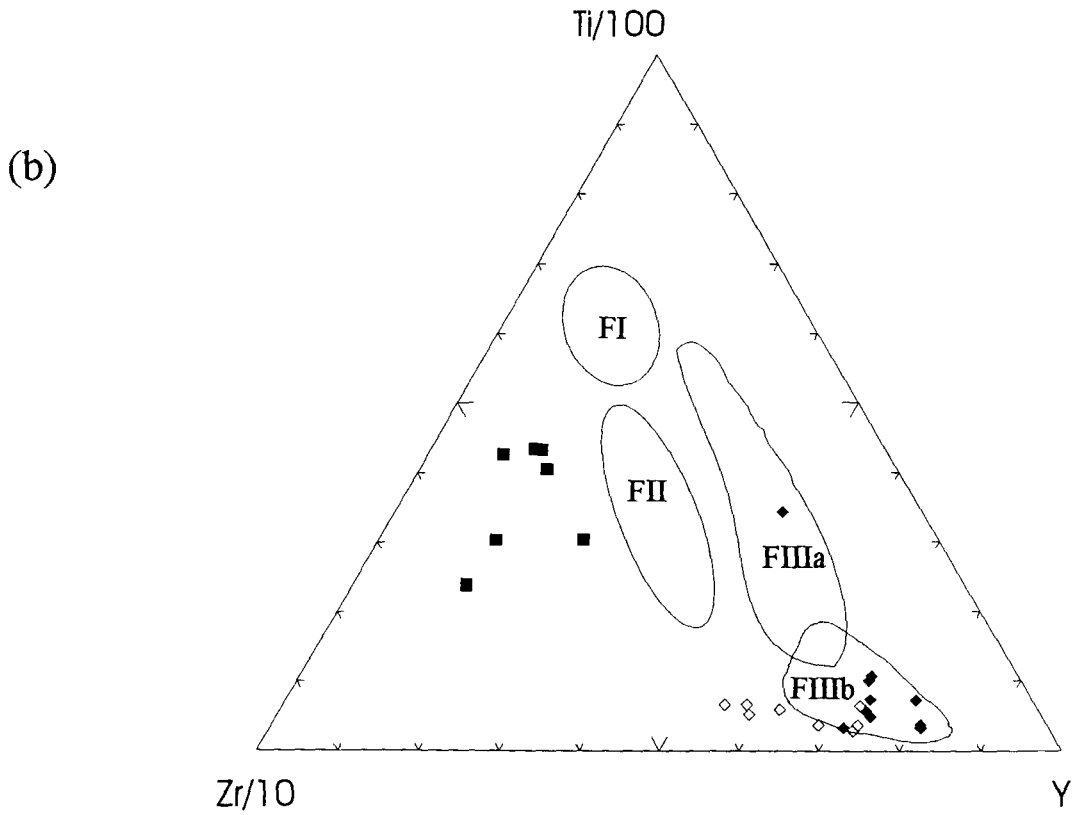
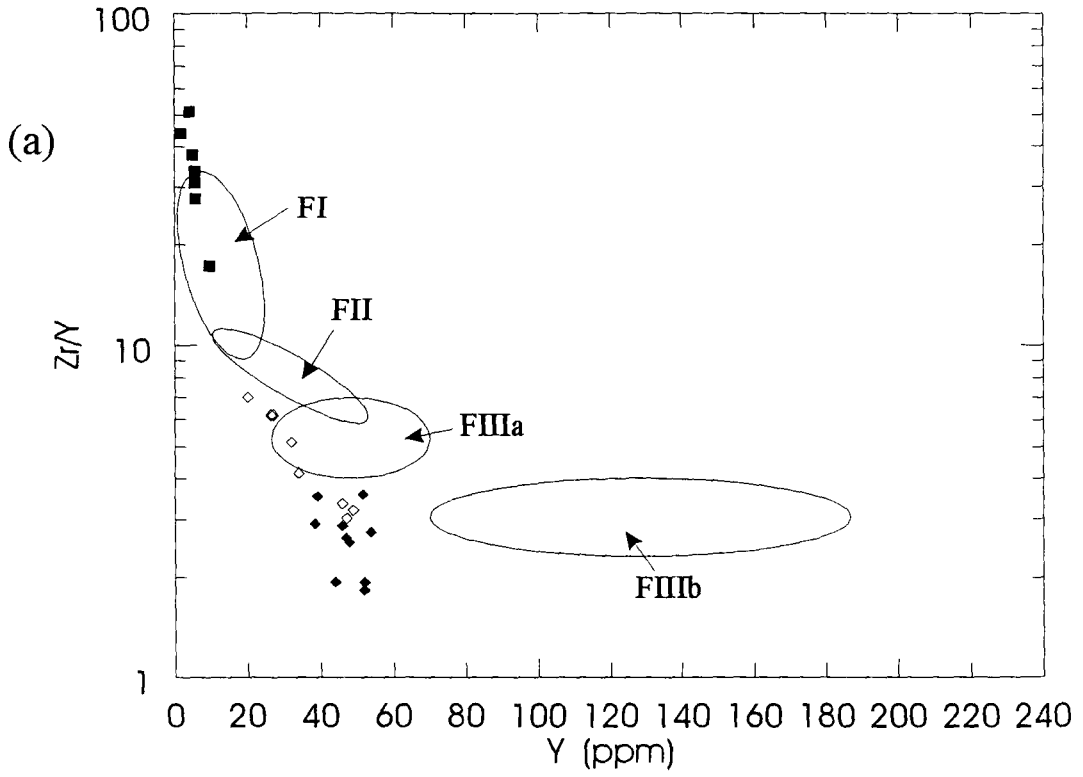
Several diagrams using Y, Zr, Ti and REE have been used by Lesher *et al.* (1986) to help clarify the classification of rhyolites. Figure 5-9 presents three such diagrams. Figure 5-9a corresponds to Lesher *et al.* (1986) figures 6 and 7, Figure 5-9b to figure 8, and Figure 5-9c to figures 3 and 4. The elliptical areas correspond to the areas defined by the samples presented in Lesher's diagrams.

From these diagrams it is apparent that the Upper and Lower Felsic horizons (empty and filled diamonds) most closely fit the FIII category. There is, however, no strong consensus as to whether they are FIIIa or FIIIb. Figures 5-9a and 5-9-c suggest the Upper and Lower Felsic horizons are a FIIIa type, while Figure 5-9b indicates they are a FIIIb type. From Table 5-3, the Zr/Y, Sr, Sc, La(n)/Yb(n) and Eu/Eu* all indicate an FIIIb type. However, given the range of overlap in values which define these rhyolite types overlaps into the FIIIa type, a combination of Figures 5-9a, b, c and Table 5-3 indicate these rhyolites would best be described as FIIIa type.

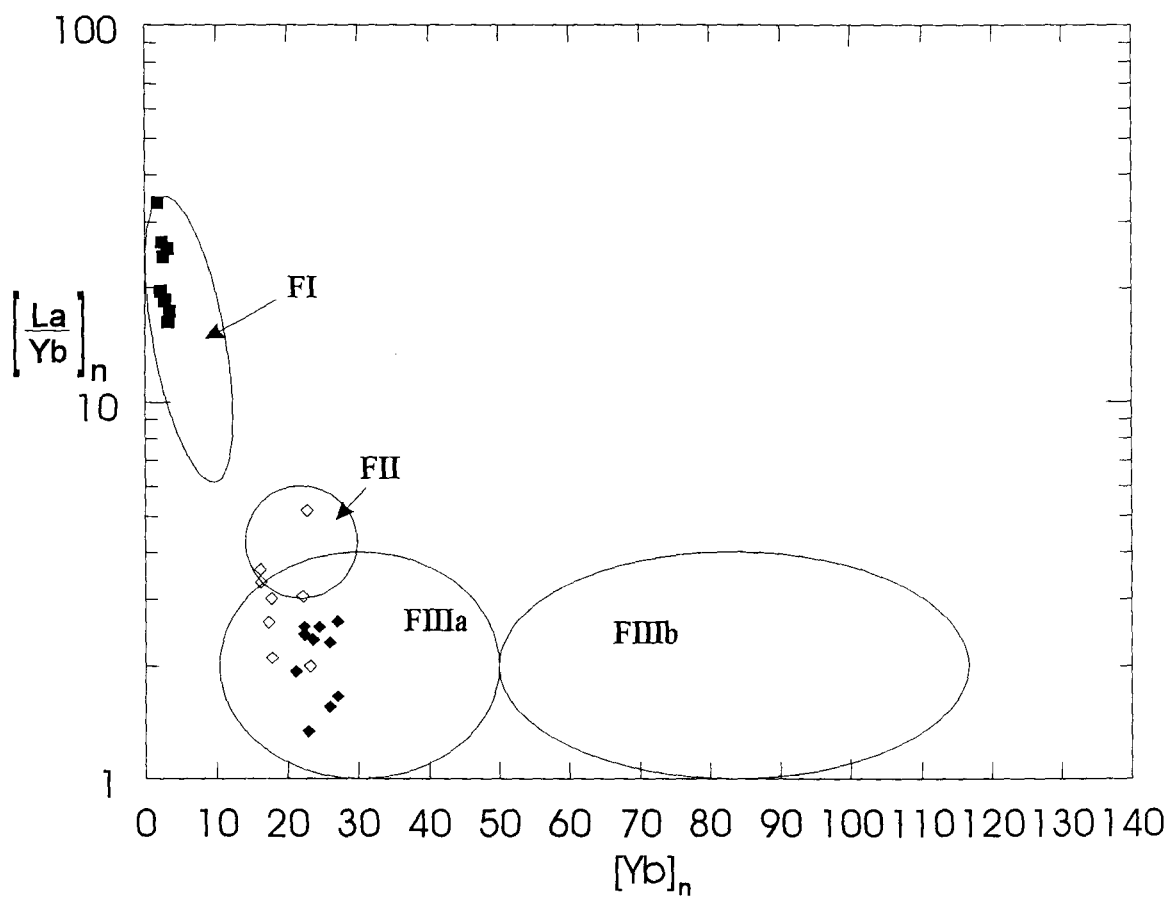
Figure 5-9a: Zr/Y vs Y rhyolite classification scheme of Lesher *et al.* (1986, figure 6 & 7). The felsic horizon samples do not quite fit the scheme, but are nearest to a FIIIa category. The quartz feldspar porphyries are best classified as FI. Symbols used:
Upper Felsic horizon - ◇
Lower Felsic horizon- ◆
quartz feldspar porphyry - ■.

Figure 5-9b: Zr/10 - Ti/100 - Y rhyolite classification scheme of Lesher *et al.* (1986, figure 8). The felsic horizon samples are best classified as FIIIb in this scheme. The quartz feldspar porphyries do not fall into a category.

Figure 5-9c (page 77): $[La/Yb]_{\text{normalized}}$ vs $[Yb]_{\text{normalized}}$ rhyolite classification scheme of Lesher *et al.* (1986, figures 3 & 4). In this scheme the felsic horizon samples are dominantly FIIIa, and the quartz feldspar porphyries are clearly FI.



(c)



5.7.2 Quartz feldspar porphyry

The quartz feldspar porphyries (City Dump and Milne Vent, see Fyon and Crocket 1986) (Table 5-3) with their steep REE profile, lack of any significant Eu anomaly, and low Zr and Y values, are mainly defined as FI type felsic volcanics. Figures 5-9 a and c place the QFP into the FI definition; however, the data does not fall into the FI or any other classification in Figure 5-9b.

5.7.3 Link Lake, Sherman Gate and South Temagami

The data for these horizons show two trends: FI for the South Temagami samples, and an FI to FII type for the Link Lake and Sherman Gate samples Figure 5-10, Table 5-3). Based on the major element, trace element and REE classification plots, these samples are undeniably calc-alkaline. As was the case with the MacLean and Barrett (1993) classification scheme (Y vs Zr), sample 108 sits very close to the FIII category, and thus may be tholeiitic.

5.8 Effects of Alteration on the Immobile Element Classification Scheme

As was discussed earlier, alteration processes can greatly change the chemistry of a rock and cause it to be improperly identified in certain classification schemes. Any element that becomes mobile during alteration cannot be used to identify the original character of its parent with great reliability. Any element that remains immobile during subsequent alteration can be used to characterize its parent. Since the immobile element is neither added to nor removed from the rock, the absolute amount of these elements will not change. If there is an addition of mobile material to the rock, then the apparent abundances of the immobile elements will decrease. If there has been a removal of mobile material from the rock, then the apparent abundances of the immobile elements will

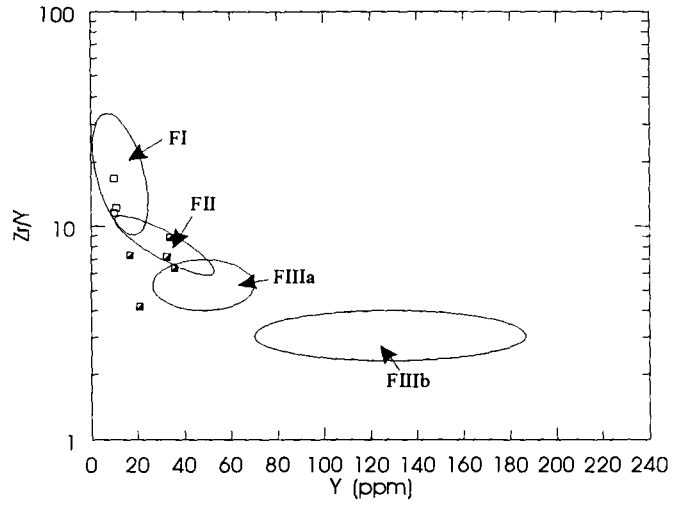
Figure 5-10: Rhyolite classification schemes of Lesher *et al.* (1986) for the Link Lake and Sherman Gate horizons (▣) and for the south Temagami samples (□).

(a) Zr/Y vs Y plot indicates the south Temagami samples are FI type rhyolites, and the Link Lake and Sherman Gate samples overlap between FII and FIIIa type rhyolites.

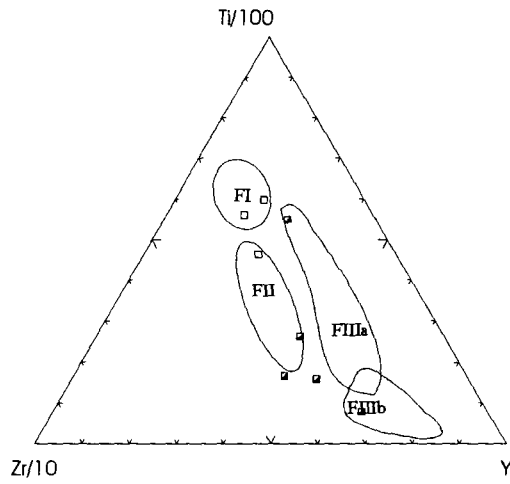
(b) $Zr/10 - Ti/100 - Y$ plot indicates the south Temagami samples are FI to FII type rhyolites, and the Link Lake and Sherman Gate samples overlap between FII and FIIIa and b type rhyolites.

(c) $[La/Yb]_{\text{normalized}}$ vs $[Yb]_{\text{normalized}}$ indicates the south Temagami samples are FI type rhyolites, and the Link Lake and Sherman Gate samples overlap between FI and FII type rhyolites.

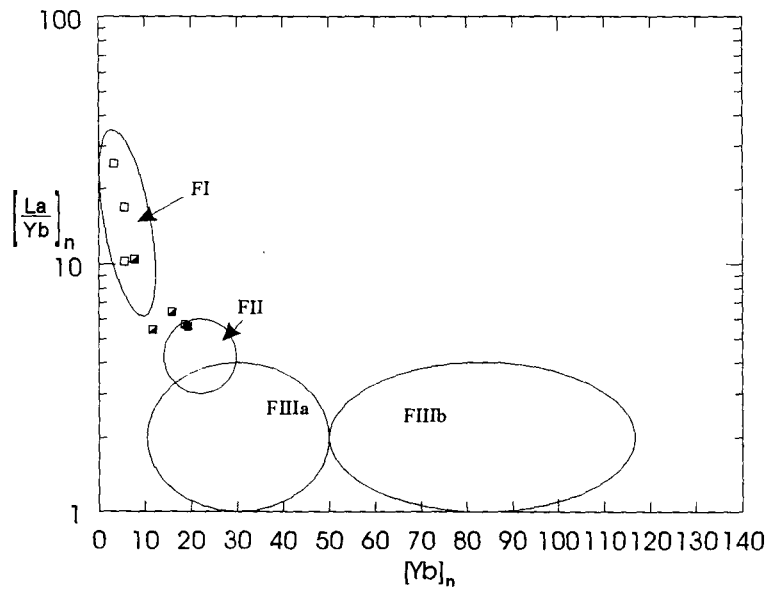
(a)



(b)



(c)



increase; however, the original ratios of immobile elements will not change during an alteration event.

The latter observation suggests that classification diagrams which either use ratios of immobile elements on both axes of a binary plot, or define classification fields based on ratios of elements, should correctly designate the pre-metamorphic or unaltered parental rock or protolith. In this respect we can conclude that the rocks identified as tholeiites and calc-alkaline in Figure 5-3a, b (immobile element Zr vs Y plots) are indeed tholeiites and calc-alkaline. Similarly, Figure 5-1d (Zr/TiO_2 vs Nb/Y) is best to determine the rock types (ie. rhyolites, rhyodacites, dacites etc.). The mobility of certain elements, in response to metamorphism, also means that any classification diagrams that use mobile elements are not necessarily accurate as guides to original protolith, and it is best not to use these types of classifications when working in an area of significant alteration.

For REE diagrams such as Figures 5-4 to 5-6, any metasomatic addition of material will cause all of the samples to show a lower chondritic normalized value than normal, and a subtraction of material will cause an apparent increase in chondritic normalized values. In the case of the classification scheme of Lesher *et al.* (1986) (Table 5-3) it is best to use element ratios for classification purposes. Assuming a net addition of mass to the Temagami samples, those plotted on Figures 5-7a and c will not move vertically, but only horizontally, such that FIIIa felsic rocks could become FIIIb as indicated in Figure 5-7b.

5.8.1 Net transfer of material

To determine if apparent alteration has resulted in a net addition or subtraction of material several methods can be used. The first is to compare the rocks in question with rocks of similar magmatic affinity to determine whether specific elements have been gained

or lost; that is, to determine what apparent mass changes may have occurred. In the Temagami case, the Upper and Lower Felsic horizons have been defined as tholeiitic rhyolites according to Zr vs Y criteria. A comparison of these samples to the tholeiitic rhyolites described by McBirney (1984, Tables 7-4, 9-1) indicates the Temagami samples have higher in Si and Mg, but lower concentration of all other major elements plus Zr.

A similar comparison of the Temagami samples to those of the Don rhyolite from the Noranda area (Ujike and Goodwin, 1987) indicates an increase in Si and Mg, and a decrease in all of the major elements as well as in Zr. A final comparison to the Amulet rhyolite, Noranda area (Barrett *et al.*, 1991c) indicates an increase in Si and K, and a decrease in all of the major elements as well as Zr.

Clearly, from these examples, there has been an apparent increase in Si, \pm Mg \pm K and a decrease in all of the other elements including Zr. The difficulty which arises is to determine whether the apparent Si increase indicates Si was added to the system, or whether the other components were lost from the system.

A commonly used method to determine how much of a specific element has been gained or lost from the rock is to consider the element concentration in a least altered sample. This sample would then presumably represent the parent or the rock composition prior to metamorphism, metasomatism or alteration. Several methods have been devised to make such comparisons including those of Gresens (1967), Pearce (1968), Grant (1986) and MacLean (1990). The theory behind these methods is that some element has remained immobile throughout the alteration event, and thus the absolute abundance of this element has not changed. By determining the apparent change of this element compared to the parent or least altered sample, it is possible to determine which element abundances have truly increased, and which have decreased.

Initial inspection of all of the samples for the Upper and Lower Felsic horizons indicate they are highly sericitized and silicified. It was decided that none of the clastic horizons should be used as a least altered sample for three reasons: 1) some of these samples have more than one clast type, 2) most of the volcanoclastics are situated in the LLDZ, a zone where more than one alteration process may have occurred, 3) the clastic nature of these rocks suggests they would undergo a greater degree of alteration as compared with a massive lava flow under the same alteration regime. Sample 119, a massive flow banded rhyolite, has the least amount of sericite and carbonate of the three massive lavas samples (ie. 23, 46, 119) and was chosen as the least altered sample.

The technique of MacLean (1990) was chosen for its simplicity in determining mass changes for the samples. The steps used to determine the mass changes as outlined by Barrett and MacLean (1994) are as follows:

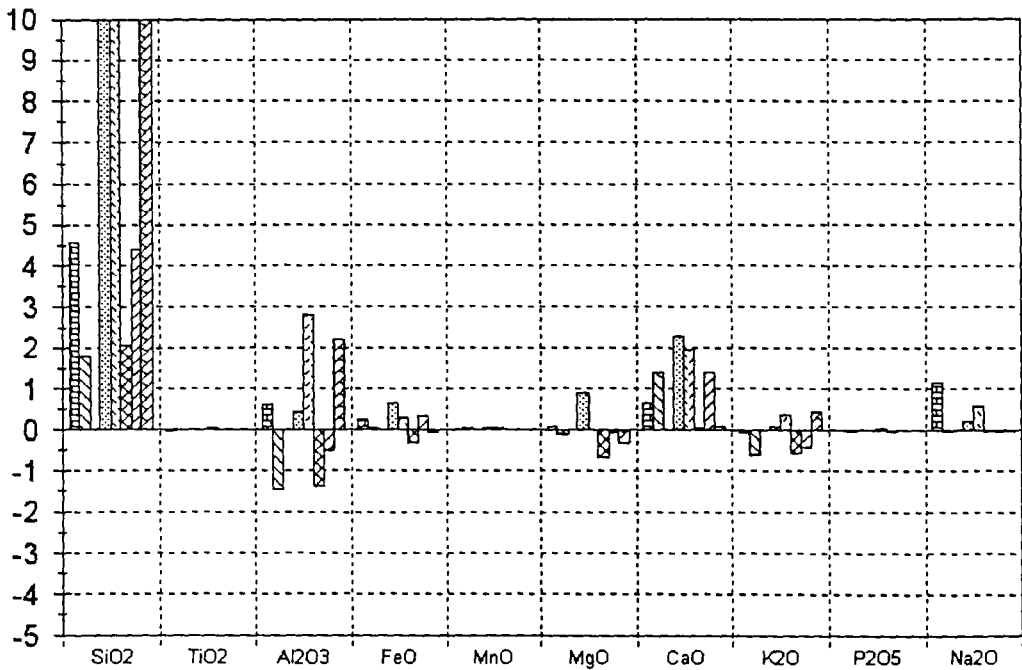
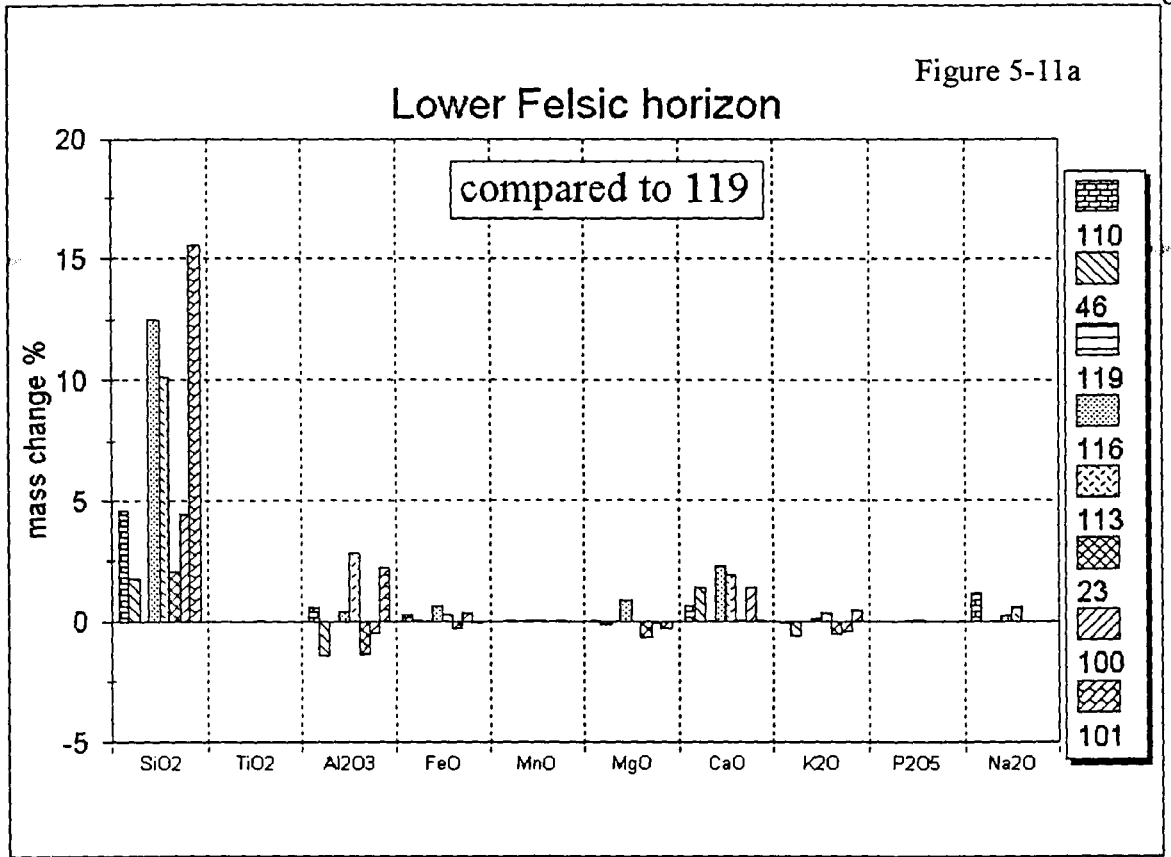
- 1) Calculate an enrichment factor (EF) for an element which is immobile; thus, for each sample : $EF = \frac{\text{immobile element}_{\text{precursor}}}{\text{immobile element}_{\text{altered sample}}}$.
- 2) Calculate a reconstructed composition (RC) for each component on an LOI-free basis: $RC = EF \times \text{wt\% or ppm component (altered sample)}$.
- 3) Calculate the mass change for the altered sample: $\text{Mass Change} = RC - \text{precursor}$.

Reconstructed compositions and mass changes are computed for each major and trace element component of the altered rocks. Mass changes are not calculated for the immobile element used in the calculation for the result will always be zero.

Figures 5-11 a, b are the results for the Upper and Lower Felsic horizon using sample 119 as the precursor and Zr as the immobile element. The data indicates there was a major addition of material to the system, and little in the way of losses. The major additions to the Upper and Lower Felsic horizons were Si and Al which increased by as

Figure 5-11: Calculated mass change (weight %) of the major elements as compared to sample 119 for (a) Lower Felsic horizon with an enlargement of the -5 to 10 range (bottom); (b) Upper Felsic horizon with an enlargement of the -2 to 10% range (bottom). The technique of MacLean (1990) was used for the calculation of element gains and losses.

Figure 5-11a



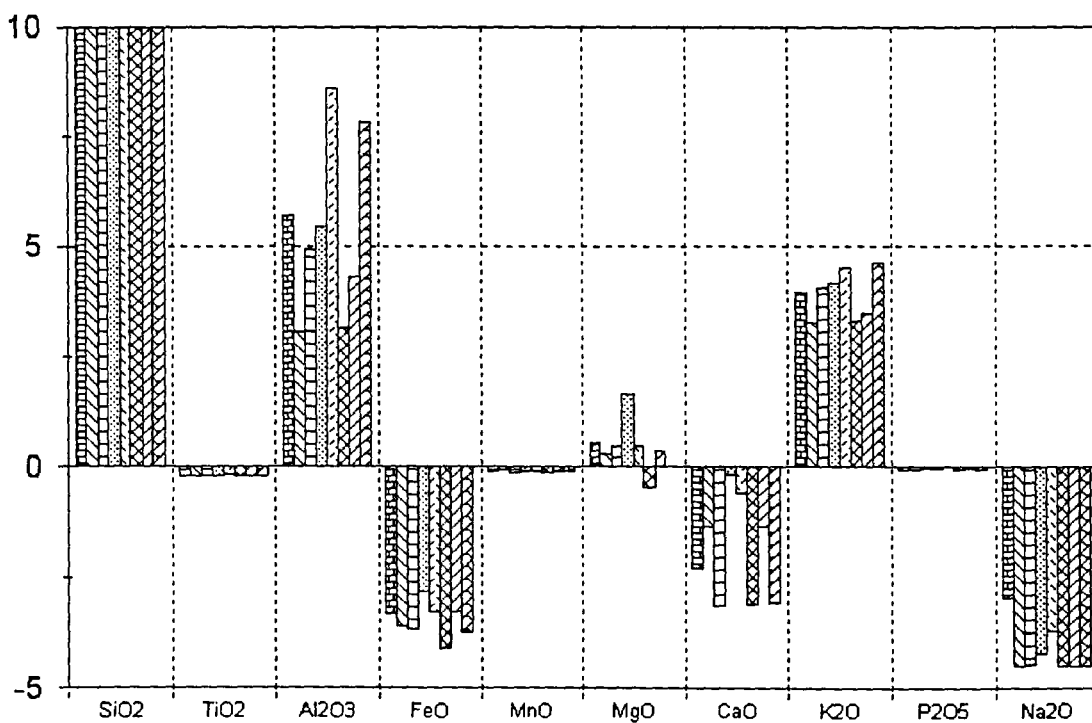
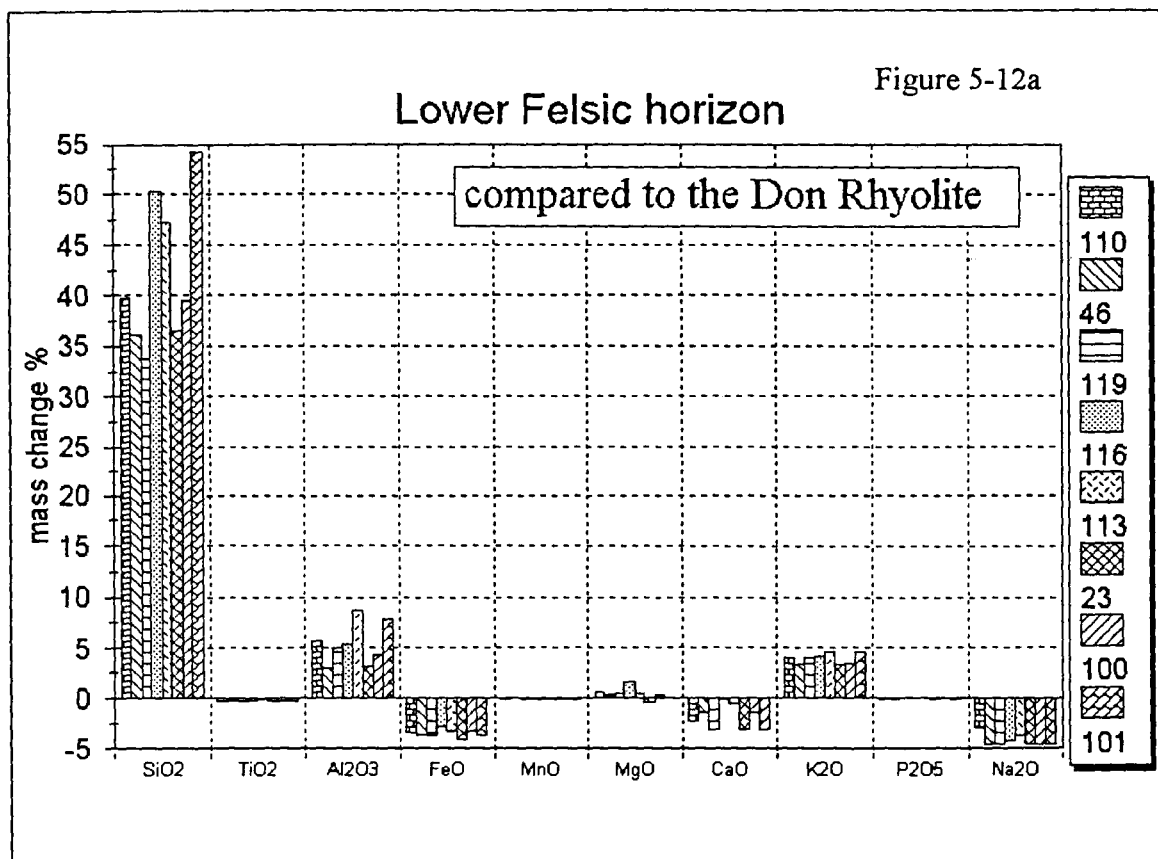
much as 79% (sample 109) and 8% (sample 106) for the two oxides respectively. The greatest positive mass changes are found along the Link Lake deformation zone, suggesting that it has greatly influenced the chemistry of the rocks.

With respect to sample 119, the data indicates there has been very little or no mass change for the elements Ti, Mn, P and Na, minimal gains for Mg, Ca and K, while Al has moderate gains. It is difficult to ascertain the true mass changes of these samples simply because there is no sample that shows no significant alteration. In this respect, the fact that there has been little or no gain of Ti, Mn, P and Na does not mean these elements have remained immobile, but rather relative to sample 119 they have not changed. As mentioned earlier, Na has apparently been mobile in this area.

A second mass change diagram was constructed using the Don rhyolite from the Noranda area (Figure 5-12a, b) as a protolith comparator (ie. original composition). This rhyolite (sample 725-2) is a FIIIa tholeiite according to Lesher *et al.* (1986) and Ujike and Goodwin (1987). It has a similar chemistry to the Lower Felsic horizon samples. As was the case with the comparison to sample 119, the greatest mass changes occur with Si and Al; however, the effects are much more extreme. Additions of Si to the Upper and Lower Felsic horizons are as much as 137%, while additions of Al can be in excess of 15%, again the greatest additions are along the Link Lake deformation zone.

In this comparison, there is also little or no change in Ti, Mn and P, suggesting these elements may have remained immobile during the alteration event. A major difference in mass change here is that Fe and Na were both removed from the system by as much as 5 wt%.

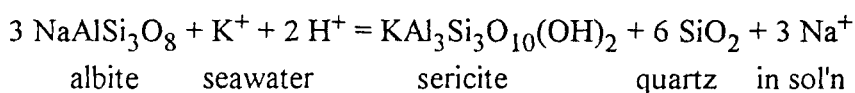
Figure 5-12: Calculated mass change (weight %) of the major elements as compared to the Don rhyolite, Noranda area (Ujike and Goodwin, 1987; sample 725-2) for the (a) Lower Felsic horizon with an enlargement of the -5 to 10% range (bottom); (b) Upper Felsic horizon with an enlargement of the -5 to 15% range (bottom). The technique of MacLean (1990) was used for the calculation of element gains and losses.



5.8.2 Explanation for the observed mass changes

5.8.2.1 Felsic horizons

As noted in Chapter 4, all of the samples contain abundant sericite, and have a high quartz content. According to Barrett and MacLean (1994) the most important reaction forming sericite is:



This reaction requires an increase in K, obtained from seawater, and the removal of Na from the system by an aqueous solution. All Al needed for this reaction can be derived from the break down of feldspar and epidote (Barrett and MacLean 1994). Excess quartz is produced by this reaction, and will either be precipitated as quartz or chert, or stay in solution and be removed from the immediate area.

Overall, the mass of Si should not increase, but either decrease or remain the same. Thus, a problem arises with the apparent mass changes in the Temagami rocks. In comparison to the Don Rhyolite, the sericite reaction explains the changes in Na and K, but in comparison to sample 119 it cannot explain the gains of Na and variable gains and losses of K. It is likely, however, that the sericite alteration has resulted in gains and losses of K and Na from the volcanoclastic material respectively. If a hydrothermal alteration event removed or added elements proportionally among the rocks, then by use of the methods of Barrett and Maclean (1994), there should be very little or no gains or losses of mass from the Temagami rocks indicated. This may have been the case for Na, K and other elements in the Upper and Lower Felsic horizon rocks.

The presence of dolomite could be responsible for the additions of Mg and Ca but the major addition of Si cannot be explained by the albite - seawater reaction. This

suggests that silicification, either during or after the deposition of the rocks, must have been part of the alteration process to affect this area.

The evidence from the thin sections suggest that the order of deposition of the alteration mineralogy was quartz - sericite / chlorite - carbonate. Since the carbonitization event was coincident with the Link Lake deformation (LLD) event, the silicification and sericitization are pre-LLD and likely related to the original deposition of the felsic volcanics.

A few quartz veins were noted in the rhyolite lava flows (Plate 4-6) suggesting some late stage fluid movements did take place after emplacement of the various flows, and may have been responsible for the higher Si values. However, since there are very few quartz veins in the area, it is more likely that Si rich fluids were contemporaneous with the formation of the felsic horizons. Since the clastic units would have been much more permeable than the lava flows, we should expect a greater addition of Si to the clastic units than to the lava flows. Based on the comparison to sample 119 (Figure 5-11a, b) this is the case.

From the comparison of the felsic horizons to the Don rhyolite (Figure 5-12 a, b) we can see that the additions and subtractions of the various elements is more pronounced, but that Si still has the greatest increase of any of the elements. While the mass changes should not be taken at face value, they do serve to indicate that these rocks have gone through some major chemical changes. One should not expect the parents of these two volcanic systems to be the same, yet based on their felsic classifications they should have gone through similar processes. The larger apparent changes in chemistry of the felsic horizons, compared to that of the Don rhyolite, is in part explained by the greater enrichment factor calculated using the larger Zr value of the Don rhyolite, as compared to sample 119.

The Zr/Hf ratio of the Don rhyolite and the Upper and Lower felsic horizons suggests the parents of these rocks actually went through dissimilar processes. The calculated Zr/Hf ratio should be a measure of fractionation processes in the magma chamber, and similar ratios for the two areas would indicate similar magmatic processes (Dr. M. Gorton, University of Toronto, pers. comm). The average Zr/Hf value for the felsic horizons is ~27.5 (Table 5-4) while the ratio for the Don rhyolite is ~43 (Ujike and Goodwin 1987). These large differences cannot be explained by experimental error, and thus are a product of different magmatic processes. It has been suggested (Dr. M. Gorton, pers. comm) that if the parent for the felsic horizons is related to an iron-tholeiite basalt, then Zr can be enriched relative to Hf in the basalt, thus depleting a tholeiitic rhyolite differentiate of Zr and lowering the Zr/Hf ratio. As mentioned in Chapter 3, the tholeiitic basalts of this area are considered iron-tholeiites and thus their formation may have resulted in a depletion of Zr in the tholeiitic rhyolites. The positive correlation for Fe and Zr has been observed for the Cerro Toledo Rhyolite (Stix and Gorton 1990).

Table 5-4
Zr/Hf ratios for the Temagami samples

quartz feldspar porphyry sample	Zr/Hf	Upper Felsic horizon sample	Zr/Hf	Lower Felsic horizon sample	Zr/Hf
03	31	11	30	23	30
12	43	26	29	46	31
13	43	27	30	100	27
14	47	30	28	101	22
15	45	32	39	110	26
16	43	36	31	113	27
17	42	43	28	116	27
102	23	106	23	119	26
		109	22		
		114	49		
average	39.6		27.9		27.0

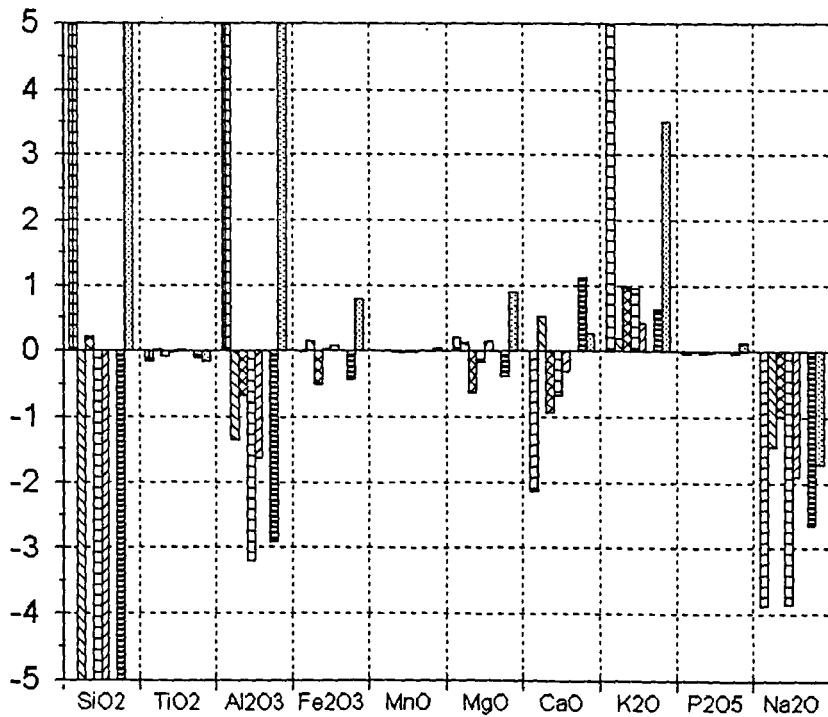
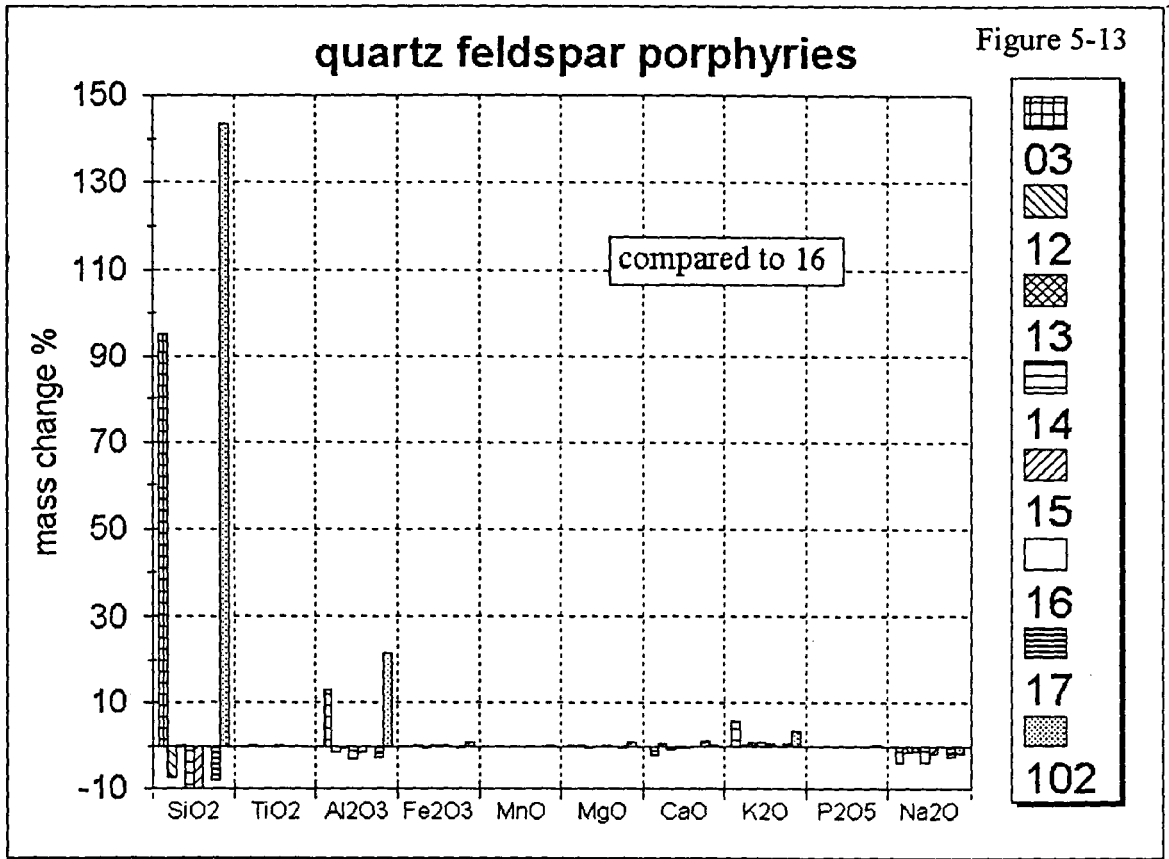
Thus the calculated enrichment factor for the Don rhyolite comparison may be more misleading in terms of additions and subtractions of materials that previously mentioned because magmatic fractionation may have reduced the initial concentration of Zr in the parent rock of the Temagami samples relative to the Don rhyolite parent.

5.8.2.2 Quartz feldspar porphyries

In the same manner that the mass changes for the felsic horizons were calculated, mass changes for the QFP's were also determined. The least altered sample for this set of rocks is sample 16, in which primary minerals and textures are well preserved, and the smallest amount of sericitization and chloritization is found. Mass changes are shown in Figure 5-13.

This set of calculated mass changes is more consistent with the dominant sericitization of the other samples. For the QFP suit, most samples show a loss of Si and Na, and gains in K. There are however, two examples, 03 and 102, with large gains in Si and Al. Sample 03 is associated with quartz veining and the Si addition may be associated with the veining. Sample 102 does not appear to have any quartz veining, but is found in the LLDZ. It is very possible then, given the apparent relative differences in age of the felsic horizons and the QFP's, that the LLDZ has produced a silicification event. If this supposition is correct, the major gains of Si in both the felsic Upper Felsic horizon and the QFP's near the area of the LLDZ can in part be attributed to the LLD event.

Figure 5-13: Calculated mass change of the major elements for the quartz feldspar porphyries as compared to sample 16.



CHAPTER 6

PYRITE CLASTS

6.1 Introduction

Sulphide clasts, consisting dominantly of pyrite, occur within several of the felsic volcanoclastic horizons including the Hydro debris flow, the Upper Felsic horizon and the Link Lake and Sherman Gate felsic horizons. The presence of sulphide fragments, or clasts, in this area is of interest from an economic point of view because sulphide fragments are known to occur in areas surrounding VMS deposits (Rokachev 1965; Sinclair 1971; Zhabin 1978; Calhoun and Hutchinson 1981; Clark 1983; Barrett *et al.* 1992), and these fragments may be an indicator of proximity to a VMS deposit. The following is a discussion of the petrological and chemical characteristics of the sulphide clasts, from the part of the Temagami greenstone belt under study, as a means of determining their origin.

6.2 Description

Sulphide clasts were obtained from several horizons including the Upper and Link Lake Felsic horizons, Sherman Gate horizon and the Hydro debris flow. The clasts vary in size from <1 cm to 35 cm in the longest dimension on surface (Plate 6-1). Surficial

Plate 6-1: Examples of some of the larger sulphide clasts from the study area:

a) Cut open clast from the Upper Felsic horizon. Both pyrite (dark grey) and volcanoclastic material (light brown) are visible in the photograph. The long dimension is parallel to the vertical component of the foliation. This clast has been pulled apart thus resulting in a brecciated texture. This is sample PY-47.

b) This large pyrite clast originates in the Link Lake horizon. As with the majority of all the pyrite clasts, this example is elongate in the plane of the foliation. Canadian nickel for scale (approximately 2cm). North is to the top of the photo.

c) This is the largest pyrite clast in the Lower Felsic horizon. Unlike most clasts, the longest surface dimension is perpendicular to the foliation. Note the iron staining on the surrounding rocks. South is to the top of the card.



weathering often produces a halo of iron stain around the clasts, creating the illusion that the clasts are larger than their true size. Where visible on road cuts, clasts were measured with width - length - height ratios ranging from 1:2:3 to 1:3:10. The longest dimension is parallel to the dip of the regional foliation, and the smallest dimension is perpendicular to the regional foliation.

While the pyrite clasts are concentrated mainly at the base of the debris flows, they can be present throughout the entire thickness of any one individual flow. Clast size decreases in the same manner as the fining up sequence of the volcanic rock fragments in the felsic volcanoclastic flows, indicating they were deposited as part of the volcanoclastic flows. The horizons rich in pyrite clasts are not laterally extensive, and do not appear to be present west of L20W.

Clasts that were cut or broken open reveal that they are dominated by massive pyrite, although cubic forms, concentrically banded and radiating crystal (reniform) textures are also present (Plate 6-2).

6.3 Petrography of the Sulphide Clasts

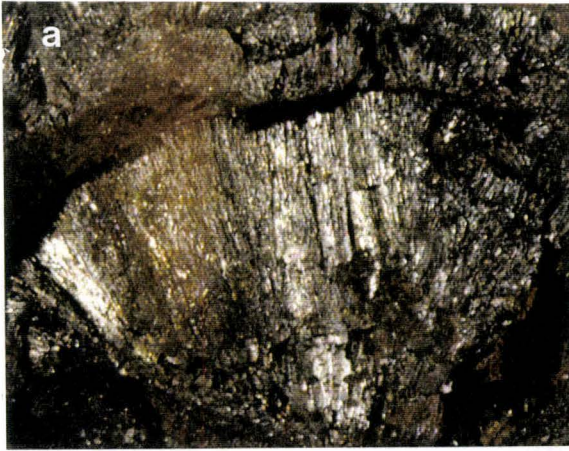
6.3.1 Mineralogy

Polished thin sections of several of the clasts were examined by reflected light microscopy which indicated the primary sulphide mineralogy of the clasts is virtually pyrite alone. Modal estimates of the mineralogy within the sulphide clasts indicates a single clast is made of >90% pyrite. Other minerals within a clast include quartz, micaceous minerals and carbonate, with quartz being the most abundant accessory mineral.

Sample PY-32 revealed one piece of sphalerite, <1mm across which was the only sphalerite found in all of the samples. Only sample PY-2 was found to contain

Plate 6-2: Several examples of pyrite textures visible in hand sample:

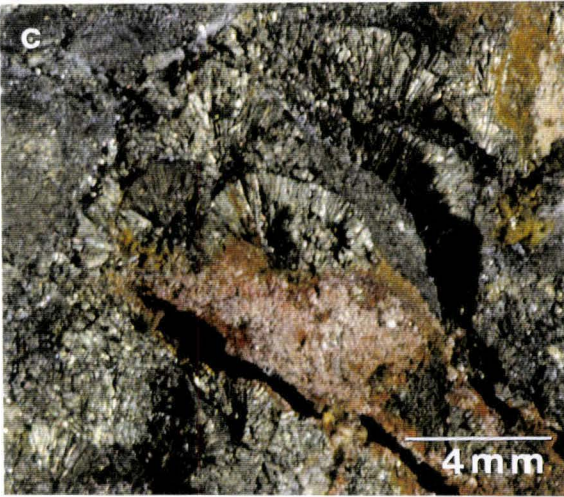
- a) Partial pyrite sphere with radiating crystals and convex edge.
- b) Broken and rotated remnant pyrite sphere with preserved convex edges (arrow).
- c) Cluster of partial pyrite spheres with radiating crystals and convex edges.
- d) Example of remnant concentric bands in a partially rotated pyrite sphere. Quartz and carbonate in the pressure solution shadow just above the pyrite.
- e) Example of radiating crystals and convex edges.
- f) Broken surface of a pyrite clast with radiating crystals and partial spheres. Often broken pieces reveal spherical 'bumps' (arrow) indicating the original spherical nature of the pyrite.



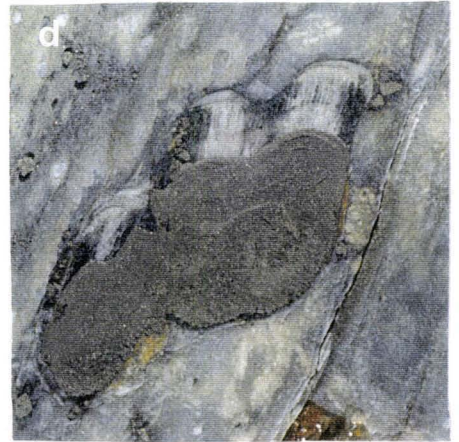
5mm



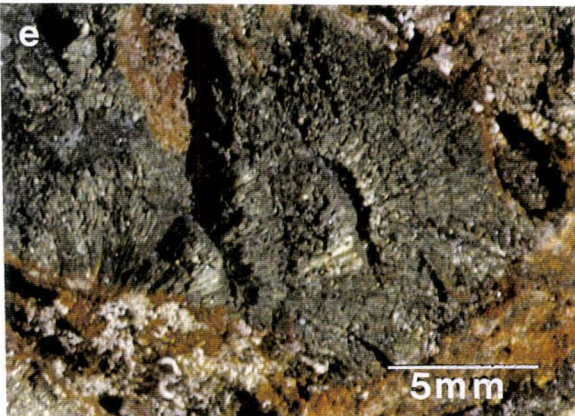
1cm



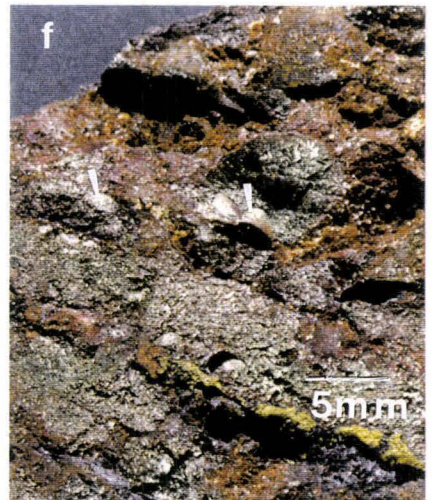
4mm



1cm



5mm



5mm

chalcopyrite. This speck of chalcopyrite, ~0.04mm across, was found in a fracture in a subhedral piece of pyrite ~2mm across (Plate 6-3) indicating it is a secondary mineral, and not part of the original pyrite.

Some additional work, using a Philips model 510 scanning electron microscope (SEM) with a Link QX 200 xray spectrometer, on sample PY-32 a spherical shaped pyrite, revealed that there are many small inclusions of molybdenite, all <1 micron in diameter (Plate 6-3). The SEM also indicated that a piece of secondary (see section 6.3.2) pyrite contained a veinlet of Mo, suggesting that during the recrystallization of this pyrite sphere the small inclusions of Mo became mobilized. Since SEM analysis was conducted on only the one sample, the extent to which molybdenum is present in other samples is not known. If it is present, it is only a minor constituent of the samples as molybdenite was not identified in reflected light microscopy.

From the SEM analysis it was also found that most of the inclusions within the pyrite sphere are quartz. From the reflected light microscopy it was determined that some of these inclusions appear to be graphite. Secondary pyrite has very few inclusions indicating the inclusions are primary constituents of the clasts.

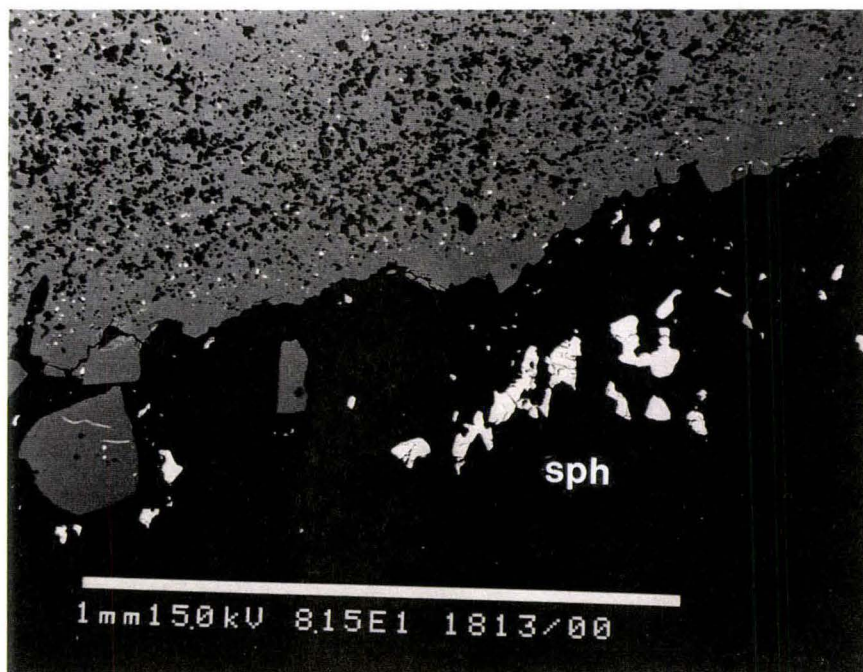
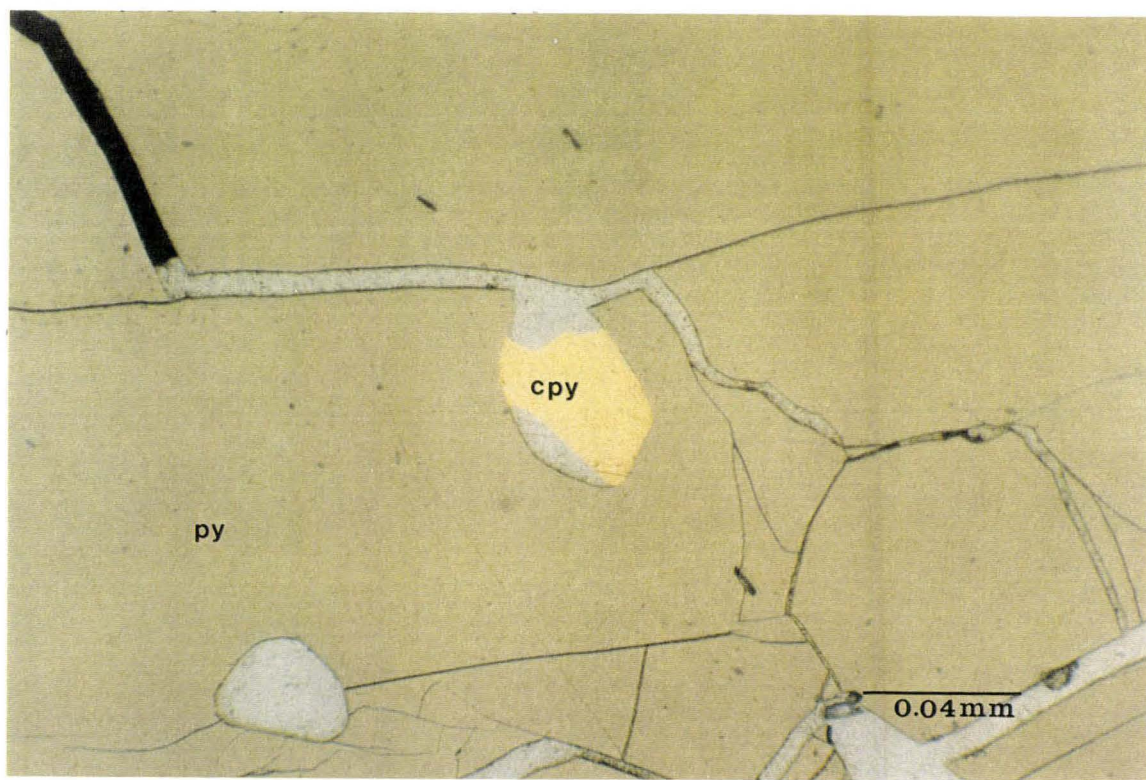
6.3.2 Textures

Several primary and secondary textural forms of pyrite have been recognized in the polished thin sections. Spherical shapes, concentric banding, radiating crystals or a lattice work of pyrite crystals are considered to be primary textures, while cubic and massive forms present as overgrowths, replacement of spheres or as individual clasts, are considered to be secondary textures.

Plate 6-3: Photomicrograph examples of the sulphide minerals associated with the pyrite clasts:

a) A subhedral piece of pyrite (py) with the only piece of chalcopyrite (cpy) found in the pyrite clasts. This example demonstrates that the chalcopyrite precipitated in a fracture within the pyrite and not as part of the pyrite. This indicates the chalcopyrite is a secondary sulphide mineral, and not a primary component of the pyrite clasts. Sample was photographed in plane polarized reflected light.

b) SEM photograph of the spherical and concentrically banded pyrite visible in Plate 6-2d. This photo reveals the presence of a sphalerite (sph) cluster outside of the pyrite sphere (light grey) and in the pressure solution texture (black). The small bright dots in the pyrite sphere are molybdenite, and the black inclusions are quartz. Note the subhedral pyrite along the edge of the pyrite sphere indicating secondary pyrite growth.



6.3.2.1 Spherical pyrites

Many of the samples contain partial to whole spheres of pyrite, the edges of which are defined by a convex boundary (Plate 6-2). In thin section this boundary is recognized by the termination of a set of radiating crystals, or by a convex boundary (Plate 6-4). These spheres range in size from 1 mm up to a 2-3 cm diameter. Spheres can be present as aggregates or as individuals, and are often concentrically banded (Plate 6-2).

6.3.2.2 Concentric banding

The concentric banding, associated with the spherical pyrites, was found in only a few samples (Plate 6-2), and in thin section is best observed with a low powered lens. Bands are generally <0.3 mm in width with gradational margins, and are defined by changes in proportions of pyrite and quartz. The number of bands is a function of the size of the spheres with larger spheres having more bands. In reflected light, bright bands are rich in pyrite, while dark bands are rich in quartz .

6.3.2.3 Radiating crystals

The radiating texture is difficult to observe in thin section, as the isotropic nature of the pyrite tends to obscure crystal edges. The radiating structure can best be seen where quartz has been incorporated along the edges of the crystal faces, or where crystals have been broken apart. If the polished thin section has slightly oxidized, then the individual crystals will stand out (Plate 6-4). Individual crystals are up to .05mm wide, with a length dependant on the size of individual spheres. From the large spheres it appears that long grains radiating from core to periphery of the sphere are made up of several pyrite crystals, not just a single crystal.

Plate 6-4: Several photomicrograph examples of textures within the pyrite clasts. All photographs were taken using plane polarized reflected light.

- a) Radiating crystals and convex edges of a partial pyrite sphere. As with this example, crystals will often break along their crystal faces and enhance the radiating nature of the pyrite.
- b) Convex edged pyrite with no apparent radiating structure in association with radiating structure of irregularly shaped pyrite. The loss of a convex edge is an indication of breakage of the pyrite during incorporation into the surrounding volcanoclastic.
- c) Lattice pyrite common to most samples. This texture is characteristic of marcasite rather than pyrite, suggesting some of the pyrite may have originally been marcasite.



Plate 6-4 continued

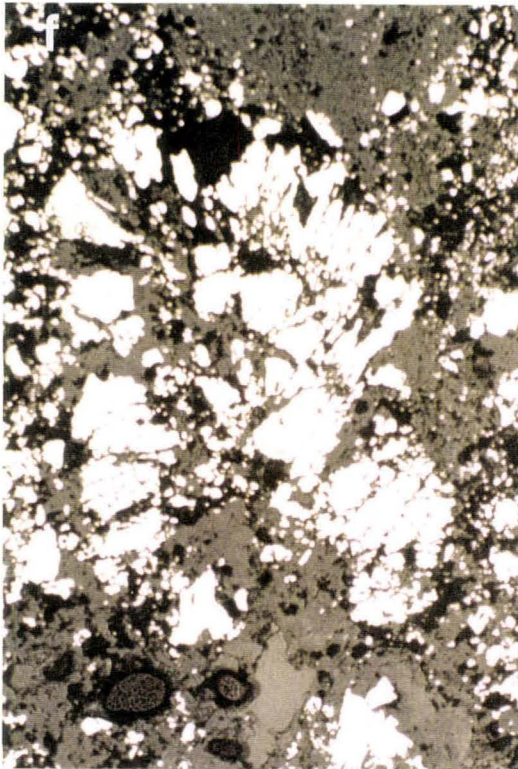
d, e) Progressive destruction of three pyrite spheres. Well preserved spheres have a quartz rich core, as in Plate 6-5a. During metamorphic and hydrothermal alteration of the host rock, pyrite tends to recrystallize and the spheres are destroyed. If the pyrite is not dispersed throughout the host rock, then cubic pyrite forms and often produces an atoll structure of pyrite (e).

f) Remnant pyrite sphere with radiating structure in massive pyrite from the nose of the fold at the Fold Nose trench. Even under extreme conditions of deformation, the primary textures of the pyrite can be partially preserved.

g) A cluster of secondary pyrite. Note that there are several examples of convex edges within this cluster which are possible remnant spherical pyrite edges.



1 m m



6.3.2.4 Lattice pyrite

Most pyrite is massive, but some pyrite occurs in arrays of intersecting blades and/or acicular crystals giving rise to a network of lattice work of pyrite grains. This texture has been recognized in conjunction with massive, radiating and concentrically banded pyrites and is the most frequently recognized texture in thin section (Plate 6-4). The individual pyrite needles or blades are a maximum of 2 microns wide, and 15 microns long. Intersection of the needles varies from orthogonal to 35-145°. Quartz and limonite are the most common minerals within the lattice; however, graphite can also be found in a few of these lattice works.

6.3.2.5 Secondary pyrite

Modal abundance of secondary pyrite varies from a few percent to 100% of an individual sample, and it is the most common pyrite in the sample set as a whole. Massive anhedral pyrite is the most common form of secondary pyrite. It is generally low in, or free of, any mineral inclusions, often occurs as overgrowths on the spherical pyrite and may represent the total destruction of original spherical pyrites

Cubic pyrite is commonly disseminated throughout any one sample, and often occurs as overgrowths or as a complete replacement of spherical forms (Plate 6-3, 6-4). As with the massive pyrite, cubic forms are generally low in, or free of, any inclusions. They vary in size from 0.1 mm to 4 mm in the largest dimension. The cubic pyrite does occur as overgrowths on the massive pyrite, and represents the last stage of pyrite growth.

6.3.2.6 Destruction of a pyrite sphere

As mentioned earlier, some cubic pyrite has completely replaced the spheres of pyrite. Most often the center of a sphere is dominantly quartz, and as one moves away

from the center, or core, the sphere is dominated by pyrite. During progressive alteration and/or metamorphism of the surrounding rock, the core is cleansed of pyrite and completely replaced by quartz. At the same time the concentric banding, radiating and lattice textures are destroyed, and cubic pyrite replaces these original textures. This replacement of the pyrite spheres is depicted in Plate 6-5a, and 6-4d, e consecutively. These atoll like structures can be found in several of the polished thin sections and also helps to identify the original presence of pyrite spheres.

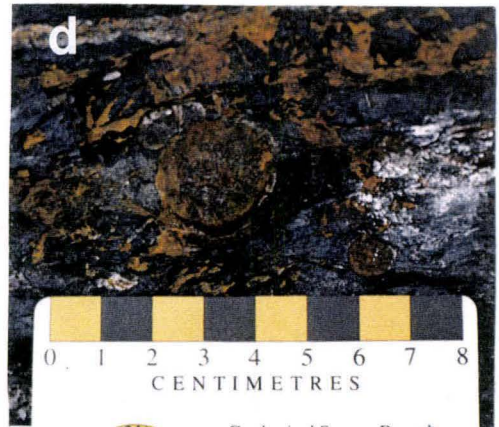
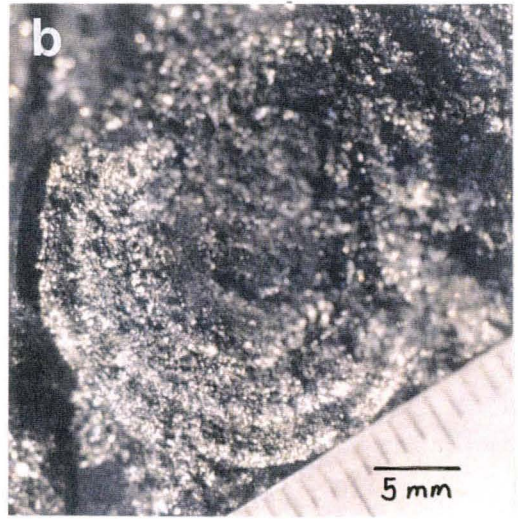
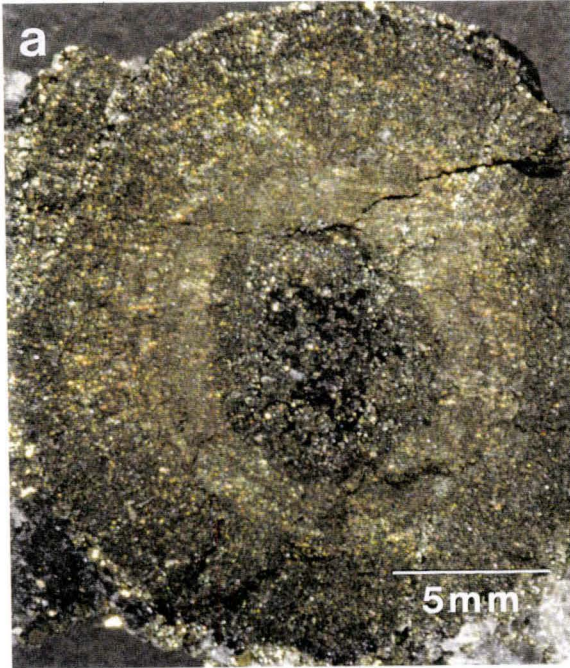
6.4 Textures of Pyrite from the Carbonaceous Shales

Pyrite clasts exhibiting spherical shapes, concentric banding and radiating textures are found in most of the felsic horizons. This wide distribution and the preservation of primary texture, suggests a common origin for these sulphide clasts. Concentrically banded pyrite ranging in size from 0.5 to 2 cm, spherical remnants of limonite after pyrite also in this size range, and massive pyrite are present in the carbonaceous shale of the Garbage Dump trench and Fold Nose trench localities, in shale along the Trans Canada pipe line, as well as in the graphitic cherts of the Sherman Mine (Bowins and Crockett 1994) (Plate 6-5a). Several shale clasts within the felsic horizons also have these remnant spherical pyrites associated with them (Plate 6-5b-e).

The presence of the spherical pyrites in the various shale horizons, the presence of concentric banding and in the case of sample 145, radiating structure (Plate 6-4f), suggests that the pyrite clasts within the volcanoclastics originated from these, or stratigraphically equivalent, shales. More will be said about this later.

Plate 6-5: Several examples of pyrite spheres from the carbonaceous shales.

- a) Concentric banding and radiating texture in a whole pyrite sphere from the Sherman Mine.
- b) Concentric banding of a partially destroyed pyrite sphere from the Garbage Dump trench carbonaceous shales.
- c, d) Examples of remnant pyrite spheres at the Garbage Dump trench. On surface these spheres are usually entirely replaced by limonite.
- e) Carbonaceous shale clast in the Lower Felsic horizon with pyrite spheres still present (arrows). Other examples of shale clasts with pyrite are present in the Upper Felsic horizon, however, completely spherical pyrites are rarely preserved.



6.5 Ag, Cu, Zn, Co and Ni in Pyrite from the Temagami Area

Chemical analysis was conducted on the pyrite clasts, shale pyrites and a vein pyrite. This was done for two reasons: 1) To determine if the pyrite clasts from the volcanoclastics are chemically similar to the pyrites from the shales or veins of pyrite in the study area. 2) To determine if the pyrite clasts may have come from some source other than the shales or pyrite vein within the Temagami study area, by comparing their chemistry to the chemistry of pyrites with known ancestries.

6.5.1 Sample preparation and analytical methods

Pyrite samples were collected from the volcanoclastics, carbonaceous shales and a pyrite vein. When possible, these sample were extracted from the host rock in the field. Pyrite samples were then further separated from the host rock by coarse crushing and hand picking. Samples were crushed to a >50 mesh (nylon bolting cloth), and when warranted, additional hand picking was conducted to further reduce host rock contamination. Final crushing was done to >200 mesh. Approximately 100 mg of each sample was separately weighed out and then digested with 5ml of double-distilled concentrated HNO_3 in teflon containers for 6 hours. The samples were then taken to dryness, and a second digestion using 5ml of concentrated HNO_3 was done. This digestion was allowed to run for 6 hours, after which the samples were again taken to dryness.

After completion of the second digestion the samples were taken up in 1.04M HNO_3 and transferred to polyethylene bottles. The total weight of solution was made up to 100mg. High purity 1.04M HNO_3 was prepared by dilution of double-distilled concentrated HNO_3 . An insoluble residue was left in only two samples indicating the other samples were nearly pure pyrite. The insoluble residual was analysed by x-ray diffraction and found to be a combination of quartz and graphite.

6.5.2 Results

Six pyrite samples from the volcanoclastics (samples PY-32, 47, 145, 146, 147, 148) were analysed for Co, Ni, Cu, Zn and Ag by Dr. Bob Bowins (McMaster University) on an Elan model 250 inductively coupled plasma mass spectrometer (ICP/MS) system, the results for which are presented in Table 6-1. Analytical error, determined from duplicate analysis of sample PY-32, is estimated at 20% for Cu, Zn, Co and Ni, and at 48% for Ag. For simplicity in description, the prefix PY- (for pyrite) has been omitted in the following discussions, and the pyrites are referred to by the host rock type.

6.5.2.1 Silver

Silver values for the volcanoclastic pyrite range from <5 ppm to 120 ppm with an average value of 49 ppm, and from 5 to 20 with an average value of 13 for the shale pyrite. This average volcanoclastic pyrite is comparable to VMS pyrite according to Roberts 1982; Bajwah *et al.* 1987; Huston *et al.* 1993, and to VMS, hydrothermal vein and sedimentary (found in pyritiferous sandstones) pyrite according to Sutherland (1967), but is higher than the shale, and lower than the vein pyrite samples for the Temagami area.

6.5.2.2 Copper

Copper content for the volcanoclastic pyrite range from 35 to 840 ppm with an average of 372 ppm, and range from 160 to 410 with an average of 305 for the shale pyrite. While this is within the range of VMS, sedimentary and vein pyrites analysed by Sutherland (1967), and of the VMS pyrites analysed by Roberts (1982) and Huston *et al.* (1993), they are significantly below the mean of 4200 ppm (Sutherland 1967) and 3185 ppm (Roberts 1982) Cu for VMS deposits. The average Cu content for the volcanoclastic pyrite is higher than for the shale pyrite but less than the vein pyrite of the Temagami

study area. The volcanoclastic pyrite copper values are more comparable to vein and sedimentary deposits than for massive sulphide deposits in which copper content in pyrite is in the several thousand ppm range.

TABLE 6-1
Trace element contents (ppm) in pyrite from the Temagami area

sample	host rock	Ag	Cu	Zn	Co	Ni	Co/Ni
ss11	shale (standard)	5	220	110	160	152	1.1
PY-1	shale	5	160	80	200	140	1.4
PY-143	shale	20	410	75	140	200	0.7
PY-144	shale	6	300	98	240	500	0.5
PY-145	shale	20	350	120	84	68	1.2
PY-48	vein	55	750	4700	110	150	0.7
PY-32	volcanoclastic	42	450	280	76	68	1.1
PY-132	duplicate of #32	120	580	360	120	94	1.3
PY-47	volcanoclastic	18	280	170	660	870	0.8
PY-146	volcanoclastic	<5	35	35	270	11	24.5
PY-147	volcanoclastic	74	840	190	180	81	2.2
PY-148	volcanoclastic	41	48	40	340	540	0.6
	Average shale	13	305	93	166	227	1.0
	Ave. volcanoclastic	49	372	179	274	277	1.2*
	Average duplicate	81	515	320	98	81	
	S.D.	39	65	40	22	13	
	PREC %	48	13	13	22	16	

Average volcanoclastic = average of samples 32, 132, 47, 146, 147, 148.

Average shale = average of samples 1, 143, 144, 145

* does not include Co/Ni ratio for sample 146

Average duplicate = average of the duplicates 132, 32.

S.D. = standard deviation of the duplicates 132, 32.

PREC % = reproducibility = S.D./ average duplicate*100.

6.5.2.3 Zinc

Zinc has the largest range of any of the elements varying from 35 ppm to 360 ppm with an average of 179 ppm for the volcanoclastic pyrite, and a range from 75 to 120 and average of 93 ppm for the shale pyrite. These values for the volcanoclastic pyrites fall within the ranges defined by Sutherland (1967), Bajwah *et al.* (1987) and Huston *et al.* (1993), but the average of 179 ppm is ~4 times higher than the 44 ppm reported by Bajwah *et al.* (1987), and significantly lower than the reported 6322 ppm average for pyrite from VMS ore derived from New Brunswick (Sutherland 1967).

6.5.2.4 Cobalt and nickel

Several studies have used Co and Ni variation to discriminate between pyrites of various origins including submarine exhalative (VMS), hydrothermal veins produced during tectonism, but not necessarily a result of volcanism, and diagenetic sedimentary pyrite (eg. Carstens 1941; Hawley and Nichol 1961; Loftus-Hills and Solomon 1967). Recent investigations confirm that Co/Ni ratios can be used as a reliable indicator of the origins of pyrites (Price 1972; Bralía *et al.* 1979; Mookherjee and Philip 1979; Kaneda *et al.* 1986; Bajawah *et al.*, 1987). A summary of their findings is presented below and in Table 6-2.

Carstens (1941) studied both hydrothermal veins and sedimentary pyrite and concluded that vein pyrite has Co contents >400 ppm and a Co/Ni ratio of >1, whereas sedimentary pyrite has Co contents <100 ppm and Co: Ni ratios of <1.

Sutherland (1967) demonstrated that Co/Ni ratio for massive sulphide (VMS) pyrite is generally > 6 and as high as 200, with Co and Ni contents > 400 and >10 ppm respectively. Vein pyrite has Co/Ni ratios <6, with a highly variable range of Co and Ni

Table 6-2
Summary of Co and Ni contents in pyrite and their origins

Author	Type of Pyrite		
	VMS	vein	sedimentary
Carstens, 1941	-----	>400 ppm Co Co/Ni ratio >1	<100 ppm Co Co/Ni ratio <1
Loftus-Hills and Solomon, 1967	Low Ni Co < 10 ppm Co/Ni ratio <1 (with Pb and Zn minerals) Co/Ni >1 (no Pb and Zn minerals)	-----	Co/Ni <1
Sutherland, 1967	Co/Ni ratio 6 to 200 Co > 400 ppm Ni >10 ppm	Co/Ni ratio <6 variable Co and Ni contents	Co/Ni ratio 1 Co = 100 Ni = 100
Price, 1972	Co > 500 ppm Ni <100 ppm Co/Ni ratio 5 to 50	Variable Co and Ni contents Co/Ni ratio <5	Low Co and Ni contents Co/Ni <1
Bralia <i>et al.</i> , 1979	Co >200 ppm Ni < 100 ppm Co/Ni ratio 5 to 50	Variable Co and Ni contents Co/Ni ratio <5	
Kaneda <i>et al.</i> , 1986	-----	Large range 200 to 6000 ppm Co 100 to 3000 ppm Ni Co/Ni ratio <2	-----
This study	-----	Co = 110 Ni = 150 Co/Ni ratio 0.7	84 to 240 ppm Co 68 to 500 ppm Ni Co/Ni ratio 0.5 to 1.4

values. His one sedimentary pyrite example has a Co/Ni ratio of 1 and Co and Ni values of 100 ppm.

Price (1972) summarized the work of several authors and was able to compare Co and Ni for vein, sedimentary and volcanic (VMS) pyrite. He concluded that the Co and Ni content of vein pyrite tends to be variable, but the Co/Ni ratio is always <5 . Sedimentary pyrite generally has low abundances of Co and Ni, but the Co/Ni ratio is usually <1 . His work on various VMS deposits including Flin Flon, Noranda, Matagami and Chibougamau deposits, reveals Co content in pyrite from these areas is generally >500 ppm, Ni content is <100 ppm, and the Co/Ni ratio is between 5 and 50.

Bralia *et al.* (1979) demonstrated that Co and Ni contents of vein pyrite is variable, but that Co/Ni ratio is <5 , and Co and Ni contents >200 ppm and <100 ppm respectively, and a Co/Ni ratio between 5 and 50 for pyrite associated with volcanic exhalative (VMS) deposits.

The Kaneda *et al.* (1986) study of vein pyrites associated with Au-Ag mineralization reveals a large range of Co and Ni values but a consistent Co/Ni ratio of <2 .

In summary, hydrothermal vein pyrite is associated with variable Co and Ni values, but a consistent Co/Ni ratio of <6 . Sedimentary pyrite has low Co and Ni values, and a Co/Ni ratio generally <1 . Pyrites associated with volcanic exhalative processes generally have Co contents >200 , and more often >500 ppm, Ni contents <100 ppm, and Co/Ni ratios >5 and <200 . While there is considerable overlap of abundances of Co and Ni in the three types of pyrites, the ratio of Co/Ni is a very good indicator of the origin of the pyrite (Bralia *et al.*, 1979; Mookherjee and Philip, 1979; Campbell and Ethier, 1984; Kaneda *et al.* 1986; Bajwah *et al.* 1987).

Co and Ni values were obtained to compare the Temagami pyrite clasts with the above literature as a means of assessing their origin. The following discussion is based on the chemistry of pyrite clasts from the felsic volcanoclastic horizons including samples 32, 47, 146, 147 and 148. Comparative data for Co and Ni is given in Figure 6-1.

The cobalt content in the pyrites range from 76 to 660 ppm, a range which overlaps the contents previously discussed for VMS, vein and sedimentary pyrite. Nickel content ranges from 11 to 870 ppm, which is also a range of values that overlaps the three pyrite types. With the exclusion of sample 146, this set of pyrite has Co/Ni ratios ranging from 2.2 to 0.6. This suggests the pyrite samples from the volcanoclastics originate from veins or sediments. While sample 147 has a Co/Ni ratio of 24.5, the absolute abundances of Co and Ni suggests it too has a vein or sedimentary origin.

6.5.3 Shale- and vein-hosted Temagami pyrites

6.5.3.1 Vein pyrite

Sample (48) was obtained from a 20 cm by >10m long vein of pyrite along the railway track (L19+90W). This vein is oriented at 020/80 west, and is parallel to the various small faults in the area. It cross cuts the stratigraphy and has not developed the intense foliation of the LLDZ. The orientation and location of the vein suggests it may have formed as a result of dilation of a fault and was subsequently filled with sulphide rich hydrothermal fluids either during or post LLD.

Surficial weathering has resulted in the transformation of much of the pyrite to limonite. A thin section of the sample reveals pyrite is the dominant sulphide, but that traces of sphalerite and arsenopyrite are also present. Chemical analyses indicates a 4700 ppm Zn content which confirms the presence of sphalerite. In general, Ag, Cu and Zn are greater than for the average volcanoclastic pyrite, while Co and Ni and the Co/Ni ratio are

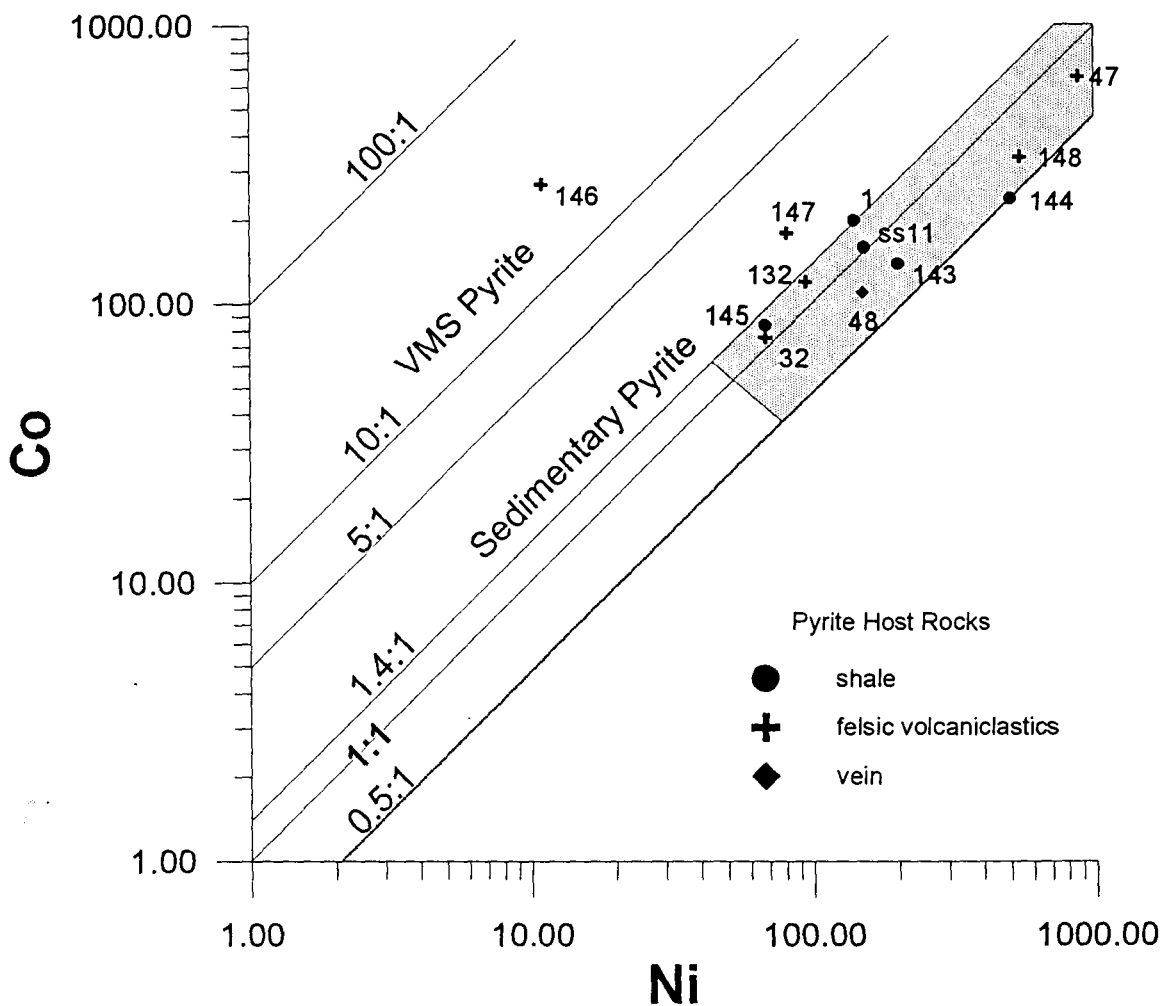


Figure 6-1: Co/Ni ratios for the pyrite samples from the study area. The shaded area defines the maximum and minimum Co/Ni ratios for pyrite from the shale samples. Note that all sample except 146 and 147 fall into this range. A Co/Ni ratio of 5 is considered the cut off point for VMS pyrite (>5) and sedimentary pyrite (<5).

all lower. The Co/Ni value for this sample is 0.7 which is within the range defined as vein by others.

6.5.3.2 Shale pyrite

The shale pyrite includes samples taken from the shale on the Trans Canada pipe line (143), Garbage Dump trench (144), the Fold Nose trench (145) and the south pit of the Sherman Mine (1) (see appendix A and sample location map back pocket for grid location).

Sample 1 was taken from part of the suite of pyrite bearing chert samples studied by Bowins and Crocket (1994). Their study concluded that this pyrite formed in sediments by bacterial sulphate reduction, and therefore could not have formed as a result of volcanic processes, although the sulphur may have originated from volcanism. The similarities between the textures and host rocks of samples 143, 144 and 145 to that of sample 1 suggests they too formed in their host sediments (the carbonaceous shales) by sulphate reducing processes.

All of the samples from the shale horizons (1, 143, 144 145), have Co/Ni ratios of ≤ 1.4 and average 1.0. This is within the range of values previously defined as sedimentary in origin. The Co and Ni contents in these pyrites range between 84 and 240 ppm, and 68 and 500 ppm respectively. The maximum and minimum Co/Ni ratios, 1.4 and 0.5 respectively, for the pyrites from the shale samples defines an envelope in which all of the shale pyrites fall (Figure 6-1).

6.6 Origin of the Pyrite Clasts

6.6.1 Chemistry

The origin of the pyrite clasts can be determined by comparing the absolute abundances and ratios of Co and Ni for the shale pyrite and vein pyrite to that of the pyrite clasts. With the exception of samples 146 and 147, all of the volcanoclastic hosted pyrites have Co/Ni ratios which are within the envelope defined by the Temagami shale pyrites. By taking into account experimental error of 20%, then on the basis of the Co/Ni ratio discriminator, only sample 146 could not be categorized as sedimentary.

As mentioned earlier, pyrite derived from veins has a Co/Ni ratio <5 . The only vein sample for the area (48) also falls within the shale pyrite envelope. While one cannot reject the hypothesis that the pyrite clasts came from eroded veins, the fact that the one vein sampled cross cuts the stratigraphy and is definitively post depositional to the volcanoclastics, indicates it is not the source for the volcanoclastic pyrites. Also, the low abundances of Cu and Zn in the volcanoclastic pyrites relative to literature values also suggests they do not originate from veins.

6.6.2 Incorporation of molybdenite into the pyrite

SEM analysis of sample 32 revealed the presence of molybdenite inclusions in the pyrite sphere. According to the literature, the presence of the molybdenite is an indication of sedimentary or vein origin for the pyrite. Sutherland (1967) indicates low abundances of <100 ppm Mo for all deposit types, from which the highest abundances are present in the vein and sedimentary pyrites. Raiswell and Plant (1980) have determined that trace element abundances in sedimentary pyrite are related to the source of the iron from which the pyrite formed. By this rationale a source of iron rich in Mo should enrich the pyrite with

Mo. Studies by Coveney *et al.* (1991) and Emerson and Huested (1991) indicate that Mo from sea-water will concentrate in sediments forming in anoxic conditions. Anoxic sediments should also be favourable for the formation of pyrite and marcasite during diagenesis. The pyrites from the shales of the study area may therefore have preferentially incorporated Mo in the form of molybdenite.

In contrast to such a possible origin, the extensive although localized introduction of Mo by the intrusion of the Strathy-Chambers batholith into the Temagami greenstone belt (Baknes 1990) might be responsible for the Mo in the pyrite sample. However, a variety of physical evidence suggests that this is not the case. The lack of any visible molybdenum in outcrops of the thesis area, and a separation distance of approximately three kilometers from the Strathy-Chambers batholith / greenstone contact, suggests there was not a wide enough dispersion of Mo from the batholith to have had an effect on the rocks of the thesis area. Even if this batholith is present at some depth below the thesis area, there are no molybdenite bearing veins in the immediate area to indicate mobilization of Mo into the area.

Textural evidence from sample 32 indicates that the molybdenite within the pyrite occurs as inclusions, not replacement of the pyrite. The only clear replacement of pyrite by molybdenite is where pyrite has clearly been recrystallized (Figure 6-3). Thus based on physical evidence, molybdenite seems to have been incorporated in the pyrites from the depositional environment in which the pyrite formed.

6.6.3 Textures

In reflected light the optical properties of the sulphide clasts are consistent with pyrite, yet some of the textures in the clasts are not strictly characteristic of pyrite. In particular the radiating or reniform and lattice structures are characteristic of marcasite

and not pyrite (Teodorovich 1961; Ramdohr 1980). These types of structures are described by Zimmermann and Spreng (1984) and are thought to have formed as a result of microorganic activity. Bowins and Crocket (1994) concluded on isotopic grounds that texturally similar pyrites from carbonaceous chert layers of the Sherman Mine formed as a result of organic activity.

The close similarities between the pyrite spheres of the Sherman Mine to those of the pyrite clasts suggests they may be related. While there is no marcasite in these samples, because of the metastable nature of marcasite as compared to pyrite (Gronvold and Westrum 1976), it is likely that diagenesis during subsequent burial of the shales, along with the regional metamorphism of the area has transformed any marcasite to pyrite.

Much of the pyrite is filled with micron scale pore spaces, similar to those described by Murowchick (1992). Murowchick describes these pores as forming during the inversion of marcasite to pyrite. During this inversion process to pyrite, as much as 2.6 volume percent pore space can form.

In many of the samples a lattice work of pyrite is present. This texture is similar to that of figure 15 of Zimmermann and Spreng (1984). In this example most of the sample is marcasite, and this type of texture is representative of termination of marcasite blades that intersect one and other.

Epigenetic replacement of volcanic clasts (eg. pumice or shards) by pyrite could be possible if hydrothermal activity was very common in the area. In this case, considering the large size of many of the clasts, replacement textures of volcanic clasts by pyrite should be readily observed. This is not the case, and the only replacement textures involving the pyrite are on millimeter scales and involve the local replacement of carbonate and quartz by pyrite.

The removal of material and replacement by pyrite could produce botryoidal and colloform textures, much as occurs during the formation of Mississippi Valley Type galena/ sphalerite/ pyrite deposits. However, an extensive network of cavities would be needed to transport enough fluids through the rocks to deposit pyrite as colloid. This is certainly not the case in this area, and this type of replacement is not feasible.

While Melnikovite pyrite can form concentric layering and radiating structures, it forms in low temperature environments and is often associated with marcasite (Ramdohr 1980). Such conditions would include sedimentary environments and very low temperature thermal springs. The nearest hospitable environment for such formation would be that of the carbonaceous shales.

Colloform textures and massive pyrite are common for many VMS deposits (eg Chen 1978; Barrett *et al.* 1992) and it is conceivable that these clasts are from such a deposit. However, the reniform structure suggests the clasts did not form in the high temperature environments associated with most VMS deposits.

The textural evidence is overwhelmingly in favour of a low temperature and/or organically produced marcasite and/or Melnikovite pyrite \pm pyrite origin for the spheres, and clasts in general.

Sample 145 is unique with respect to the other samples in that it is massive pyrite in the shale in the nose of the fold (Figure 3-2, and Plate 3-2a), and as mentioned earlier, the chemistry for this sample indicates it is sedimentary in origin. While this sample does exhibit strong remobilization textures, such as overgrowths and euhedralism of the pyrite, considering that this pyrite lies exclusively in the shale horizon and still has some convex and radiating textures preserved (Plate 6-3), it is considered to be sedimentary in origin . The massive nature of the pyrite is interpreted to have formed as the result of

remobilization of the pyrite from the surrounding shale into the nose of the fold during the folding event.

6.7 Source of Pyrite

With the exclusion of the Hydro debris flow, all of the pyrite clasts are found above the Lower Felsic horizon. The only shale horizons in the thesis area are found along the uppermost part of the Lower Felsic horizon, and these horizons contain pyrite with the aforementioned textures. As described in Chapter 4, the Upper Felsic horizon is made up of a series of thin debris flows, within which the pyrite clasts are concentrated along the base of the flows. By inducing a debris flow higher up in the water column and having it sweep down the flanks of a submerged volcano, these debris flows could travel lengthy distances into deeper water. It is in this deeper water that the organic rich muds were being deposited. Since this would likely be a reducing environment, marcasite and pyrite spheres could form in the muds. As a debris flow sweeps across the muds, it would entrain the pyrite clasts and tend to leave the mud in suspension in the water column. The debris flow would continue to carry the pyrites until it loses its momentum and stops.

While much of the mud would go into suspension, some of it would be entrained in the debris flow. While turbulence within the flow would be responsible for distributing the mud throughout the flow, debris deposited proximal to the source muds would be expected to contain some of the mud fragments (now shale). Such fragments are visible to the east of the Hydro debris flow and along L19W (Figure 4-3), and some of them still contain pyrite spheres (Plate 6-5).

In summary, on the basis of the textural and chemical evidence for the pyrites, the presence of spherical pyrite in shales in the area, and the presence of these shales with

spherical pyrites in the debris flows, it is concluded that most if not all of the pyrite clasts in all of the felsic horizons have originated from shales stratigraphically equivalent to those associated with the Lower Felsic sequence.

CHAPTER 7

VOLCANOLOGICAL DISCUSSION

7.1 Petrology

7.1.1 Definition of volcanoclastic

Throughout the previous Chapters the terms volcanoclastic and volcanoclastic debris have been used to describe the fragmental felsic volcanic rocks in the study area. Cas and Wright (1988) define volcanoclastic as a non-genetic term for any fragmental aggregate of volcanic parentage irrespective of origin. The term pyroclastic should only be used when it can be demonstrated that the mode of fragmentation and mode of transport of the fragments is a direct result of eruptive activity (Cas and Wright 1988).

While Fyon and Crocket (1986) have referred to the rocks of the study area as pyroclastic, many of the fragments exhibit a subrounded nature suggesting they have been deposited by secondary means, and are not primary pyroclastic rocks. Much of the fragmental rock has been deformed by the LLDZ destroying primary textures and elongating clasts such that they appear angular even though less deformed areas indicate they are subrounded (see Chapter 4 for discussion).

Cas (1992) indicates that most primary fragmental rocks are deposited in marine environments with water depths shallower than 500m. The Upper and Lower Felsic horizons contain a relatively thin unit of fragmental rocks with subordinate amounts of carbonaceous shales and rhyolitic lavas surrounded by pillow lavas with low vesicularity. This indicates a relatively deep marine environment for the fragmental rocks, further suggesting they are not primary pyroclastic deposits.

For the aforementioned reasons, it is suggested that the Upper and Lower Felsic, Sherman Gate and Link Lake horizons all be referred to as volcanoclastic in future studies.

7.1.2 Pumice

Bennett (1978) indicates that dark wisps present in the felsic volcanoclastics are pumice. While pumice, recognized by the presence of amygdules, is present in some of the felsic volcanoclastics or the Upper Felsic horizon, some of the dark wisps described by Bennett may in fact be pieces of shale. In thin section some of the samples do superficially resemble flattened pumice, but they are entirely replaced by chlorite and do not contain vesicles. In the case of the Upper Felsic horizon, they occur in greatest abundance in the beds which have pyrite clasts. It has already been established that these pyrite clasts originate from shales, and for this reason it is likely that much of the flattened pumice in this horizon are actually pieces of shale.

7.1.3 Proximity to a vent

It may be possible to classify the Upper and Lower Felsic horizons in terms of proximity to a central vent. Proximal, distal and medial are terms used to indicate deposition of volcanoclastic material very near, very far and at intermediate distances from a vent. These terms are based on relative locations; however, Williams and McBirney

(1979) indicate proximal deposits lie between 5 and 15 km from a central vent, and distal deposits are >15 km from a vent.

De Rosen-Spence *et al.* (1980) have identified proximal to distal facies variations, relative to the point of extrusion, in Archean lavas. The proximal facies is homogeneous, consisting mainly of massive lava with a thin capping of flow breccia. The median facies is heterogeneous, consisting of lava lobes and fragments of lobes in hyaloclastite microbreccia. The distal facies consists mainly of breccia composed of lava lobe fragments in a matrix of autobreccia and hyaloclastite.

The Garbage Dump trench consists of a ~8.5 m section of massive lava capped with ~9 m of hyaloclastic material (including the black rhyolite). The Hydro Station lava flows total ~10 m but do not appear to have a capping of hyaloclastics. This suggests the Hydro Station is relatively proximal to its point of extrusion, while the Garbage Dump is medial to its point of extrusion.

At the Garbage Dump trench the lava flow has a total thickness of ~17 m while the Hydro Station lavas are ~10 m. One would expect that a rhyolite flow proximal to a vent would be at least as thick if not thicker than the same flow farther from the vent. This suggests that both areas, while related to the same magma source, may not have been extruded from the same vent or fissure. It is possible that the rhyolite lavas at the Garbage Dump and the Hydro Station erupted from fissures along the structural margin of a cauldron, rather than from the main vent of a cauldron, producing several lobes of lava. Thus the massive lavas at the two ends of the study area could be from different lobes of rhyolite.

Relative to the point of ejection, proximal and distal facies variations for primary subaqueous volcanic fragmental rocks is usually defined by the size, shape, sorting and abundance of volcanic material (eg. Fisher and Schmincke 1984; Cas and Wright 1988).

Proximal deposits are usually thick with abundant large clasts and poorly sorted, while distal deposits are dominated by a small grain size, better sorting and parallel laminations. The presence of deep-water hemipelagic muds can be an indication that fragmental material has travelled some distance from a vent.

According to these criteria, the larger clasts found at the Hydro Station suggests a proximal deposit, while the presence of the carbonaceous shales at the Garbage Dump suggests it is at some distance from the vent. The presence of poor grading and parallel laminations in the Upper Felsic horizon suggests it is a medial deposit. Since the fragmental rocks were deposited by secondary processes, these proximity characteristics are related to the point of mass movement, which may have been at some distance from a central vent.

Even though the fragmental rocks in the Upper and Lower Felsic horizons have been deposited by epiclastic processes, we can still make inferences to proximity of a central vent. The preserved shales and greywacke at the Garbage Dump area indicate it was not affected by volcanism to the extent the Hydro Station was, and must have been more remote from volcanic activity. Thus, the Garbage Dump is more distal from a central vent than the Hydro Station area.

7.2 Chemistry

It has already been demonstrated that the Upper and Lower Felsic horizons are of tholeiitic magmatic affinity, and from the same parent source. Fyon and Cole (1989) indicated that the granitic phase of the Strathy-Chambers batholith has a similar REE pattern to their sequence B, which includes the Upper and Lower Felsic horizons. Baknes (1990) confirmed the flat REE pattern ($[La/Yb]_n < 2$) with a significant negative Eu

anomaly ($\text{Eu}/\text{Eu}^* < 0.1$) in the marginal phases of the Strathy batholith. He also determined that the Zr/Hf ratio is ~ 30 . These values are nearly the same as for the Upper and Lower Felsic horizons, suggesting the Strathy-Chambers batholith is the parent for these rocks.

The samples taken along Strathy road south of Temagami (samples 41, 103, 105) have a REE pattern similar to that of the quartz feldspar porphyries (QFP) (Figure 7-1). Thus, the QFP are apparently not from the granitic phase of the Strathy-Chambers batholith, but rather may be related to sequence E of Fyon and Cole (1988) and therefore related to the Iceland Lake trondhjemite or the trondhjemitic phase of the Strathy-Chambers batholith.

The Link Lake and Sherman Gate horizons, while poorly understood in a petrologic sense, have differences in their chemical signatures indicating they are from different magma sources. Although all of the samples from these horizons have similar REE patterns (45, 108, 117, 120, 121), sample 45 and 108 both have a weak negative Eu anomaly and the others do not (Figure 5-8b). The $[\text{La}/\text{Yb}]_n$ ratios for the Link Lake and Sherman Gate horizons (< 11 Table 5-3) are less than for the QFP and south Temagami samples (most > 16) and suggests they are not related to the same parent magma.

Originally Fyon and O'Donnell (1987) and Fyon *et al.* (1988) had correlated sequences B and E on the basis of lithology and apparent repetition on either side of the Tetapaga syncline. Subsequently Fyon and Cole (1989) correlated the felsic and mafic volcanics of sequence A and E on the basis of lithology and REE chemistry. The present data indicates that the chondrite-normalized REE pattern of the QFP are similar to that of sequence E. Therefore, as a complete package of rocks sequence B and E are not one in the same, but rather sequence B may represent a zone of volcanic accumulation influenced

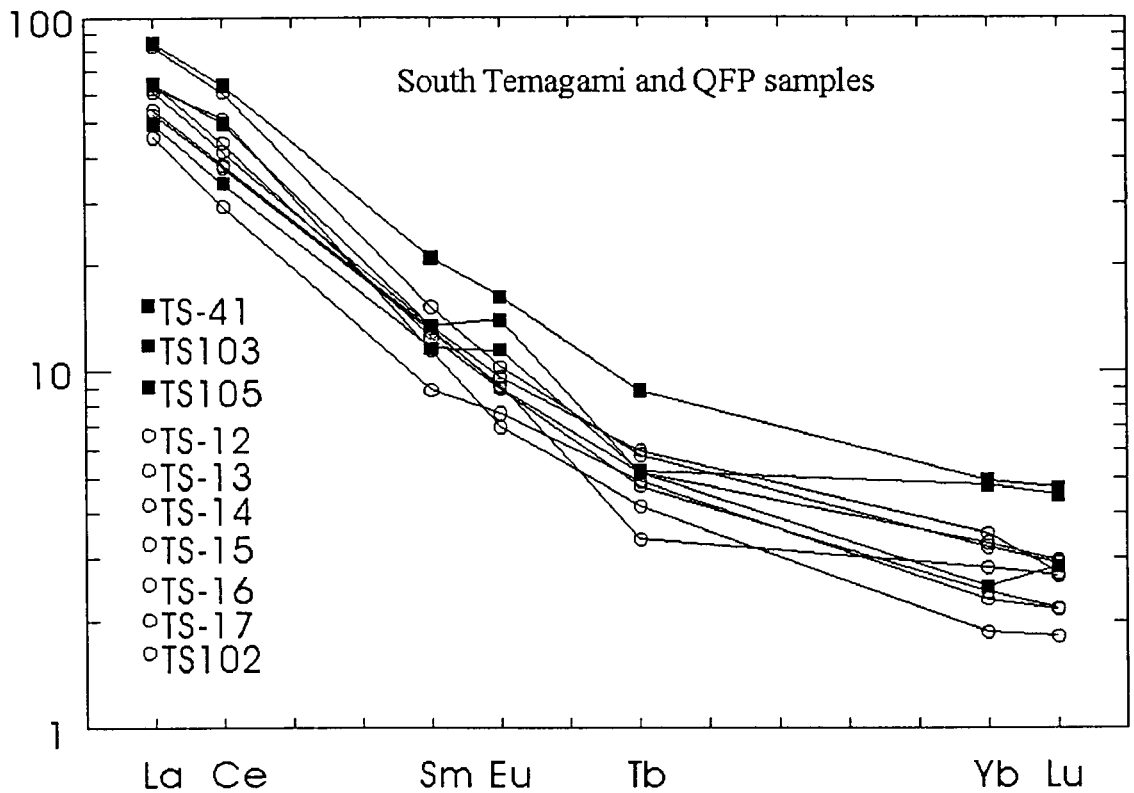


Figure 7.1: REE chondrite normalized plot comparing the south Temagami samples (■) to the QFP (○) demonstrating the similar relationship between the two rock types.

by volcanism from more than one center. These sources may be the Iceland Lake Pluton and the various phases of the Strathy-Chambers batholith.

As mentioned in section 5.5.2, no past study of the Temagami greenstone belt has definitively stated that there are tholeiitic felsic volcanics present in this greenstone belt. Hurley (1985), on the basis of petrology, demonstrated samples which were identified as tholeiitic on the Jensen cation plot are calc-alkaline. However, several samples identified as calc-alkaline by Hurley on the Jensen cation plot are identified as tholeiitic on the Y vs

Zr plot of MacLean and Barrett (1993) (eg. TDH-22, 25, 26, 29, 30; see Hurley 1985). These samples have a Zr/Y ratio of ~4, which is clearly tholeiitic on the Y vs Zr plot. This indicates alteration has played an extensive role in changing the chemistry of the Temagami rocks, and may have lead to the misidentification of the magmatic affinities of other rock units in this area as well.

7.3 Geologic Reconstruction of the Thesis Area Rocks

The stratigraphic sequence of the thesis area rocks from the base to the top is as follows: tholeiitic basalts, calc-alkaline basalts, tholeiitic rhyolites, calc-alkaline mafic sill, calc-alkaline QFP, calc-alkaline basalts, calc-alkaline volcanics (Figure 7-2). However, this stratigraphic sequence is not the original eruptive order for these rocks.

There are no major chemical differences between the Lower Felsic horizon and the Upper Felsic horizon suggesting they are part of the same horizon. The physical separation of these rocks is due mainly to the presence of the Sill, indicating the Lower and Upper Felsic horizons were originally in contact with each other, possibly separated by a basaltic flow throughout their entire length.

Chemical and stratigraphic evidence indicate the QFP, and in particular the Milne Vent was intruded into the Felsic horizons and into the Link Lake horizon (see field map back pocket and Figure 7.2). Thus the emplacement of the QFP occurred after the deposition of the Link Lake horizon.

7.3.1 Depositional history

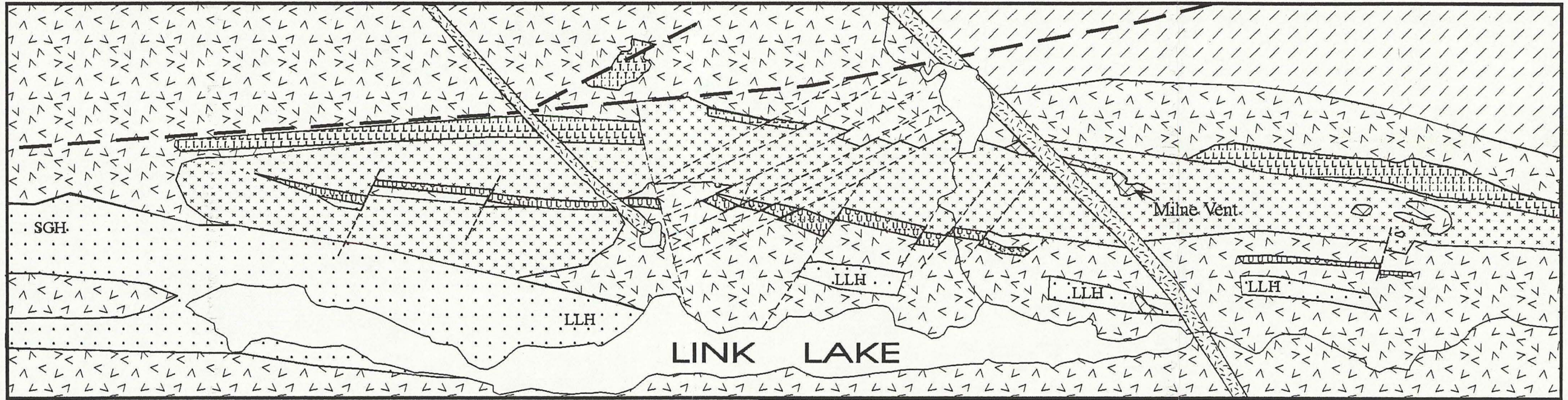
Prior to the formation of the Lower Felsic horizon, both tholeiitic and calc-alkaline volcanism had already deposited a thick sequence of pillow basalts, sheet flows and basaltic fragmental rocks. The initiation of felsic volcanism is marked by the

Figure 7.2: Geologic map of the thesis area indicating present stratigraphic position of the main horizons. Correlation of the felsic horizons is based on trace element chemistry. The geology on this map is a simplification of the field map. Stratigraphic top is to the south.



79° 50

79° 48



LINK LAKE

SCALE



79° 50

79° 48

LEGEND

- | | | | |
|--|-------------------------------------|--|---|
| | diabase | | Upper (U) and Lower (L)
Felsic tholeiitic metavolcanic |
| | mafic to ultramafic intrusive rocks | | mafic calc-alkaline metavolcanic |
| | felsic calc-alkaline metavolcanic | | mafic tholeiitic metavolcanic |

SYMBOLS

- LLH Link Lake horizon
- SGH Sherman Gate horizon
- — regional fault
- - - - local fault

deposition of basaltic dominated debris flows. These debris flows are present at both the Hydro Station and Garbage Dump trenches indicating the volcanic process which initiated these debris flows were wide spread. The apparent abrupt termination of the debris flow against a topographic high in the underlying basalts at the Hydro Station, suggests much of the deposition of the debris flow was topographically controlled. The presence of the thick package of fragmental material at the Hydro Station and the presence of the carbonaceous shale at the Garbage Dump suggest the Hydro Station area may have been more proximal to a central vent than the Garbage Dump.

Rhyolitic lava flows were emplaced in both locations; however, it appears that the lava flow at the Garbage dump may have been emplaced after some carbonaceous shale had been deposited. The textural characteristics of the rhyolite at the Garbage Dump suggests that as the rhyolite lava was moving over this area it entrained both fragments from the lower debris flow, and pieces of the carbonaceous shale, as well as forming a hyaloclastic skin. (Figure 4-1 and Plate 4-3). The presence of the carbonaceous shale and greywacke at the Garbage Dump indicate there was a relatively long interval during which volcanism did not affect this area.

With the removal of the Sill and the Milne Vent, the next rock type found above the Hydro Station area are basaltic lavas. No chemical data is available for this basalt, so it has not been determined if this is truly a calc-alkaline basalt as mapped by Fyon and Crocket (1986) or tholeiitic. Immediately overlying this basalt is the Upper Felsic horizon.

The Upper Felsic horizon marks the resurgence in volcanism much in the way the lower debris flows at the base of the Lower Felsic horizon marked the initiation of felsic tholeiitic volcanism in this area. Relative to the lower debris flows, the Upper Felsic horizon is several times thicker. This suggests there was a relatively large accumulation of tholeiitic pyroclastic rocks somewhere in the Temagami greenstone belt, possibly in the

area now east of the Hydro Station. There must have been a relatively long hiatus in volcanism to produce enough pyrite rich carbonaceous shale for it to be subsequently incorporated into several debris flows in the Upper Felsic horizon.

The end of felsic tholeiitic volcanism and epiclastic deposition of the rocks is marked by the presence of calc-alkaline basalts on top of the Upper Felsic horizon. How long the time interval was between the deposition of the Link Lake horizon and the intrusion of the Milne Vent and other QFP is not known. However, the Milne Vent did intrude into both the Upper Felsic horizon and the Link Lake horizon. The textural similarities between the small circular quartz feldspar intrusion at the Hydro Station and the QFP suggest they are a product of the same eruptive cycle.

Eventually this area was intruded by the Sill, separating the rocks which now make up the Lower and Upper Felsic horizons, and encompassing the Milne vent. The separation of the relatively thin Upper Felsic horizon from the Lower Felsic horizon suggests there was a structural weakness in this area which would preferentially allow for the Sill to intrude at this spot.

7.3.2 Silicification of the Upper and Lower Felsic horizons

The histograms of mass gains and losses (Figure 5-1-1) indicate there is no consistent mass gain (or loss) of one element relative to a mass gain (or loss) for another element in any individual sample. There is also no apparent pattern of gains and losses across the length of these horizons. Since the modal abundances of sericite, the second most abundant alteration mineral, is consistent throughout the area, and there are no mass gain and loss patterns, the alteration of the Upper and Lower Felsic horizons appears to be regional with respect to the study area. The individual mass gains and losses are then a

product of the nature of the lithology at the individual sample sites. For instance, fragmental samples with a greater surface area and higher permeability have a greater addition of Si than do the lava flows (23, 46) in comparison to sample 119. It is also possible that because the density of samples relative to the length of the map area is quite low, a pattern of mass gains or losses which would suggest a local alteration event (such as a bulls eye Si high) could not be discerned at this scale.

The cause of this Si alteration is not known with certainty. The Sill itself does not exhibit any Si addition in hand sample or thin section (ie. quartz veining or replacement of minerals by quartz), and with the exception of sample 3 and 102, neither do the QFP. Thus, the silicification associated with the LLDZ was not the cause of the primary silicification of the Upper and Lower Felsic horizons. If the intrusion of the Sill itself was responsible for the silicification, then there should be evidence of this in the Milne Vent. However, samples taken from this intrusive are of the least altered QFP, yet some stoped pieces of pillow basalts within the Sill are silicified. It is therefore likely that the silicification of the Upper and Lower Felsic horizons, and those basalts in between, occurred prior to the intrusion of the Milne Vent. Some basalts and felsic volcanics above the Upper Felsic horizon are also silicified, but it is not known if this silicification was produced during the silicification of the Upper and Lower Felsic horizons, or just from the LLD event.

7.4 Comparison to other Archean and Modern Volcanism

The Upper and Lower Felsic horizons were determined to be FIIIa high silica rhyolites. Several Phanerozoic examples of high silica rhyolites have been documented (eg. Cerro Toledo rhyolite, Stix *et al.* 1988). These rhyolites are crystal poor, with <20%

phenocrysts, contain >75 wt% SiO₂, have large negative Eu anomalies and low La/Lu ratios (Mahood and Hildreth 1983; Stix and Gorton 1993). These rhyolites are the products of the most fractionated liquids that collect at the top of a magma chamber (Stix *et al.* 1988). A main physical difference between the Archean and Phanerozoic equivalents is the Archean examples are dominantly subaqueous, and the Phanerozoic examples are subareal.

Archean examples of this rhyolite type are known to occur in the Rouyn-Noranda area, Quebec, and includes the Don, Waite, Amulet and Beecham rhyolites (Leshner *et al.* 1986), all part of the Blake River Group of the Abitibi greenstone belt. Most of the Noranda rhyolites are associated with and lie within the bounds of an interpreted shield volcano (Kerr and Gibson 1993). Those rhyolites which lie outside of this area are of FII type (Barrett *et al.* 1991b) rather than an FIII type, typical of most but not all of the cauldron sequence rhyolites (Leshner *et al.* 1986). Leshner *et al.* (1986) notes that this FIII characteristic is not present anywhere else in the Blake River group, suggesting it forms only under special conditions. Unlike the thesis area, the rhyolitic flows of the Noranda cauldron are up to 500m thick, volumes up to 3 km³ and areal extents of up to 22 km² (Gibson 1990). This indicates the Upper and Lower Felsic horizon are either derived from a minor volcanic center, or are distal from a main volcanic center.

Barrie *et al.* (1993) categorized several areas of the Abitibi greenstone belt into five groups as follows:

Group I is composed of bimodal, tholeiitic basalt-basaltic andesite, and high silica rhyolite. The basaltic andesites and high silica rhyolites are characterized by high abundances of high field strength elements and HREE, and [La/Yb]_n ratios from 0.8 to 3, and all known examples host a VMS deposit.

Group II is composed of bimodal, transitional tholeiitic to calc-alkalic andesite and rhyolite, characterized by intermediate high field strength element contents and $[La/Yb]_n$ ratios from 1-4. All known examples host a VMS deposit.

Group III contains calc-alkalic andesite-rhyolite with relatively low high field strength element and REE contents, and $[La/Yb]_n$ ratios from 3-9, and only one example from the Abitibi greenstone belt is known to host a VMS deposit.

Group IV are calc-alkalic basaltic andesite to rhyodacite, with low high field strength element and $[La/Yb]_n$ ratios from 8-20, and with no known VMS deposits.

Group V are mafic to felsic alkalic volcanic rocks with $[La/Yb]_n$ ratios from 12-62, and are not known to host a VMS deposit.

Using the Th/Yb vs Ta/Yb diagram of Pearce (1983) for basaltic magmas, Barrie *et al.* (1993) determined group II volcanics are produced in a rifting environment, specifically related to rifted island arc volcanism. Using his criteria, the Upper and Lower Felsic horizons are classified as group II type volcanics, indicating they are a product of arc volcanism. In comparison to the data of Macdonald *et al.* (1990), the rare-earth element pattern for the tholeiitic rhyolites of the study area are similar to anomalous mid ocean ridge rhyolites of eastern Iceland. However, Barrie *et al.* (1993) feel that group I volcanics are more comparable to the anomalous mid ocean ridge rhyolites. Jackson *et al.* (1994) have categorized the Temagami greenstone belt as an IRON-type supracrustal assemblage (ie. a supracrustal assemblage of which a major proportion is banded iron formation) which formed in an arc tectonic environment. Thus, the present data would suggest the study area was formed in an arc environment.

7.5 Summary

Despite the apparent angularity of clasts along the LLDZ, subrounding of clasts in areas away from the LLDZ, the debris flow characteristics of the beds and inferred deep water depositional setting for these rocks indicates the term volcanoclastic should be used in reference to the fragmental rocks from this area. While pumice is present in these fragmental rocks, much of the so called flattened pumice is associated with the pyrite clasts. Since these pyrite clasts originate from shales, it is likely much of the flattened pumice in these horizons are actually pieces of shale.

The thesis area consists of both tholeiitic and calc-alkaline felsic volcanoclastic rocks, deposited in proximity to an island arc. The tholeiitic felsic volcanics are related to the Strathy-Chambers batholith, and maybe a product of rift associated volcanism. The QFP are intrusives which post date the Link Lake horizon, and are either related to the Iceland Lake pluton or the trondhjemite phase of the Strathy-Chambers batholith. Both volcanoclastic and extrusive felsic tholeiites indicate the Hydro Station is proximal to a central vent relative to the Garbage Dump.

CHAPTER 8

VOLCANOGENIC MASSIVE SULPHIDE EXPLORATION

8.1 Introduction

As was mentioned in section 1.4, the felsic horizons along the Sherman Mine road, has a flat REE pattern which suggests these horizons are favourable host rocks for an Archean VMS deposit. What follows is a discussion of how the chemistry and textures of volcanic rocks can be used to define potential locations of VMS style mineralization, and how this relates to the rocks of the study area.

8.2 Definition and Origin of a VMS Deposit

Volcanogenic massive sulphide deposits (VMS), also known as volcanic hosted massive sulphide deposits (VHMS) and volcanic-associated massive sulphide deposits (VMS), are a subdivision of a more general class of massive sulphide deposits and form as a direct consequence of volcanic activity (Franklin *et al.* 1981). The oldest example of this class of deposit is located in the pre-3700 Ma supracrustal rocks of Greenland (Appel 1979) and the youngest equivalent are the present day black smokers. Of relevance to this study are those VMS deposits which are Precambrian in age.

8.2.1 Precambrian VMS deposits

The following is a summary of the characteristics of a Precambrian VMS deposit as described by Lydon (1990*a, b*), and Figure 8-1 is provided as a simplified cross section of an idealized VMS deposit for reference to the following discussion.

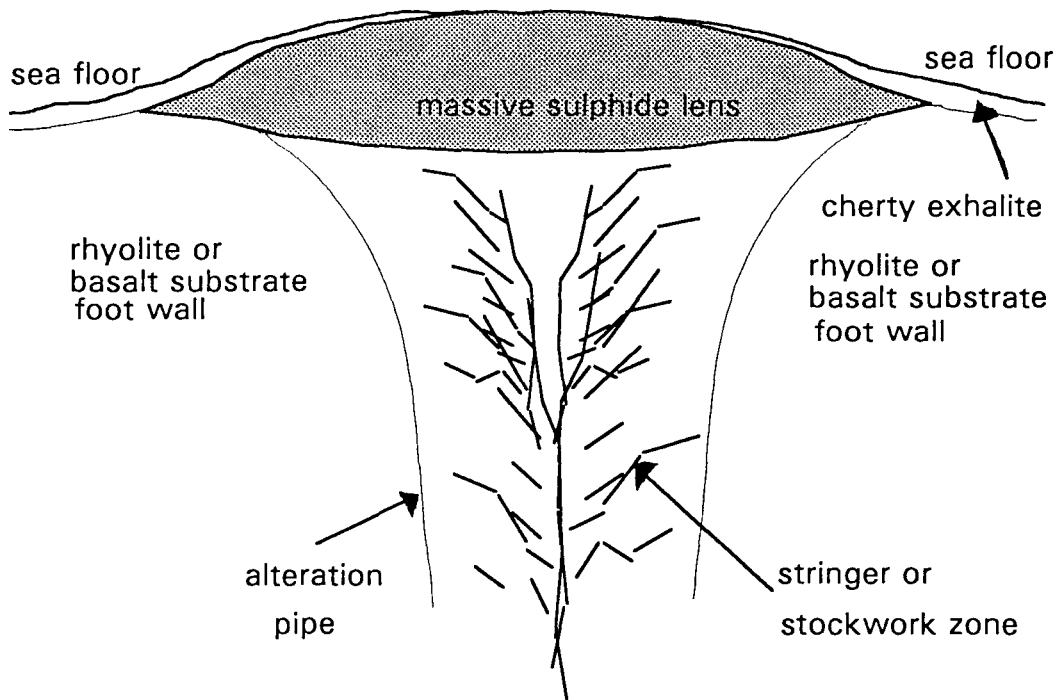


Figure 8-1: Idealized cross section of a VMS deposit .

Precambrian VMS deposits are dominated by felsic volcanic rocks overlain by mafic volcanic rocks, and are often overlain by sedimentary rocks. The ore from these deposits is stratiform, and is usually located directly on top of the felsic volcanics. Whether these deposits formed in relation to plate boundaries is not known for sure, although Sillitoe (1982) states that the generation of rhyolite-hosted massive sulfide deposits is restricted to extensional habitats. Stringer zones of mineralization and large alteration pipes have been observed in many of these deposits, but are not present in others. The lithology of these deposits indicates they formed subaqueously.

The formation of a VMS deposit can be divided into two general groups: 1) those deposits that formed directly over the hydrothermal channel way, termed proximal deposits; 2) those that formed away from the hydrothermal channel way, termed distal deposits. The size, shape, distribution and mineral content of a VMS deposit is related to hydrothermal fluid interaction during the formation of a deposit more than to the underlying lithology (Lydon 1990*b*). In this way, we can use the chemical signature and alteration minerals produced by the hydrothermal fluids, to locate the proximity to the alteration pipe of a VMS deposit.

The hydrothermal channel way is commonly referred to as the alteration pipe (Figure 8-1). It is in this area that hydrothermal fluids, rich in metals and other elements, travel toward the surface and interact with sea-water depositing various sulphide and other alteration minerals. Some of these minerals are deposited below surface in a stock work of veins, some are deposited on the ocean floor in a mound and some are dispersed in the water column. If, as a result of primary sea-water hydrothermal fluid interactions, or post depositional tectonism, a VMS deposit is not overlying the alteration pipe, then chemical signatures produced by the hydrothermal fluids may not lead the prospector to the VMS deposit.

Textural features such as the size of clasts within fragmental rocks, the presence of sulphide clasts, abundant mineralized veins, changes in mineralogy (chloritization, silicification and sericitization), the presence of cherty exhalative horizons and the presence of a large accumulation of base metals, all help to determine proximity to a VMS deposit. It is not the scope of this study to explain all the characteristics of VMS deposition, but rather to compare both the chemical and textural features observed in known VMS deposits to those of the study area, as an indication of the potential for VMS occurrence in this area.

8.3 VMS Potential of Temagami Rocks

A number of geochemical and geological properties of the Temagami rocks from the thesis area are relevant to the question of whether this area is likely to host a VMS deposit. The most important factors including composition, especially REE, of the rhyolites, rock alteration characteristics and lithological characteristics of the area are considered below.

8.3.1 REE rhyolite classifications

Geochemical methods to evaluate the potential of volcanic horizons to host VMS deposits have been researched by several authors (eg. Campbell *et al.* 1981*b*; Thurston 1981; Campbell *et al.* 1982*a, b*; Leshner *et al.* 1986; Barrie *et al.* 1993). All of their research is based on a comparison of high field strength and rare-earth element chemistry of felsic volcanic rocks which do and do not host VMS deposits. The work of Leshner *et al.* (1986, see p.74 this thesis) summarizes the data for barren and mineralized rhyolites showing that mineralized rhyolites belong to the F category of Condie (1976, 1981).

In summary, FI type rhyolites are not known to host VMS deposits. FII type rhyolites are known to host VMS deposits, although there are very few Archean examples. With the possible exception of the Garrison felsic tuffs, Abitibi greenstone belt (Leshner *et al.* 1986), all known FIII type rhyolites host a VMS deposit, although not all of these deposits are economic.

Leshner *et al.* (1986) indicate the FI and FII are from deep magma chambers which have escaped significant fractionation. The FI rhyolite maybe a differentiate of a magma derived from a 10-20% melting of a eclogite (Condie 1976), and a FII rhyolite maybe a differentiate of a magma produced by a 30-60% melting of a siliceous granulite (Condie 1976). In contrast, FIII type rhyolites are differentiates derived from relatively shallow magma chambers which have undergone a plagioclase-dominated fractionation (Leshner *et al.* 1986). Partial melting and Rayleigh fractional crystallization modeling of andesites and rhyolites from the Noranda area were conducted by Ujike and Goodwin (1987). They indicate rhyolites classified as FIIIa by Leshner *et al.* (1986) are differentiates produced during shallow-level fractional crystallization of a 7-14% partial melt of a primitive mantle source.

All three of these rhyolite types have been recognized in the study area. The QFP and the south Temagami samples are FI, and therefore are unlikely to host a VMS deposit. The Link Lake and Sherman Gate horizons border on an FI to FII type and so have a low potential of hosting a VMS deposit. Thus, the horizons that are most likely to host a VMS deposit, are the Lower and Upper Felsic horizons if compared to all other mineralized FIII type rhyolites.

A second discrimination between productive and barren felsic horizons is outlined by Barrie *et al.* (1993, see p.131, this thesis). As mentioned in Chapter 7, this

discrimination classification is divided into five groupings. Groups I and II are productive horizons, group III maybe productive horizons and groups IV and V are barren horizons.

The felsic rocks of groups I and II correspond to groups FIIIb and FIIIa respectively (Barrie et al. 1993). In this respect the rocks of the Upper and Lower Felsic horizons are part of the group II type rocks and have a good potential of hosting a VMS deposit. The QFP's correspond to a group V type and are not expected to host a VMS deposit. As a bright note, the Link Lake and Sherman Gate horizons appear to be a group III type, and while there is only one known example in the Abitibi, there is a chance that these horizons might be the host to a deposit.

Most of the work of Lesher *et al.* (1986) and Barrie *et al.* (1993) is based on comparisons to greenstone belts in the Superior province with emphasis on the Abitibi, and therefore comparisons are related to these greenstone belts. It does not appear, however, that these classifications for barren and productive cycles necessarily apply outside the Abitibi greenstone belt let alone the Superior province. For example, using the negative Eu anomaly as an indicator of a fertile horizon (Lesher *et al.* 1986) the host rocks to the Scuddles VMS deposit, Australia, which lack negative Eu anomalies would be predicted to be barren (Whitford and Ashley 1992).

Even within the Abitibi a FII horizon may be more fertile than is perceived. Barrett *et al.* (1991a, b) indicate that the Aldermac and Horne mines respectively are FII types. For this reason the Link Lake and Sherman Gate horizons should not be excluded from VMS exploration without further chemical definition of these horizons.

8.3.2 Rock alteration characteristics

As was mentioned in Chapter 5, both major and trace elements can become mobile under conditions of hydrothermal alteration. The major elements can become mobile under low to moderate conditions of hydrothermal alteration (ie. low temperatures, weak chemical activity and small volumes of hydrothermal fluids), while it takes a greater degree of hydrothermal alteration to cause most trace elements, especially high field strength and rare-earth elements, to become mobile. By determining which elements have been mobile, and if this mobility has enriched or depleted the surrounding rocks of these elements, then it should be possible to determine proximity to the main hydrothermal system. In the case of a VMS deposit, it would determine proximity to the alteration pipe, and thus to the massive sulphide mound.

Considering that, on the basis of chemical classifications, the QFP lack any potential of hosting a VMS deposit, and there is not enough chemical definition of the Link Lake and Sherman Gate horizons, these horizons will be excluded from the following discussions.

8.3.2.1 Major elements

Since the major elements including Na, K, Si, Fe, Mg, Ca and Mn tend to be the most mobile of elements, any deviations in the chemical signatures of an altered rock as compared to the parent, should be most noticeable in these elements. MacGeehan and MacLean (1980) and Amor and Nichol (1983) noted that rocks outside and below the alteration pipe can exhibit additions of Si and Na and losses in Mg, Fe, Ca, Mn, and Ti for up to several kilometers from the alteration pipe, and that within the alteration pipe the reverse is true. However, Amor and Nichol (1983) note that these changes are not consistent from one deposit to the next.

Both the Upper and Lower Felsic horizons exhibit large increases in Si with minor changes in other elements compared to sample 119, and large increases in Si with nominal decreases in Fe, Ca and Na as compared to the Don rhyolite. There are no systematic increases or decreases in the major elements, suggesting these horizons, if related to a VMS deposit, are at a uniform distance from the main alteration pipe.

If the Upper and Lower Felsic horizons were permeable enough to act as reservoir rocks for a large geothermal system, then a regional uniform alteration pattern could be imparted on these rocks. This type of regional alteration has been documented for the Garon Lake VMS deposits (MacGeehan and MacLean 1980). In such a case, one would need to look at the overlying rocks for a chemical signature indicative of a discharge point (ie. alteration pipe).

8.3.2.2 Trace elements

Trace elements usually become mobile only in the alteration pipe, and any variability in their abundance would indicate a close proximity to the alteration pipe. In Chapter 5 it was determined that the trace elements appear to have remained immobile in this area (Table 5-1). However, it was also noted that the LREE of the Upper Felsic horizon have a greater range of values suggesting they have been slightly mobilized. If this is a consequence of hydrothermal alteration and not sample heterogeneity, then this signature is an indication the rocks are outside of an alteration pipe, although in relative terms not too far from the pipe (MacLean 1988).

In both the Upper and Lower Felsic horizons this LREE enrichment is observed in the eastern section of the study area. This enrichment is from sample 27 to 11 in the Upper Felsic horizon, and from sample 23 to 101 in the Lower Felsic horizon (see sample location map back pocket). The LREE enrichment in the eastern area of the thesis area

suggests there is a stronger alteration signature in this area, and the area may be more proximal to a VMS alteration pipe. Conversely, the City Dump Vent intrudes the stratigraphy just to the east of these samples, and may have mobilized the LREE in such a manner as to produce this signature.

8.3.3 Lithological characteristics

Lithological characteristics of the rocks, such as the presence of volcanoclastics, cherty tuffs, sulphide clasts, lava flows and shales, can be used to target an area for the exploration of a VMS deposit. While the presence of the features might increase the chance of finding a deposit, none of these characteristics alone guarantees the presence of a deposit.

Lydon (1990a) noted Precambrian VMS deposits are dominated by felsic volcanic rocks overlain by mafic volcanic rocks. This is the case for the Upper Felsic horizon which is overlain by basaltic calc-alkaline pillow and flow lavas. The Upper Felsic horizon is also dominated by volcanoclastic material, considered necessary by some for the formation of an Archean VMS deposit (eg. Gilmour 1965; Boldly 1968). Barrie *et al.* (1993) indicate the VMS deposits of the Abitibi are associated with felsic volcanic rocks with thicknesses greater than 150m. The maximum thickness of the Upper and Lower felsic horizons combined is ~75m. So, while the stratigraphy seems favourable to hosting a VMS deposit, the thickness is not.

As mentioned in Chapter 6, pyrite clasts are often an indication of proximity to a VMS deposit. However, it has already been determined that these clasts are not from a VMS deposit, and therefore are not a measure of proximity to such a deposit.

Spence (1975) and Scott *et al.* (1983) indicate cherty tuffaceous exhalites can be used as exploration guides for VMS deposits. Spence (1975) indicates that cherty tuffs at

the Vauze sulphide deposit, Noranda, lie between the massive sulphide (below) and pillowed andesite (above). Cherty tuffs were recognized by Fyon and Crocket (1986) and are present in the Upper Felsic horizon (samples 33 and 36). These tuffs are not laterally continuous, and in some cases may be the upper most part of a debris flow cycle (Chapter 4). While these tuffs do not indicate proximity to a VMS deposit, they could be used as a marker horizon for exploration purposes.

Cas (1992) suggests that some common properties which can be used to evaluate the potential prospectivity of ancient volcanic successions for VMS deposits includes: 1) facies characteristics which indicate a deep water setting, including turbidites, pillow lavas and hemipelagic muds; 2) quenched-fragmented felsic lavas such as hyaloclastites. These features are present in the study area horizons. The Lower Felsic horizon has black shales and hyaloclastics, and pillow lavas are present below and above the Upper and Lower Felsic horizons, indicating favourable conditions for the presence of a VMS deposit.

Hopwood (1976) and Berge (1981) indicate that quartz porphyritic felsic rocks (referred by them as quartz-eye-bearing) are closely related to the occurrence of VMS deposits, and can be used as a prospecting guide. The formation of such rocks is controversial, but may be a result of metamorphism, hydrothermal alteration, or rapid intrusion. There are several quartz porphyry rocks in the Temagami study area. The most easily recognized is the QFP including the Milne Vent, but the chemistry suggests it is not a likely host to a VMS deposit. Most of the rhyolite flows have quartz phenocrysts, but these are primary quartz crystals. Sample 117 also has quartz-eyes, and traces of pyrite; however, it is not laterally extensive and is a FII type rock. In all, the use of quartz phenocrysts to determine the proximity to a VMS deposit does not appear to be a useful tool in this area.

The Sill is another consideration for determining host potential for a VMS deposit. Campbell *et al.* (1981a) state most Canadian Precambrian massive sulphides have large subvolcanic sills in their footwalls. These sills are thought to be the heat engines that drive hydrothermal systems that forms the VMS deposit. As such these sills play a passive role, but could be used to identified potential locations of VMS deposits. It has been suggested that these sills are intruded contemporaneously with the deposition of volcanic material which hosts the deposits, and has a similar REE pattern to these host rocks.

While only one sample was analysed from the Sill (05) it has a rare earth pattern similar to the Link Lake and Sherman Gate horizons. The overall abundance of the REE is lower than for these horizons, but it is too dissimilar to the Upper and Lower Felsic horizons and the QFP, to be related to them. As such, the area directly above the Sill, and possibly along the upper contact of the Link Lake and Sherman Gate horizons could be a good area to conduct further exploration for a VMS deposit.

8.4 Comparison of the Temagami Thesis Area to other VMS Host Rocks

Of the various Archean examples of VMS deposits, the Upper and Lower Felsic horizons appear to be equivalent to a Noranda Type deposit. The Noranda Type deposit has FIIIa rhyolites (Leshner *et al.* 1986) and is classified as a group II type (Barrie *et al.* 1993). They contain mafic and felsic flows and hyaloclastites (Morton and Franklin 1987), can contain tuffaceous exhalites (Spence 1975; Scott *et al.* 1983), and often have a larger quartz (silica) semiconformable alteration halo in the foot wall rocks (Morton and Franklin 1987). In contrast, the Matabi type VMS deposit is a FII type (Leshner *et al.* 1986), and the Kidd Creek type VMS deposit is a FIIIb type (Leshner *et al.* 1986) and a group I (Barrie *et al.* 1993).

The only major differences between the Noranda type and the Upper and Lower Felsic horizons are the very thin nature of the latter and apparently only one cycle of FIIIa volcanism for the Upper and Lower Felsic horizons.

8.5 Conclusions

Based on the FIIIa and group II chemical classifications alone, of all the felsic rocks in the study area, the Upper and Lower Felsic horizon have the greatest potential for hosting a VMS deposit. The relative uniformity of the alteration mineralogy along these horizons suggests if one main conduit cross cuts the stratigraphy, it is at an equal distance from any section of these horizons. It is also possible that these rocks served as a reservoir rock for a geothermal system, thus producing the relatively homogenous alteration pattern.

The REE chemistry, specifically the LREE chemistry suggests a slight enrichment of these elements has taken place towards the eastern extent of the study area. Therefore a alteration pipe may be present in the far eastern section of the study area.

The presence of tuffaceous cherts, hyaloclastites, carbonaceous shales and pillow lavas are all indications that this area could host a VMS deposit. As such, the tuffaceous cherts and the contact between the Upper Felsic horizon and overlying basalts could be used as a marker horizon for further exploration.

The presence of the Sill indicates it may have been a heat source for a hydrothermal system, and thus a VMS deposits could be located somewhere above it. Since the chondrite normalized REE pattern of the Sill is most similar to the FII volcanics of Link Lake and Sherman Gate horizons, then if the Sill did act as a heat source for a hydrothermal system, the VMS deposit produced by such a system would be located along the Link Lake and Sherman Gate horizons, and directly above the Sill.

The QFP, which includes the Milne and City Dump vents, is a FI type and group V type felsic volcanic. Since these types of volcanic rock are not favourable host for VMS deposits, it is recommend they not be used as guides in the exploration for VMS mineralization.

Since the pyrite clast are determined to be sedimentary in origin, and they lack any significant amounts of Cu and Zn, they should not be used as a guide to locating VMS deposits.

REFERENCES CITED

- Alderton D.H.M., Pearce, J.A. and Potts, P.J. 1980. Rare earth element mobility during granite alteration: Evidence from southwest England. *Earth and Planetary Science Letters*, **49**: 149-165.
- Amor, S.D., and Nichol, I. 1983. Identification of diagnostic geochemical alteration in the wallrocks of Archean volcanic-exhalative massive sulfide deposits. *Journal of Geochemical Exploration*, **19**: 543-562.
- Appel, P.W. 1979. Stratabound copper sulfides in a banded iron-formation and in basaltic tuffs in the early Precambrian Isua supracrustal belt, west Greenland. *Economic Geology*, **74**: 45-52.
- Bajwah, Z.U., Seccombe, P.K. and Offler, R. 1987. Trace element distribution, Co:Ni ratios and genesis of the Big Cadia iron-copper deposit, New South Wales, Australia. *Mineralium Deposita*, **22**: 292-300.
- Baknes, M.E. 1990. A structural-geochemical investigation of a mineralized breccia and associated vein system at the contact between the Strathy Batholith and the Temagami Greenstone Belt, Strathy TWP., Ontario. Unpublished M.Sc. thesis, McMaster University, Hamilton, Ontario, 331p.
- Barlow, A.E. 1907. Second edition of a report on the geology and natural resources of the area included by the Nipissing and Timiskaming Map-Sheets. *Canadian Geological Survey, Report Number 962*, 303p.
- Barrett, T.J., Cattalani, S., Chartrand, F., and Jones, P. 1991*a*. Massive sulfide deposits of the Noranda area, Quebec. II. The Aldermac Mine. *Canadian Journal of Earth Sciences*, **28**: 1301-1327.
- Barrett, T.J., Cattalani, S., and Maclean, W.H. 1991*b*. Massive sulfide deposits of the Noranda Area, Quebec. I. The Horne Mine. *Canadian Journal of Earth Sciences*, **28**: 465-488.

- Barrett, T.J., Maclean, W.H., Cattalani, S., Chartrand, F., Hoy, L., and Riverin, G. 1991c. Massive sulfide deposits of the Noranda area, Quebec. III. The Ansil Mine. *Canadian Journal of Earth Sciences*, **28**: 1699-1730.
- Barrett, T.J., Cattalani, S., Hoy, L., Riopel, J., and Lafleur, P.J. 1992. Massive sulfide deposits of the Noranda area, Quebec. IV. The Morbrun Mine. *Canadian Journal of Earth Sciences* **29**: 1349-1374.
- Barrett, T.J. and MacLean, W.H. 1994. Chemostratigraphy and hydrothermal alteration in exploration for VHMS deposits in greenstones and younger volcanic rocks. *In* Alteration and Alteration Processes associated with Ore-forming Systems. *Edited* by D.R. Lentz, Geological Association of Canada, Short Course Notes, 11, 433-467.
- Barrie, C.T., Ludden, J.N., and Green, T.H. 1993. Geochemistry of volcanic rocks associated with Cu-Zn and Ni-Cu deposits in the Abitibi subprovince. *Economic Geology*, **88**: 1341-1358.
- Bennett, G. 1978. Geology of the Northeast Temagami area, District of Nipissing. Ontario Geological Survey, Report 163, 128p.
- Berge, J.W. 1981. Recent investigations of two quartz eye porphyroidal rock-volcanogenic massive sulfide occurrences. *Economic Geology*, **76**: 1211-1216.
- Beswick, A.E. and Soucie, G. 1978. A correction procedure for metasomatism in an Archean greenstone belt. *Precambrian Research*, **6**: 235-248.
- Blum, N. 1986. Geochemical studies of Archean iron formations and associated volcanic rocks. Ph.D. Thesis, McMaster University, Hamilton, Ontario, 410p.
- Boldly, J. 1968. Geological observations on the Delbridge massive sulphide deposit. *Canadian Institute of Mining and Metallurgy, Transactions* **71**: 247-256.
- Bowins, R.J. 1989. Rare earth and other geochemical studies of Archean banded iron formation: Sherman and Adams Mines, Ontario. Ph.D. Thesis, McMaster University, Hamilton, Ontario, 399p.
- Bowins, R.J. and Crocket, J.H. 1994. Sulfur and carbon isotopes in Archean banded iron formations: Implications for sulfur sources. *Chemical Geology*, **111**: 307-323.
- Bowins, R.J. and Heaman, L.M. 1991. Age and timing of igneous activity in the Temagami greenstone belt, Ontario: a preliminary report. *Canadian Journal of Earth Sciences*, **28**: 1873-1876.

- Boynton, W.V. 1984. Cosmochemistry of the rare earth elements: Meteorite studies. *In* Rare Earth Element Geochemistry, *Edited by* P. Henderson. Elsevier New York 63-114.
- Bralia, A., Sabatini, G. and Troja, F. 1979. Revaluation of the Co/Ni ratio in pyrite as a geochemical tool in ore genesis problems. *Mineralium Deposita*, **14**: 353-374.
- Brons, D.J. 1989. Stratigraphy and metamorphism of mafic volcanic rocks near Arsenic Lake, Temagami, Ontario. Unpublished M.Sc. thesis, Laurentian University, Sudbury, Ontario, 146p.
- Busby-Spera, C.J. and White, J.D.L. 1987. Variation in peperite textures associated with differing host-sediment properties. *Bulletin of Volcanology*, **49**: 765-775.
- Calhoun, T.A. and Hutchinson, R.W. 1981. Determination of flow direction and source of fragmental sulphides, Clementine deposit Buchans, Newfoundland. *In* The Buchans Orebodies: Fifty years of geology and mining, *Edited by* E.A. Swanson, D.F. Strong and J.G. Thurlow, Geological Association of Canada Special Paper 22, 187-204.
- Campbell, F.A. and Ethier, V.G. 1984. Nickel and cobalt in pyrrhotite and pyrite from the Faro and Sullivan orebodies. *Canadian Mineralogist*, **22**: 503-506.
- Campbell, I.H., Franklin, J.M., Gorton, M.P., Hart, T.R., and Scott, S.D. 1981*a*. The role of subvolcanic sills in the generation of massive sulfide deposits. *Economic Geology*, **76**: 2248-2253.
- Campbell, I.H., Coad, P., Franklin, J.M., Gorton, M.P., Hart, T.R., Scott, S.D., Sowa, J., and Thurston, P.C. 1981*b*. Rare earth elements in felsic volcanic rocks associated with Cu-Zn massive sulphide mineralization. Ontario Geological Survey Miscellaneous Paper 98: 45-53.
- Campbell, I.H., Coad, P., Franklin, J.M., Gorton, M.P., Hart, T.R., Sowa, J., and Thurston, P.C. 1982*a*. Rare earth elements in felsic volcanic rocks associated with Cu-Zn massive sulphide mineralization. Ontario Geological Survey Miscellaneous Paper, 103: 45-53.
- Campbell, I.H., Coad, P., Franklin, J.M., Gorton, M.P., Scott, S.D., Sowa, J., and Thurston, P.C. 1982*b*. Rare earth elements in volcanic rocks associated with Cu-Zn massive sulphide mineralization: a preliminary report. *Canadian Journal of Earth Sciences*, **19**: 619-623.

- Campbell, I.H., Lesher, C.M., Coad, P., Franklin, J.M., Gorton, M.P. and Thurston, P.C. 1984. Rare-earth element mobility in alteration pipes below massive Cu-Zn sulfide deposits. *Chemical Geology*, **45**: 181-202.
- Cann, J.R. 1970. Rb, Sr, Y, Zr, Nb in some ocean-floor basaltic rocks. *Earth and Planetary Science Letters*, **10**: 7-11.
- Carstens, C.W. 1941. Om geokjemiske undersøkelser av malmer. *Norsk Geol. Tids.* **21**: 213-221.
- Cas, R.A.F. 1992. Submarine volcanism: eruption styles, products, and relevance to understanding the host-rock successions to volcanic-hosted massive sulfide deposits. *Economic Geology*, **87**: 511-541.
- Cas, R.A.F. and Wright, J.V. 1988. Volcanic successions modern and ancient. A geological approach to processes, products and successions. Unwin Hyman, London. 528p.
- Chen, T.T. 1978. Colloform and framboidal pyrite from the Caribou Deposit New Brunswick. *Canadian Mineralogist*, **16**: 9-15.
- Christiansen, R.L. and Lipman, R.W. 1966. Emplacement and thermal history of a rhyolite lava flow near Fortymile Canyon, Southern Nevada. *Geological Society of America Bulletin* **77**: 671-684.
- Clark, L.A. 1983. Genetic implications of fragmental Ore texture in Japanese Kuroko deposits. *CIM Bulletin* **76**: 105-114.
- Condie, K.C. 1976. Trace-element geochemistry of Archean Greenstone Belts. *Earth-Science Reviews*, **12**: 393-417.
- Condie, K.C. 1981. Archean greenstone belts. Elsevier, New York, NY, 434 p.
- Coveney, R.M., Watney, W.L., and Maples, C.G. 1991. Contrasting depositional models for Pennsylvanian black shale discerned from molybdenum abundances. *Geology* **19**: 147-150.
- De Rosen-Spence, A.F., Provost, G., Dimroth, E., Gochnauer, K. and Owen, V. 1980. Archean subaqueous felsic flows, Rouyn-Noranda, Quebec, Canada, and their Quarternary equivalents. *Precambrian Research* **12**: 43-77.

- Dostal, J., Strong, D.F. and Jamieson, R.A. 1980. Trace element mobility in the mylonite zone within the Ophiolite Aureole, St. Anthony Complex, Newfoundland. *Earth and Planetary Science Letters*, **49**: 188-192.
- Elliott-Meadows, S.R. and Appleyard, E.C. 1991. The alteration geochemistry and petrology of the Lar Cu-Zn deposit, Lynn Lake area, Manitoba, Canada. *Economic Geology*, **86**: 486-505.
- Emerson, S.R., and Husted, S.S. 1991. Ocean anoxia and the concentrations of molybdenum and vanadium in seawater. *Marine Chemistry* **34**: 177-196.
- Finlow-Bates, T. and Stumpfl, E.F. 1981. The behaviour of so-called immobile elements in hydrothermally altered rocks associated with volcanogenic submarine-exhalative ore deposits. *Mineralium Deposita*, **16**: 319-328.
- Fisher, R.V. and Schmincke, H.U. 1984. *Pyroclastic Rocks*. Springer-Verlag, Berlin, Heidelberg, New York, Tokyo. 472p.
- Franklin, J.M., Lydon, J.W. and Sangster D.F. 1981. Volcanic-associated massive sulfide deposits. *Economic Geology*, 75th Anniversary Volume, p 485-627.
- Fyon, J.A., and Crocket, J.H. 1986. Exploration potential for base and precious metal mineralization in part of Strathy Township, Temagami area. Ontario Geological Survey, Open File Report 5591, 46p.
- Fyon, J.A., and O'Donnell, L. 1987. Metallogenic studies in the Temagami Greenstone Belt, district of Nipissing. *In* Summary of Field Work and Other Activities 1987, Ontario Geological Survey, Miscellaneous Paper 137, 190-197.
- Fyon, J.A., Hrabi, R.B. and Maitland, W.M., 1988. Relationships between lithological, alteration, and structural features and precious metal occurrences in the Temagami Greenstone Belt, district of Nipissing. *In* Summary of Field Work and Other Activities 1988, Ontario Geological Survey Miscellaneous Paper 141, 271-275.
- Fyon, J.A., and Cole, S. 1989. Geology of part of the Temagami Greenstone Belt, district of Nipissing, including relationships between lithologic, alteration, and structural features and precious-metal occurrences. *In* Summary of Field Work and Other Activities 1989, Ontario Geological Survey Miscellaneous Paper 146, 108-115.
- Gibson, H.L., Watkinson, D.H. and Comba, C.D.A. 1983. Silicification: Hydrothermal alteration in an Archean geothermal system within the Amulet rhyolite formation, Noranda, Quebec. *Economic Geology*, **78**: 954-971.

- Gibson, H.L. 1990. The Mine Sequence of the central Noranda volcanic complex: Geology, alteration, massive sulphide deposits and volcanological reconstruction. Unpublished Ph.D. thesis, Carleton University, Ottawa, Canada, 715p.
- Gilmour, P. 1965. The origin of the massive sulphide mineralization in the Noranda district, Northwestern Quebec. Geological Association of Canada, Proceedings **16**: 63-81.
- Grant, J.A. 1986. The isocron diagram-A simple solution to Gresens' equation for metasomatic alteration. Economic Geology, **81**: 1976-1982.
- Gresens, R.L. 1967. Composition-volume relationships in metasomatism. Chemical Geology, **2**: 47-55.
- Gronvold, F., and Westrum, E.F. 1976. Heat capacities of iron disulfides. Thermodynamics of marcasite from 5 to 700K, pyrite from 350 to 700K, and the transformation of marcasite to pyrite. Journal of Chemical Thermodynamics **8**: 1039-1048.
- Hawley, J.E. and Nichol, I. 1961. Trace elements in pyrite, pyrrhotite and chalcopyrite of different ores. Economic Geology, **56**: 467-471.
- Hellman, P.L., Smith, R.E. and Henderson, P. 1979. The mobility of the rare earth elements: Evidence and implications from selected terrains affected by burial metamorphism. Contributions to Mineralogy and Petrology, **71**: 23-44.
- Hopwood, T.P. 1976. "Quartz-Eye" bearing porphyroidal rocks and volcanogenic massive sulfide deposits. Economic Geology, **71**: 589-612.
- Hurley, T.D. 1985. Petrology and geochemistry of the volcanic host rocks to the west and north pits of the Sherman Mine iron formation, Temagami, Ontario. Unpublished M.Sc. thesis, McMaster University, Hamilton, Ontario, 154p.
- Huston, D.L., Sie, S.H., Suter, G.F. and Ryan, C.G. 1993. The composition of pyrite in volcanogenic massive sulfide deposits as determined with the proton microprobe. Nuclear Instruments and Methods in Physics Research. **B75**: 531-534.
- Ireland, J.C., Zalierunas, R.V. and Basa, E.M. 1993. Cobalt resident geologist's district-1992; *In* Report of activities 1992 resident geologists. Ontario Geological Survey Miscellaneous Paper 161: 307-333.

- Irvine, T.N. and Baragar, W.R.A. 1971. A Guide to the chemical classification of the common volcanic rocks. *Canadian Journal Of Earth Sciences*, **8**: 523-548.
- Jackson, S.L. and Fyon, J.A. 1991. The Western Abitibi Subprovince in Ontario; In: *Geology of Ontario*, Ontario Geological Survey Special volume 4, Part 1. 405-482.
- Jackson, S.L., Fyon, J.A and Corfu, F. 1994. Review of Archean supracrustal assemblages of the southern Abitibi greenstone belt in Ontario, Canada: products of microplate interaction within a large-scale plate-tectonic setting. *Precambrian Research* **65**: 183-205.
- Jacobs, J.W., Korteve, R.L., Blanchard, D.P. and Haskin, L.A. 1977. A well-tested procedure for Instrumental Neutron Activation Analysis of silicate rocks and minerals. *Journal of Radioanalytical Chemistry* **40**: 93-114.
- Jensen, L.S. 1976. A new cation plot for classifying subalkalic volcanic rocks. Ontario Division of Mines, Miscellaneous Paper 66, 22p.
- Kaneda, H., Shimazaki, H., and Lee, M.S. 1986. Mineralogy and geochemistry of the Au-Ag ore deposits of the South Korean Peninsula. *Mineralium Deposita*, **21**: 234-243.
- Kerr, D.J. and Gibson, H.L. 1993. A comparison of the Horne volcanogenic massive sulfide deposit and intracauldron deposits of the mine sequence, Noranda, Quebec. *Economic Geology*, **88**: 1419-1442.
- Leshner, C.M., Goodwin, A.M., Campbell, I.H., and Gorton, M.P. 1986. Trace-element geochemistry of ore-associated and barren, felsic metavolcanic rocks in the Superior Province, Canada. *Canadian Journal Of Earth Sciences*, **23**: 222-237.
- Loftus-Hills, G. and Solomon, M. 1967. Cobalt, nickel and selenium in sulphides as indicators of ore genesis. *Mineralium Deposita*, **2**: 228-242.
- Lydon, J.W. 1990a. Volcanogenic massive sulphide deposits part 2: A descriptive model. *In Ore Deposit Models*, Edited by R.G. Roberts and R.A. Sheahan. Geoscience Canada Reprint Series 3, 145-154.
- Lydon, J.W. 1990b. Volcanogenic massive sulphide deposits part 2: Genetic models. *In Ore Deposit Models*, Edited by R.G. Roberts and R.A. Sheahan. Geoscience Canada Reprint Series 3, 155-181.

- Macdonald, R., McGarvie, D.W., Pinkerton, H., Smith, R.L. and Palacz, Z.A., 1990. Petrogenetic evolution of the Torfajokull volcanic complex, Iceland, I. Relationship between the magma types. *Journal of Petrology*, **31**: 429-459.
- MacGeehan, P.J. and MacLean, W.H. 1980. An Archean sub-seafloor geothermal system, calc-alkali trends, and massive sulfide genesis. *Nature*, **286**: 767-771.
- Maclean, W.H. 1988. Rare earth element mobility at constant inter-REE ratios in the alteration zone at the Phelps Dodge massive sulphide deposit, Matagami, Quebec. *Mineralium Deposita*, **23**: 231-238.
- Maclean, W.H. 1990. Mass change calculations in altered rock series. *Mineralium Deposita*, **25**: 44-49.
- MacLean, W.H. and Barrett, T.J. 1993. Litho-geochemical techniques using immobile elements. *Journal of Geochemical Exploration*, **48**: 109-133.
- MacLean, W.H. and Kranidiotis, P. 1987. Immobile elements as monitors of mass transfer in hydrothermal alteration: Phelps Dodge massive sulfide deposit, Matagami, Quebec. *Economic Geology*, **82**: 951-962.
- Mahood, G. and Hildreth, W. 1983. Large partition coefficients for trace elements in high-silica rhyolites. *Geochimica et Cosmochimica Acta*, **47**: 11-30.
- McBirney, A.R. 1984. *Igneous Petrology*. Freeman Cooper and Company, San Francisco, CA. 504p.
- McLennan, S.M. and Taylor, S.R. 1979. Rare earth mobility associated with uranium mineralization. *Nature*, **282**: 247-250.
- Middlemost, E.A.K. 1985. *Magmas and magmatic rocks*. Longman Group Limited, Essex.
- Miyashiro, A. 1974. Volcanic rock series in island arcs and active continental margins. *American Journal of Science*, **274**: 321-355.
- Mookherjee A. and Philip R. 1979. Distribution of copper, cobalt and nickel in ores and host-rocks, Ingaldhal, Karnataka, India. *Mineralium Deposita*, **14**: 33-55.
- Moorehouse, W.W. 1942. The northeastern portion of the Temagami Lake area. Ontario Department of Mines 51, pt.6, 42p.

- Morton, R.L., and Franklin, J.M. 1987. Two-fold classification of Archean volcanic-associated massive sulfide deposits. *Economic Geology*, **82**: 1057-1063.
- Murowchick, J.B. 1992. Marcasite inversion and the petrographic determination of pyrite ancestry. *Economic Geology*, **87**: 1141-1152.
- Nesbitt, R.W., Mastins, H., Stolz, G.W. and Bruce, D.R. 1976. Matrix corrections in trace-element analysis by x-ray fluorescence: An extension of the Compton scattering technique to long wavelengths. *Chemical Geology*, **18**: 203.
- Nicholls, G.D. and Islam, M.R. 1971. Geochemical investigations of basalts and associated rocks from the ocean floor and their implications. *Philos Trans Royal Society of London*. **268**: 469-486.
- Norrish, K. and Hutton, J.T. 1969. An accurate X-ray spectrographic method for the analysis of a wide range of geological samples. *Geochimica et Cosmochimica Acta*, **33**: 431-453.
- Osterberg, S.A., Morton, R.L. and Franklin, J.M. 1987. Hydrothermal alteration and physical volcanology of Archean rocks in the vicinity of the Headway-Coulee massive sulfide occurrence, Onoman area, northwestern Ontario. *Economic Geology*, **82**: 1505-1520.
- Pearce, T.H. 1968. A contribution to the theory of variation diagrams. *Contributions to Mineralogy and Petrology*, **19**: 142-157.
- Pearce, J.A. 1983. Role of sub-continental lithosphere in magma genesis at active continental margins. *In* *Continental basalts and mantle xenoliths*, Edited by C.J. Hawkesworth and M.J. Norry. Shiva Publishing, Orpington, England, 230-249.
- Price, B.J. 1972. Minor elements in pyrites from the Smithers map area, British Columbia and exploration applications of minor element studies. Unpublished M.Sc. thesis, University of British Columbia, 270p.
- Raiswell, R., and Plant, J. 1980. The incorporation of trace elements into pyrite during diagenesis of black shales, Yorkshire, England. *Economic Geology* **75**: 684-699.
- Ramdohr, P. 1980. *The ore minerals and their intergrowths*. Pergamon Press, Toronto.
- Roberts, F.I. 1982. Trace element chemistry of pyrite: a useful guide to the occurrence of sulfide base metal mineralization. *Journal of Geochemical Exploration*, **17**: 49-62.

- Rokachev, S.A. 1965. More facts about fragmental sulfide concentrations in roof rocks of the Urals Sibay ore deposit. *Doklady Akademii Nauk SSR, Geology*, **158**: 85-87.
- Schandl, E.S., Davis, D.W., and Krogh, T.E. 1990. Are the alteration halos of massive sulfide deposits syngenetic? Evidence from U-Pb dating of hydrothermal rutile at the Kidd Volcanic Center, Abitibi Subprovince, Canada. *Geology*, **18**: 505-508.
- Schandl, E.S., and Gorton, M.P. 1991. Postore mobilization of rare earth elements at Kidd Creek and other Archean massive sulfide deposits. *Economic Geology*, **86**: 1546-1553.
- Scott, S.D., Kalogeropoulos, S.I., Shegelski, R.J., and Siriunas, J.M. 1983. Tuffaceous exhalites as exploration guides for volcanogenic massive sulphide deposits. *Journal of Geochemical Exploration* **19**: 500-502.
- Sillitoe, R.H. 1982. Extensional habitats of rhyolite-hosted massive sulfide deposits. *Geology*, **10**: 403-407.
- Sinclair, W.D. 1971. A Volcanic origin for the No. 5 zone of the Horne Mine, Noranda, Quebec. *Economic Geology*, **66**: 1225-1231.
- Sopuck, V.J., Lavin, O.P., and Nichol, I. 1980. Lithochemistry as a guide to identifying favorable areas for the discovery of volcanogenic massive sulphide deposits. *CIMM Bull. (Nov.)*, 152-166.
- Soucie, G.E. 1979. A lithochemical study of metasomatic alteration in the Temagami greenstone belt, Northeastern Ontario. Unpublished M.Sc. thesis, Laurentian University, Sudbury, Ontario.
- Spence, C.D. 1975. Volcanogenic features of the Vauze sulfide deposit, Noranda, Quebec. *Economic Geology*, **70**: 102-114.
- Stanley, C.R. and Madeisky, H.E. 1994. Lithochemical exploration for hydrothermal ore deposits using pearce element ratio analysis. *In Alteration and Alteration Processes associated with Ore-forming Systems. Edited by D.R. Lentz, Geological Association of Canada, Short Course Notes, 11*, 193-211.
- Stix, J., Goff, F., Gorton, M.P., Heiken, G. and Garcia, S.R. 1988. Restoration of compositional zonation in the Bandelier silicic magma chamber between two caldera-forming eruptions: Geochemistry and origin of the Cerro Toledo Rhyolite, Jemez Mountains, New Mexico. *Journal of Geophysical Research*, **93**: 6129-6147.

- Stix, J. and Gorton, M.P. 1990. Changes in silicic melt structure between the two Bandelier caldera-forming eruptions, New Mexico, USA: Evidence from zirconium and light rare earth elements. *Journal of Petrology*, **31**: 1261-1283.
- Stix, J. and Gorton, M.P. 1993. Replenishment and crystallization in epicontinental silicic magma chambers: evidence from the Bandelier magmatic system. *Journal of Volcanology and Geothermal Research*, **55**: 201-215.
- Sutherland, J.K. 1967. The chemistry of some New Brunswick pyrites. *Canadian Mineralogist*, **9**: 71-84.
- Teodorovich, G.I. 1961. Authigenic minerals in sedimentary rocks. Consultants Bureau, New York, 120p.
- Thurston, P.C. 1981. Economic evaluation of Archean felsic volcanic rocks using REE geochemistry. *In Archean Geology Edited by J.E. Glover and D.I. Groves*, 439-450.
- Ujike, O. and Goodwin, A.M. 1987. Geochemistry and origin of Archean felsic metavolcanic rocks, central Noranda area, Quebec, Canada. *Canadian Journal of Earth Science*, **24**: 2551-2567.
- Whitford, D.J., Korsch, M.J., Porritt, P.M. and Craven, S.J. 1988. Rare-earth element mobility around the volcanogenic polymetallic massive sulfide deposit at Que River, Tasmania, Australia. *Chemical Geology*, **68**: 105-119.
- Whitford, D.J., McPherson, W.P.A., and Wallace, D.J. 1989. Geochemistry of the host rocks of the volcanogenic massive sulfide deposit at Que River, Tasmania. *Economic Geology*, **84**: 1-21.
- Whitford, D.J. and Ashley, P.M. 1992. The Scuddles volcanic-hosted massive sulfide deposit, western Australia: geochemistry of the host rocks and evaluation of litho-geochemistry for exploration. *Economic Geology*, **87**: 873-888.
- Williams, H. and McBirney, A.R. 1979. *Volcanology*. Freeman, Cooper and Company, San Francisco, 397p.
- Willis, J.P. 1989. Compton scatter and matrix correction for trace element analysis of geological materials. *In X-ray fluorescence analysis in the geological sciences, advances in methodology, Edited by S.T. Ahmedali*. Geological Association of Canada Short Course, **7**: 91-.

- Winchester, J.A. and Floyd, P.A. 1977. Geochemical discrimination of different magma series and their differentiation products using immobile elements. *Chemical Geology*, **20**: 325-343.
- Zhabin, A.G. 1978 Rate of lithification of sulfide volcanogenic-sedimentary ores and the origin of ore-clasts. *International Geology Review*, **21**: 847-856.
- Zimmermann, R.A. and Spreng, A.C. 1984. Sedimentary and diagenetic features in the sulfide-bearing sedimentary dikes and strata of lower ordovician dolomites, Decaturville, Missouri, U.S.A. *In* Syngensis and Epigenesis in the Formation of Mineral Deposits. *Edited by* A Wauschkuhn et al. Springer-Verlag Berlin Heidelberg 350-372.

APPENDIX A

SAMPLE DESCRIPTIONS, LOCATIONS AND

GEOCHEMICAL CLASSIFICATIONS

(see back pocket for sample location map)

Sample	Field Location	Field Designation	Field Name	Alteration Mineralogy ⁽¹⁾
&*TS-02	L13+65W 3+35N	2a	massive lava	chl, carb
&*TS-03	L13W 1+20N	4a	quartz feldspar porphyry	ser, carb
TS-04	L2W 3+25S	4	quartz feldspar porphyry	
&*TS-05	L9W 0+25S	6	mafic intrusive	chl, ser, carb
TS-06	L15+75W 0+40N	6	mafic intrusive	
TS-07	L13W 1+20N	6	mafic intrusive	
&*TS-11	L1W 2+80S	3e	volcaniclastic flow	ser, chl, carb
&*TS-12	L2W 0+65S	4f	quartz feldspar porphyry	ser, chl, carb
&*TS-13	L8+90E 6+20S	4f	quartz feldspar porphyry	ser, chl, carb
&*TS-14	L10+20E 4+00S	4f	quartz feldspar porphyry	ser, chl, carb
&*TS-15	L8+50E 3+00S	4f	quartz feldspar porphyry	ser, chl, carb
&*TS-16	L9+80w B L0	4f	quartz feldspar porphyry	ser, chl, carb
&*TS-17	L9+75W 0+40N	4f	quartz feldspar porphyry	ser, chl, carb
& TS-18	L0+50W 0+75N	2a,b	massive and pillowed lava	
TS-19	L0+50W 0+75N	2	mafic dike	
TS-20	L0+50W 0+75N	3e	polymictic debris flow	
& TS-21	L0+50W 0+75N	3f?, 4f?	QFP intrusive	ser
TS-22	L0+50W 0+75N	3e	polymictic debris flow	
&*TS-23	L1W 0+55N	3a	massive lava flow	ser, carb
& TS-24	L20W 0+75S	2b	pillow lava	chl, ser, carb
TS-25	L20W 0+75S	3e	volcaniclastic flow	
&*TS-26	L20W 0+75S	3e	volcaniclastic flow	ser, carb
&*TS-27	L20W 0+75S	3e	volcaniclastic flow	ser, carb
& TS-28	L20W 0+75S	2a	massive mafic flow	chl, carb
TS-29	L20W 0+75S	3e	volcaniclastic flow	
&*TS-30	L20W 0+75S	3e	volcaniclastic flow	ser, carb
TS-31	L20W 0+75S	2a	massive mafic flow	
&*TS-32	L20W 0+75S	3e	polymictic flow	ser, chl, carb
& TS-33	L20W 0+75S	3e	volcaniclastic flow	ser
TS-34	L20W 0+75S	2a	massive mafic flow	

* = geochemical sample

& = thin section sample

Alteration mineralogy ser = sericite chl = chlorite carb = carbonate

(1) = presented in order of apparent formation (chlorite and sericite are usually cogenetic)

(2) = for location of Strathy road see Figure 2-1

(3) = UFH - Upper Felsic horizon, LFH - Lower Felsic horizon, SGH - Sherman Gate horizon, LLH - Link Lake horizon

Sample	Field Location	Field Designation	Field Name	Alteration Mineralogy ⁽¹⁾
& TS-35	L20W 0+75S	6	mafic intrusive	chl, carb
&*TS-36	L20W 0+75S	3e	volcaniclastic flow	ser, carb
TS-37	L20W 0+75S	3e	clastic flow	
TS-38	L20W 0+75S	3e	clastic flow	
TS-39	L20W 0+75S	3e	clastic flow	
TS-40	L20W 0+75S	3e	clastic flow	
&*TS-41	HWY11-Strathy rd ⁽²⁾	4	volcaniclastic	ser, chl, carb
& TS-42	L1W 2+75S	2?	tuffaceous basalt	chl, carb
&*TS-43	L29+75W 0+25S	3	volcaniclastic flow	ser, carb
TS-44	L26+40W 2+50N	3a	clastic flow	
&*TS-45	Sherman mine gate	4a	volcaniclastic flow	ser, chl, carb
&*TS-46	L25+50W 4+75N	3a	massive lava flow	ser, carb
& TS-49	L25+75W 4N	3c	hyaloclastite	
*TS-100	L0+25W 0+25N	3e	volcaniclastic flow	
*TS-101	L1+80E 0+20S	3e	volcaniclastic flow	
*TS-102	L8+75W 3+80S	4f	volcaniclastic flow	
TS-103	Strathy road	4e	volcaniclastic flow	
*TS-105	Strathy road	4e	volcaniclastic flow	
*TS-106	L14+75W 1+75S	3e	volcaniclastic flow	
*TS-108	L29+40W 4+80S	3f?, 4f?	quartz feldspar porphyry	
&*TS-109	L35W 0+50S	3e	volcaniclastic tuff	ser, carb
*TS-110	L27W 2+20N	3e	volcaniclastic flow	
*TS-113	L6W 0+75N	3e	volcaniclastic flow	
*TS-114	L23W 0+40S	3e	volcaniclastic flow	
&*TS-116	L22W 2+10N	3e	volcaniclastic tuff	ser, carb
&*TS-117	L35+10W 2+50S	3f	quartz feldspar porphyry	
&*TS-119	L25+50W 4N	3a	massive lava flow	ser, chl, carb
*TS-120	L2+60W 3+50S	4e	volcaniclastic flow	
*TS-121	L19+50W 3S	4e	volcaniclastic flow	

Sample	Classification Maclean and Barrett (1993)	Leshner (1986) classification	Name from Fyon and Crocket (1986)	Horizon ⁽³⁾
&*TS-02	tholeiitic basalt	-----	calc-alkaline basalt	-----
&*TS-03	calc-alkaline rhyolite	F I	Milne Vent	Milne vent
TS-04	calc-alkaline rhyolite			
&*TS-05	calc-alkaline	-----	Diorite	Sill
TS-06				
TS-07				
&*TS-11	tholeiitic rhyolite	F IIIa	Felsic volcanoclastic	UFH
&*TS-12	calc-alkaline rhyolite	F I	Felsic volcanoclastic	Milne vent?
&*TS-13	calc-alkaline rhyolite	F I	City Dump vent	City Dump
vent				
&*TS-14	calc-alkaline rhyolite	F I	City Dump vent	City Dump
vent				
&*TS-15	calc-alkaline rhyolite	F I	City Dump vent	City Dump
vent				
&*TS-16	calc-alkaline rhyolite	F I	Milne vent	Milne vent
&*TS-17	calc-alkaline rhyolite	F I	Milne vent	Milne vent
& TS-18				
TS-19				
TS-20				
TS-21				
TS-22				
&*TS-23	transitional rhyolite	F IIIa		
& TS-24				
TS-25				
&*TS-26	tholeiitic rhyolite	F IIIa	Felsic volcanoclastic	UFH
&*TS-27	tholeiitic rhyolite	F IIIa	Felsic volcanoclastic	UFH
& TS-28				
TS-29				
&*TS-30	tholeiitic rhyolite	F IIIa	Felsic volcanoclastic	UFH
TS-31				
&*TS-32	tholeiitic rhyolite	F IIIa	Felsic volcanoclastic	UFH
& TS-33				
TS-34				

Sample	Classification Maclean and Barrett (1993)	Lesher (1986) classification	Name from Fyon and Crocket (1986)	Horizon ⁽³⁾
& TS-35				
&*TS-36	tholeiitic rhyolite	F IIIa	Felsic volcanoclastic	UFH
TS-37				
TS-38				
TS-39				
TS-40				
&*TS-41	calc-alkaline rhyolite	F I		South Temagami
& TS-42				
&*TS-43	tholeiitic rhyolite	F IIIa	Felsic volcanoclastic	UFH
TS-44				
&*TS-45	calc-alkaline rhyolite	F II	Felsic volcanoclastic	SGH
&*TS-46	transitional rhyolite	F IIIa	Felsic volcanoclastic	LFH
& TS-49				
*TS-100	tholeiitic rhyolite	F IIIa	Felsic volcanoclastic	LFH
*TS-101	transitional rhyolite	F IIIa	Felsic volcanoclastic	LFH
*TS-102	calc-alkaline rhyolite	F I	Felsic volcanoclastic	Milne vent ?
*TS-103	calc-alkaline rhyolite	F I		South Temagami
*TS-105	calc-alkaline rhyolite	F I		South Temagami
*TS-106	tholeiitic rhyolite	F IIIa	Felsic volcanoclastic	UFH
*TS-108	tholeiitic rhyolite	F IIIa	Felsic volcanoclastic	LLH
&*TS-109	tholeiitic rhyolite	F IIIa	Felsic volcanoclastic	UFH
*TS-110	tholeiitic rhyolite	F IIIa	Felsic volcanoclastic	LFH
*TS-113	tholeiitic rhyolite	F IIIa	Felsic volcanoclastic	LFH
*TS-114	tholeiitic rhyolite	F IIIa	Felsic volcanoclastic	UFH
&*TS-116	tholeiitic rhyolite	F IIIa	Felsic volcanoclastic	LFH
&*TS-117	transitional rhyolite	F II	Felsic volcanoclastic	LLH
*TS-119	transitional rhyolite	F IIIa	Felsic volcanoclastic	LFH
*TS-120	calc-alkaline rhyolite	F II	Felsic volcanoclastic	LLH
*TS-121	calc-alkaline rhyolite	F II	Felsic volcanoclastic	LLH

Pyrite samples

Sample	Location	Co/Ni classification	host rock	Horizon ⁽³⁾
*PY-1	South pit, Sherman mine	sedimentary	graphitic chert	-----
&*PY-32	L20W 0+75S	sedimentary	volcaniclastic	UFH
&*PY-47	L1W 2+80S	vein	pillow basalts	-----
&*PY-48	L17+90W 1+85S	sedimentary	volcaniclastic	UFH
&*PY-132	Repeat of PY-32	sedimentary	volcaniclastic	UFH
&*PY-143	L1+80E 0+20S	sedimentary	carbonaceous shale	LFH
*PY-144	L25+50W 4N	sedimentary	carbonaceous shale	LFH
&*PY-145	L6W 0+75N	sedimentary	carbonaceous shale	LFH
*PY-146	Sherman mine gate	sedimentary?	volcaniclastic	SGH
*PY-147	L0+50W 0+75N	sedimentary	volcaniclastic	LFH
&*PY-148	L19+50W 3S	sedimentary	volcaniclastic	LLH

APPENDIX B

MAJOR AND TRACE ELEMENT DATA
FOR ALL SAMPLES

Notes for Appendix B

The ten major elements expressed as oxides, SiO₂, TiO₂, Fe₂O₃, MnO, MgO, CaO, K₂O, Na₂O, P₂O₅, were determined by XRF methods.

The trace elements, Nb, Zr, Y, Sr, Rb, Ba, Pb, Zn, Cu, Ni, Co, Cr, V were determined by XRF methods.

All other elements were determined by the following INAA methods:

As, La, Sb, and Sm were determined after a 2mw epithermal irradiation.

Au, Ba, Ce, Lu, Sc, Th, Yb, Eu, Hf, Tb, Ta and Cs were determined after a 7mw thermal irradiation.

U was determined by delayed neutron counting (DNC).

B was determined by prompt gamma.

All oxides and LOI are expressed in weight percent (wt%), and all trace elements are expressed in ppm, with the exception of Au which is expressed in ppb.

Abbreviations for Appendix B

QFP = quartz feldspar porphyry, unit 4f

UFH = Upper Felsic horizon, unit 3

LFH = Lower Felsic horizon, unit 3

SGH = Sherman Gate horizon, unit 4

LLH = Link Lake horizon, unit 4

ST = south Temagami samples, Strathy road, unit 4

unit/horizon sample	Unit 1 02	Unit 6 05	Unit 6 70	QFP 03	QFP 75	QFP 12	QFP 13	QFP 14
SiO ₂	53.80	50.66	----	78.01	----	68.53	73.65	70.37
TiO ₂	1.02	0.69	----	0.05	----	0.30	0.19	0.31
Al ₂ O ₃	17.21	15.08	----	13.10	----	14.57	14.70	14.87
Fe ₂ O ₃	8.46	9.31	----	1.30	----	3.17	1.59	3.37
MnO	0.16	0.14	----	0.02	----	0.04	0.01	0.03
MgO	3.52	7.35	----	0.56	----	1.17	0.38	1.03
CaO	6.31	4.68	----	0.06	----	2.87	1.32	1.93
K ₂ O	0.16	0.45	----	3.56	----	2.23	2.94	3.52
P ₂ O ₅	0.04	0.06	----	0.01	----	0.07	0.02	0.06
Na ₂ O	4.49	2.72	----	0.00	----	2.49	2.88	0.02
LOI	4.08	8.25	----	2.20	----	3.56	1.79	3.38
Total	99.25	99.39	----	98.87	----	99.00	99.47	98.89
Nb	8	9	9	9	9	9	9	9
Zr	91	124	124	78	76	178	166	209
Y	20	13	12	2	2	6	10	4
Sr	139	84	89	34	34	83	213	72
Rb	8	19	22	112	113	60	67	102
Ba	318	396	375	397	279	415	928	674
Pb	2	10	5	4	6	2	15	4
Zn	111	117	112	18	16	41	55	48
Cu	161	34	47	30	26	20	114	40
Ni	54	217	208	5	4	7	35	23
Co	58	53	50	5	6	6	5	4
Cr	190	302	297	7	7	16	25	14
V	349	185	184	0	0	16	46	7
As	0.56	3.8	3.2	3.0	2.8	< 0.5	0.90	< 0.5
B	6.91	7.79	5.30	40.8	40.7	23.5	21.3	28.7
Ce	10	19	16	37	41	30	24	31
Cs	0.5	1.1	1.2	4.2	4.5	2.8	2.8	3.3
Eu	0.78	0.84	0.70	0.36	0.37	0.67	0.56	0.66
Hf	1.4	2.4	2.2	2.5	2.5	4.2	3.9	4.4
La	2.8	11.1	8.4	19.5	21.9	16.3	14.0	16.8
Lu	0.23	0.21	0.20	0.07	0.06	0.09	0.07	0.10
Sb	0.42	3.5	3.9	0.57	2.0	1.2	2.5	1.3
Sc	32	19	18	1.3	0.93	4.4	2.2	4.5
Sm	2.4	2.8	2.3	2.2	2.4	2.5	1.7	2.6
Ta	0.10	0.26	0.26	0.73	0.80	0.54	0.49	0.58
Tb	0.19	0.42	0.41	0.19	0.21	0.16	0.23	0.25
Th	< 0.5	1.0	1.0	5.5	6.2	3.0	3.6	3.6
U	< 0.5	0.5	< 0.5	1.5	1.5	0.86	1.1	0.94
Yb	1.5	1.4	1.2	0.54	0.52	0.59	0.48	0.69
Au	0	1	1	0	1	2	1	2

horizon	QFP	QFP	QFP	QFP	UFH	UFH	UFH	UFH
sample	15	16	17	102	11	26	27	30
SiO ₂	68.68	70.40	70.91	77.88	76.71	74.58	75.99	80.95
TiO ₂	0.31	0.25	0.17	0.04	0.12	0.09	0.05	0.11
Al ₂ O ₃	15.03	14.73	13.52	13.28	11.79	13.81	9.92	12.49
Fe ₂ O ₃	3.19	2.61	1.93	1.61	1.68	1.13	2.11	0.85
MnO	0.03	0.03	0.04	0.03	0.03	0.03	0.09	0.01
MgO	1.26	0.96	0.67	0.68	0.93	0.81	1.10	0.21
CaO	2.12	2.15	3.64	0.91	1.66	1.23	2.47	0.07
K ₂ O	2.60	1.87	2.81	1.96	2.27	3.18	2.51	3.28
P ₂ O ₅	0.08	0.06	0.03	0.07	0.00	0.00	0.01	0.01
Na ₂ O	2.14	3.69	1.33	0.77	0.54	0.33	0.00	0.00
LOI	3.27	2.67	4.28	2.28	3.79	3.88	4.35	1.48
Total	98.71	99.42	99.33	99.51	99.52	99.07	98.60	99.46
Nb	9	9	10	8	15	17	12	16
Zr	187	161	185	60	122	148	112	123
Y	6	6	5	5	48	54	38	47
Sr	59	78	71	105	77	70	42	31
Rb	80	55	92	59	77	95	70	98
Ba	365	388	455	357	410	614	153	483
Pb	2	8	3	8	9	36	32	11
Zn	34	41	19	16	14	19	16	27
Cu	22	15	32	< 5	20	20	20	27
Ni	9	8	1	7	13	10	10	9
Co	5	5	5	< 5	5	6	4	6
Cr	16	14	8	< 5	8	8	7	6
V	17	8	0	< 5	0	0	4	7
As	< 0.5	1.8	1.5	0.84	4.0	4.9	23	6.5
B	24.0	17.5	29.2	45.0	40.8	41.0	33.5	35.0
Ce	33	35	49	41	41	51	29	38
Cs	3.2	2.2	3.2	2.2	2.0	1.9	1.5	2.1
Eu	0.71	0.65	0.76	0.51	0.64	0.67	0.51	0.48
Hf	4.1	3.7	4.4	2.7	4.0	5.1	3.8	4.5
La	19.0	20.0	25.6	19.5	17.2	22.0	12.7	16.9
Lu	0.09	0.07	0.09	0.06	0.70	0.81	0.63	0.67
Sb	1.2	0.99	1.3	0.51	1.9	3.8	3.0	6.3
Sc	4.5	3.1	1.4	0.92	3.7	5.7	3.5	4.0
Sm	2.6	2.4	3.0	2.2	6.2	7.8	4.6	5.3
Ta	0.55	0.58	0.68	0.72	1.8	2.3	1.4	1.9
Tb	0.28	0.22	0.27	0.20	1.5	1.7	1.2	1.3
Th	3.2	4.1	5.2	5.6	11	16	11	13
U	0.73	1.2	1.3	1.4	3.7	4.7	3.3	3.2
Yb	0.73	0.51	0.68	0.39	4.9	5.7	4.4	4.7
Au	1	0	1	3	2	0	0	0

horizon	UFH	UFH	UFH	UFH	UFH	UFH	LFH	LFH
sample	32	36	43	106	109	114	23	46
SiO ₂	58.66	79.36	79.06	77.72	80.17	77.68	82.85	79.69
TiO ₂	0.61	0.03	0.05	0.08	0.03	0.04	0.04	0.05
Al ₂ O ₃	11.75	11.15	12.42	11.33	9.62	11.21	10.67	10.25
Fe ₂ O ₃	4.39	1.00	0.79	1.49	1.07	1.83	0.51	1.27
MnO	0.30	0.04	0.02	0.09	0.03	0.09	0.01	0.07
MgO	3.12	0.59	0.65	0.99	1.42	0.77	0.11	0.64
CaO	6.65	0.92	0.52	1.69	1.82	1.96	0.05	1.32
K ₂ O	3.04	3.03	3.57	2.81	2.40	3.00	3.24	3.08
P ₂ O ₅	0.06	0.00	0.00	0.03	0.02	0.03	0.00	0.00
Na ₂ O	0.17	0.00	0.00	0.20	0.15	0.09	0.00	0.00
LOI	10.36	3.10	2.58	3.99	3.78	3.49	1.19	3.09
Total	99.11	99.22	99.66	100.42	100.51	100.19	98.67	99.46
Nb	34	14	16	14	11	9	15	13
Zr	184	138	131	95	85	100	166	163
Y	52	39	46	52	44	52	27	26
Sr	124	29	23	35	42	11	12	16
Rb	87	89	82	79	66	65	116	111
Ba	362	534	490	461	339	222	251	202
Pb	25	11	11	12	< 5	< 5	7	6
Zn	39	8	7	70	< 5	24	7	22
Cu	26	23	19	5	< 5	< 5	22	42
Ni	6	7	11	11	11	18	9	3
Co	3	6	6	< 5	< 5	7	7	5
Cr	5	7	7	< 5	< 5	< 5	7	7
V	0	0	0	11	11	5	0	0
As	23	1.5	< 0.5	6.7	0.93	7.1	4.6	< 0.5
B	31.7	37.0	52.7	29.8	61.3	25.6	51.6	36.5
Ce	44	40	45	37	24	23	33	45
Cs	2.0	2.0	2.7	1.5	1.6	0.9	4.1	2.9
Eu	0.67	0.50	0.37	0.65	0.41	0.44	0.39	0.51
Hf	4.7	4.4	4.7	4.1	3.8	2.0	5.5	5.3
La	18.6	17.6	19.3	14.0	9.5	12.6	11.7	18.1
Lu	0.80	0.68	0.73	0.78	0.67	0.79	0.51	0.50
Sb	7.4	1.5	2.2	0.69	0.55	0.85	2.2	2.1
Sc	9.3	2.8	3.1	3.2	3.0	2.3	1.7	1.6
Sm	8.3	6.4	6.5	5.4	3.9	4.3	4.8	6.1
Ta	1.7	1.6	1.9	1.7	1.4	0.85	1.5	1.3
Tb	1.5	1.3	1.3	1.2	1.0	0.68	0.96	0.96
Th	7.8	12	13	12	10	9.4	11	10
U	4.0	3.9	4.0	4.1	3.1	4.6	2.4	2.3
Yb	5.4	4.7	5.1	5.7	4.8	5.4	3.7	3.4
Au	2	1	0	1	1	0	0	3

horizon	LFH	LFH	LFH	LFH	LFH	LFH	SGH	SGH
sample	100	101	110	113	116	119	45	117
SiO ₂	79.51	80.80	79.31	76.49	76.78	79.81	79.25	80.66
TiO ₂	0.04	0.04	0.03	0.07	0.03	0.05	0.21	0.18
Al ₂ O ₃	10.79	11.92	11.72	12.45	10.25	11.87	10.78	10.08
Fe ₂ O ₃	1.76	0.90	1.65	1.54	2.16	1.19	1.81	2.47
MnO	0.04	0.02	0.03	0.04	0.04	0.02	0.04	0.03
MgO	0.66	0.38	0.78	0.66	1.36	0.77	0.44	0.63
CaO	1.28	0.07	0.61	1.63	1.85	0.02	1.47	0.37
K ₂ O	3.13	3.54	3.44	3.48	3.18	3.73	2.23	2.21
P ₂ O ₅	0.03	0.01	0.01	0.04	0.03	0.02	0.03	0.07
Na ₂ O	0.00	0.00	1.05	0.48	0.18	0.02	0.76	0.16
LOI	2.10	1.69	1.89	2.79	3.18	1.79	2.58	2.29
Total	99.34	99.37	100.52	99.67	99.04	99.29	99.60	99.15
Nb	27	14	16	33	9	13	13	5
Zr	157	140	154	142	141	165	300	227
Y	49	20	46	47	34	32	34	36
Sr	24	< 2	23	30	41	6	70	72
Rb	126	142	132	127	128	137	50	60
Ba	245	267	305	434	372	126	580	292
Pb	14	< 5	16	11	< 5	< 5	4	8
Zn	40	17	35	24	27	10	20	33
Cu	10	< 5	< 5	< 5	< 5	< 5	38	< 5
Ni	21	12	29	9	15	8	8	11
Co	< 5	< 5	7	< 5	< 5	< 5	5	< 5
Cr	28	11	< 5	< 5	< 5	< 5	8	< 5
V	< 5	< 5	< 5	< 5	< 5	7	0	18
As	3.3	4.9	5.0	1.7	< 0.5	0.73	< 0.5	30
B	47.9	220	41.4	42.9	26.8	44.9	21.0	22.5
Ce	56	40	41	78	48	48	70	71
Cs	4.0	4.5	2.9	3.9	4.7	3.6	1.6	1.6
Eu	0.69	0.52	0.59	0.78	0.70	0.65	1.2	1.7
Hf	5.7	6.2	6.0	5.2	5.3	6.5	7.2	5.7
La	21.0	14.0	14.4	36.5	16.8	16.5	32.8	32.3
Lu	0.64	0.52	0.71	0.70	0.50	0.58	0.56	0.57
Sb	0.59	0.70	0.74	0.70	0.63	0.53	1.8	3.4
Sc	1.8	1.7	1.8	2.8	1.6	2.0	5.8	5.1
Sm	6.7	4.7	5.3	6.4	5.3	5.3	6.8	5.3
Ta	1.3	1.5	1.5	1.5	1.2	1.5	0.86	0.63
Tb	1.1	0.85	1.1	1.1	0.89	0.83	1.0	0.82
Th	11	12	12	12	10	12	6.5	6.2
U	2.7	2.9	3.6	3.5	2.5	2.8	1.8	1.4
Yb	4.6	3.6	4.8	4.8	3.4	3.7	3.9	3.8
Au	2	2	0	1	0	1	0	0

horizon	LLH	LLH	LLH	ST	ST	ST
sample	108	120	121	41	103	105
SiO ₂	84.89	70.66	61.50	64.31	62.54	61.14
TiO ₂	0.04	0.33	0.59	0.56	0.35	0.53
Al ₂ O ₃	8.16	12.21	11.29	14.27	14.24	14.89
Fe ₂ O ₃	2.47	4.57	6.88	3.13	2.91	4.59
MnO	0.06	0.06	0.14	0.06	0.09	0.08
MgO	1.07	2.10	2.73	1.78	2.09	2.35
CaO	0.25	2.08	5.26	3.69	4.41	3.73
K ₂ O	1.75	2.48	1.78	2.92	2.04	1.83
P ₂ O ₅	0.04	0.09	0.12	0.15	0.13	0.15
Na ₂ O	0.11	0.22	0.34	0.72	1.82	3.06
LOI	1.49	4.55	8.95	7.04	7.77	6.46
Total	100.33	99.35	99.58	98.63	98.39	98.81
Nb	3	9	2	9	4	6
Zr	87	235	123	166	134	115
Y	21	33	17	10	11	10
Sr	23	48	70	213	260	178
Rb	45	83	54	67	50	48
Ba	220	434	284	936	764	521
Pb	520	< 5	9	17	8	8
Zn	770	135	93	55	56	97
Cu	16	101	< 5	88	33	< 5
Ni	10	39	106	33	11	22
Co	< 5	11	12	5	6	15
Cr	< 5	< 5	< 5	23	18	13
V	< 5	39	148	47	42	77
As	79	14	14	5.0	2.5	3.8
B	25.4	100	22.2	36.1	39.8	29.9
Ce	39	68	49	52	40	27
Cs	1.0	1.7	0.9	2.3	1.2	1.5
Eu	0.58	1.6	1.4	1.2	1.0	0.84
Hf	2.9	6.3	2.7	3.1	3.3	3.1
La	18.7	30.3	23.6	26.1	20.0	15.3
Lu	0.33	0.51	0.23	0.15	0.09	0.14
Sb	11	0.87	1.7	4.6	0.84	1.4
Sc	2.2	8.4	12	9.3	5.0	8.8
Sm	2.9	5.9	4.5	4.1	2.6	2.3
Ta	0.63	0.74	0.37	0.32	0.39	0.30
Tb	0.58	0.80	0.48	0.42	0.25	0.25
Th	5.4	5.8	3.0	4.3	4.5	4.9
U	1.5	1.9	0.85	1.2	1.0	1.3
Yb	2.3	3.2	1.5	1.0	0.52	1.0
Au	0	0	0	1	1	2

APPENDIX C

PRECISION AND ACCURACY OF XRF AND INAA ANALYSES

Sample	SiO ₂	TiO ₂	Al ₂ O ₃	Fe ₂ O ₃	MnO	MgO	CaO	K ₂ O	P ₂ O ₅	Na ₂ O
MRG-1	38.93	3.81	8.47	18.06	0.18	13.55	14.70	0.16	0.07	0.79
MRG-1	39.13	3.79	8.43	17.90	0.17	13.48	14.72	0.16	0.07	0.74
MRG-1	39.14	3.82	8.47	17.90	0.17	13.50	14.73	0.17	0.06	0.79
R.V.	39.09	3.77	8.46	17.93	0.17	13.55	14.71	0.18	0.08	0.74
Average	39.07	3.81	8.46	17.95	0.17	13.51	14.72	0.16	0.07	0.77
S.D.	0.097	0.012	0.019	0.075	0.005	0.029	0.012	0.005	0.005	0.024
PREC %	0.2	0.3	0.2	0.4	2.7	0.2	0.1	2.9	7.1	3.0
VAR.	0.010	0.001	0.000	0.006	0.000	0.002	0.000	0.000	0.000	0.002
DEV	0.099	0.039	0.019	0.079	0.006	0.050	0.014	0.017	0.014	0.041
ACCU %	0.25	1.03	0.23	0.44	3.40	0.37	0.10	9.62	17.68	5.52

Sample	SiO ₂	TiO ₂	Al ₂ O ₃	Fe ₂ O ₃	MnO	MgO	CaO	K ₂ O	P ₂ O ₅	Na ₂ O
JB-1A	52.20	1.32	14.54	9.05	0.15	7.70	9.26	1.43	0.27	2.68
JB-1A	52.13	1.28	14.53	8.99	0.15	7.73	9.22	1.44	0.25	2.70
JB-1A	52.18	1.26	14.60	8.95	0.14	7.77	9.20	1.43	0.24	2.66
R.V.	52.16	1.30	14.51	9.10	0.15	7.75	9.23	1.42	0.26	2.74
Average	52.17	1.29	14.56	9.00	0.15	7.73	9.23	1.43	0.25	2.68
S.D.	0.029	0.025	0.031	0.041	0.005	0.029	0.025	0.005	0.012	0.016
PREC %	0.1	1.9	0.2	0.5	3.2	0.4	0.3	0.3	4.9	0.6
VAR.	0.001	0.001	0.003	0.012	0.000	0.001	0.001	0.000	0.000	0.004
DEV	0.031	0.028	0.056	0.111	0.006	0.033	0.025	0.014	0.014	0.062
ACCU %	0.06	2.18	0.39	1.22	3.85	0.43	0.27	1.00	5.44	2.27

R.V. Recommended value
S.D. Standard deviation about the average
PREC % Reproducibility= S.D./average*100
VAR. Variance= ((X1-R.V.)² + (X2-R.V.)² + + (Xn-R.V.)²)/n
DEV Standard deviation about the recommended value = SQRT (variance)
ACCU % Accuracy = DEV/ R.V. *100

Sample	Pb	Zn	Cu	Ni	Co	Cr	V	Ba
JB-1A	7	79	54	138	38	410	218	499
JB-1A	9	80	53	140	39	408	216	501
JB-1A	8	78	55	139	38	409	217	500
R.V.	7.2	82	55.5	140	39.5	415	220	497
Average	8.00	79	54	139	38	409	217	500
S.D.	0.82	0.82	0.82	0.82	0.47	0.82	0.82	0.82
PREC %	10.2	1.0	1.5	0.6	1.2	0.2	0.4	0.2
VAR.	1.31	9.67	2.92	1.67	1.58	36.67	9.67	9.67
DEV	1.14	3.11	1.71	1.29	1.26	6.06	3.11	3.11
ACCU %	15.88	3.79	3.08	0.92	3.19	1.46	1.41	0.63

Sample	Pb	Zn	Cu	Ni	Co	Cr	V	Ba
BHVO-1	5	99	130	119	46	288	317	139
BHVO-1	5	101	132	120	45	291	319	136
BHVO-1	5	102	134	118	47	290	316	138
R.V.	2.6	105	136	121	45	289	317	139
Average	5.00	101	132	119	46	290	317	138
S.D.	0.00	1.25	1.63	0.82	0.82	1.25	1.25	1.25
PREC %	0.0	1.2	1.2	0.7	1.8	0.4	0.4	0.9
VAR.	5.76	20.33	18.67	4.67	1.67	2.00	1.67	3.33
DEV	2.40	4.51	4.32	2.16	1.29	1.41	1.29	1.83
ACCU %	92.31	4.29	3.18	1.79	2.87	0.49	0.41	1.31

Sample	Pb	Zn	Cu	Ni	Co	Cr	V	Ba
MRG-1	11	201	137	192	88	428	528	63
MRG-1	10	202	138	190	88	431	527	62
MRG-1	9	201	135	189	87	432	526	59
R.V.	10	191	134	193	87	430	526	61
Average	10.00	201	137	190	88	430	527	61
S.D.	0.82	0.47	1.25	1.25	0.47	1.70	0.82	1.70
PREC %	8.2	0.2	0.9	0.7	0.5	0.4	0.2	2.8
VAR.	0.67	107.00	8.67	8.67	0.67	3.00	1.67	3.00
DEV	0.82	10.34	2.94	2.94	0.82	1.73	1.29	1.73
ACCU %	8.16	5.42	2.20	1.53	0.94	0.40	0.25	2.84

Sample	Nb	Zr	Y	Sr	Rb
G-2	11	310	12	480	172
G-2	12	313	11	479	171
G-2	12	309	12	482	171
R.V.	12	309	11	478	170
Average	12	311	12	480	171
S.D.	0.47	1.70	0.47	1.25	0.47
PREC %	4.0	0.5	4.0	0.3	0.3
VAR.	0.33	5.67	0.67	7.00	2.00
DEV	0.58	2.38	0.82	2.65	1.41
ACCU %	4.81	0.77	7.42	0.55	0.83

Sample	Nb	Zr	Y	Sr	Rb
BHVO-1	18	189	28	404	10
BHVO-1	19	184	28	406	11
BHVO-1	18	179	28	403	10
R.V.	19	179	27.6	403	11
Average	18	184	28	404	10
S.D.	0.47	4.08	0.00	1.25	0.47
PREC %	2.6	2.2	0.0	0.3	4.6
VAR.	0.67	41.67	0.16	3.33	0.67
DEV	0.82	6.45	0.40	1.83	0.82
ACCU %	4.30	3.61	1.45	0.45	7.42

Sample	Nb	Zr	Y	Sr	Rb
NIM-G	54	297	142	10	321
NIM-G	55	298	143	9	322
R.V.	53	300	143	10	320
Average	55	298	143	10	322
S.D.	0.50	0.50	0.50	0.50	0.50
PREC %	0.92	0.17	0.35	5.26	0.16
VAR.	2.50	6.50	0.50	0.50	2.50
DEV	1.58	2.55	0.71	0.71	1.58
ACCU %	2.98	0.85	0.49	7.07	0.49

sample	TS-03	TS-75	relative error	TS-05	TS-70	relative error
element	ppm	ppm	± %	ppm	ppm	± %
Ti	200.00	200.00	0.00	2600.00	2500.00	3.92
Nb	8.99	9.33	3.71	8.93	8.54	4.46
Zr	77.60	75.52	2.72	124.12	123.58	0.44
Y	1.77	2.23	23.00	12.58	12.34	1.93
Sr	34.10	33.79	0.91	83.60	89.27	6.56
Rb	112.44	113.49	0.93	18.64	22.11	17.03
Pb	4.10	6.10	39.22	9.70	4.60	71.33
Zn	18.00	16.00	11.76	117.10	112.10	4.36
Cu	29.80	26.10	13.24	33.50	46.70	32.92
Ni	4.50	3.50	25.00	216.60	208.10	4.00
Co	5.30	5.80	9.01	53.00	50.20	5.43
Cr	7.00	7.00	0.00	302.20	296.50	1.90
V	0.00	0.00	0.00	184.60	184.00	0.33
As	2.98	2.76	7.67	3.78	3.23	15.69
Au	0.39	0.54	32.26	0.94	1.01	7.18
Ba	397.42	279.38	34.88	396.31	374.88	5.56
Ce	36.91	41.42	11.52	19.45	15.68	21.46
Cs	4.22	4.52	6.86	1.11	1.22	9.44
Eu	0.36	0.37	2.74	0.84	0.70	18.18
Hf	2.53	2.51	0.79	2.40	2.22	7.79
La	19.49	21.91	11.69	11.09	8.37	27.95
Lu	0.07	0.06	15.38	0.21	0.20	4.88
Sb	0.57	1.98	110.59	3.54	3.87	8.91
Sc	1.26	0.93	30.14	19.06	18.49	3.04
Sm	2.17	2.39	9.65	2.81	2.28	20.83
Ta	0.73	0.80	9.15	0.26	0.26	0.00
Tb	0.24	0.26	8.00	0.24	0.23	4.26
Th	5.49	6.23	12.63	1.03	0.99	3.96
U	1.43	1.56	8.70	0.36	0.49	30.59
Yb	0.54	0.52	3.77	1.44	1.19	19.01
B	40.78	40.69	0.22	7.79	5.30	38.04

relative error: eg. Nb $(9.33-8.99)/((9.33+8.99)/2)*100 = 3.71\%$

Eu		Ce		Th	
standard and run	calculated ppm	standard and run	calculated ppm	standard and run	calculated ppm
RGM 94	0.70	RGM 94	57	RGM 94	16.5
RGM 93-1	0.74	RGM 93-1	57	RGM 93-1	16.6
RGM 93-2	0.72	RGM 93-2	55	RGM 93-2	15.9
R.V.	0.66	R.V.	47	R.V.	15.1
Average	0.72	Average	56	Average	16.3
S.D.	0.0167	S.D.	0.9703	S.D.	0.2875
PREC %	2.3	PREC %	1.7	PREC %	1.8
VAR.	0.0040	VAR.	81.9268	VAR.	1.6137
DEV	0.0630	DEV	9.0513	DEV	1.2703
ACCU %	9.55	ACCU %	19.26	ACCU %	8.41

Eu		Ce		Th	
standard and run	calculated ppm	standard and run	calculated ppm	standard and run	calculated ppm
SCo-1 94	1.12	SCo-1 94	51	SCo-1 94	8.9
SCo-1-1	1.06	SCo-1-1	52	SCo-1-1	8.8
SCo-1-2	1.09	SCo-1-2	53	SCo-1-2	9.2
R.V.	1.19	R.V.	62	R.V.	9.7
Average	1.09	Average	52	Average	9.0
S.D.	0.0252	S.D.	0.9121	S.D.	0.1595
PREC %	2.3	PREC %	1.8	PREC %	1.8
VAR.	0.0106	VAR.	99.7892	VAR.	0.5610
DEV	0.1029	DEV	9.9895	DEV	0.7490
ACCU %	8.65	ACCU %	16.11	ACCU %	7.72

Sc		Hf		Cs	
standard and run	calculated ppm	standard and run	calculated ppm	standard and run	calculated ppm
RGM 94	4.4	RGM 94	6.5	RGM 94	10.8
RGM 93-1	4.5	RGM 93-1	6.6	RGM 93-1	10.9
RGM 93-2	4.4	RGM 93-2	6.3	RGM 93-2	10.5
R.V.	4.4	R.V.	6.2	R.V.	9.6
Average	4.4	Average	6.5	Average	10.7
S.D.	0.0507	S.D.	0.0967	S.D.	0.1711
PREC %	1.1	PREC %	1.5	PREC %	1.6
VAR.	0.0027	VAR.	0.0790	VAR.	1.2900
DEV	0.0524	DEV	0.2810	DEV	1.1358
ACCU %	1.19	ACCU %	4.53	ACCU %	11.83

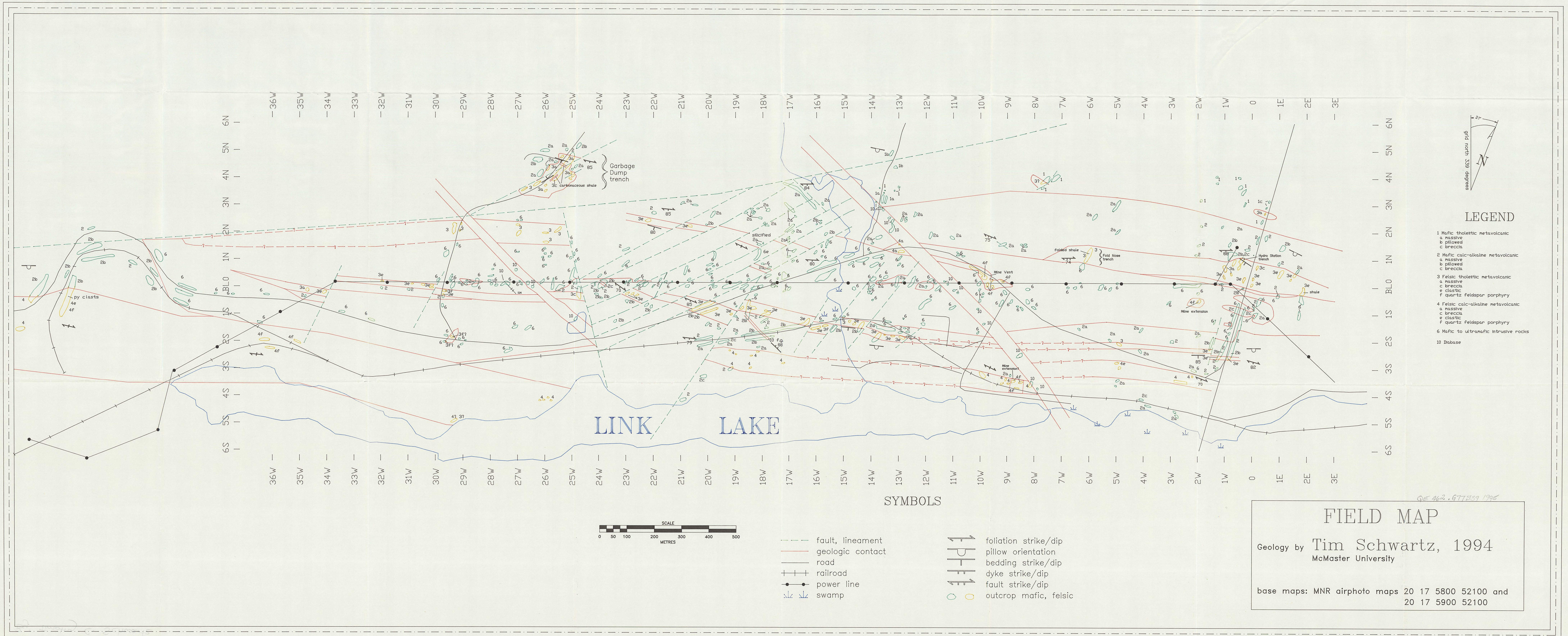
Sc		Hf		Cs	
standard and run	calculated ppm	standard and run	calculated ppm	standard and run	calculated ppm
SCo-1 94	10.8	SCo-1 94	4.4	SCo-1 94	6.9
SCo-1-1	10.6	SCo-1-1	4.3	SCo-1-1	6.9
SCo-1-2	10.9	SCo-1-2	4.5	SCo-1-2	7.1
R.V.	10.8	R.V.	4.6	R.V.	7.8
Average	10.8	Average	4.4	Average	7.0
S.D.	0.1237	S.D.	0.0661	S.D.	0.1126
PREC %	1.1	PREC %	1.5	PREC %	1.6
VAR.	0.0163	VAR.	0.0393	VAR.	0.6769
DEV	0.1276	DEV	0.1982	DEV	0.8227
ACCU %	1.18	ACCU %	4.31	ACCU %	10.55

Lu		Tb		La	
standard and run	calculated ppm	standard and run	calculated ppm	standard and run	calculated ppm
RGM 94	0.39	RGM 94	0.72	RGM 94	24.0
RGM 93-1	0.41	RGM 93-1	0.87	RGM 93-1	22.6
RGM 93-2	0.43	RGM 93-2	0.85	RGM 93-2	18.9
R.V.	0.41	R.V.	0.66	R.V.	24
Average	0.41	Average	0.81	Average	21.8
S.D.	0.0149	S.D.	0.0698	S.D.	2.1573
PREC %	3.6	PREC %	8.6	PREC %	9.9
VAR.	0.0002	VAR.	0.0285	VAR.	9.4505
DEV	0.0149	DEV	0.1687	DEV	3.0742
ACCU %	3.63	ACCU %	25.56	ACCU %	12.81

Lu		Tb		La	
standard and run	calculated ppm	standard and run	calculated ppm	standard and run	calculated ppm
SCo-1 94	0.36	SCo-1 94	0.65	SCo-1 94	29.5
SCo-1-1	0.34	SCo-1-1	0.53	SCo-1-1	31.3
SCo-1-2	0.33	SCo-1-2	0.54	SCo-1-2	37.5
R.V.	0.34	R.V.	0.70	R.V.	29.5
Average	0.34	Average	0.57	Average	32.8
S.D.	0.0124	S.D.	0.0521	S.D.	3.4231
PREC %	3.7	PREC %	9.1	PREC %	10.4
VAR.	0.0002	VAR.	0.0190	VAR.	22.6114
DEV	0.0124	DEV	0.1379	DEV	4.7551
ACCU %	3.66	ACCU %	19.70	ACCU %	16.12

Ta		Yb		Sm	
standard and run	calculated ppm	standard and run	calculated ppm	standard and run	calculated ppm
RGM 94	1.09	RGM 94	2.5	RGM 94	4.4
RGM 93-1	1.11	RGM 93-1	2.7	RGM 93-1	4.0
RGM 93-2	1.18	RGM 93-2	2.6	RGM 93-2	3.7
R.V.	0.95	R.V.	2.6	R.V.	4.3
Average	1.13	Average	2.6	Average	4.0
S.D.	0.0385	S.D.	0.0784	S.D.	0.2948
PREC %	3.4	PREC %	3.0	PREC %	7.3
VAR.	0.0334	VAR.	0.0063	VAR.	0.1500
DEV	0.1827	DEV	0.0795	DEV	0.3872
ACCU %	19.23	ACCU %	3.06	ACCU %	9.01

Ta		Yb		Sm	
standard and run	calculated ppm	standard and run	calculated ppm	standard and run	calculated ppm
SCo-1 94	0.80	SCo-1 94	2.4	SCo-1 94	5.2
SCo-1-1	0.78	SCo-1-1	2.2	SCo-1-1	5.6
SCo-1-2	0.74	SCo-1-2	2.3	SCo-1-2	6.2
R.V.	0.92	R.V.	2.27	R.V.	5.3
Average	0.78	Average	2.3	Average	5.7
S.D.	0.0260	S.D.	0.0685	S.D.	0.4131
PREC %	3.4	PREC %	3.0	PREC %	7.3
VAR.	0.0216	VAR.	0.0049	VAR.	0.2993
DEV	0.1470	DEV	0.0698	DEV	0.5471
ACCU %	15.98	ACCU %	3.08	ACCU %	10.32

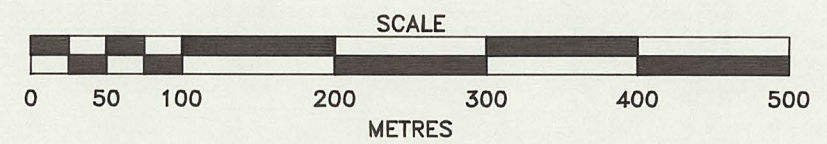


LEGEND

- 1 Mafic tholeiitic metavolcanic
 - a massive
 - b pillowed
 - c breccia
- 2 Mafic calc-alkaline metavolcanic
 - a massive
 - b pillowed
 - c breccia
- 3 Felsic tholeiitic metavolcanic
 - a massive
 - b breccia
 - c shale
 - e clastic
 - f quartz feldspar porphyry
- 4 Felsic calc-alkaline metavolcanic
 - a massive
 - b breccia
 - c clastic
 - f quartz feldspar porphyry
- 6 Mafic to ultramafic intrusive rocks
- 10 Diabase

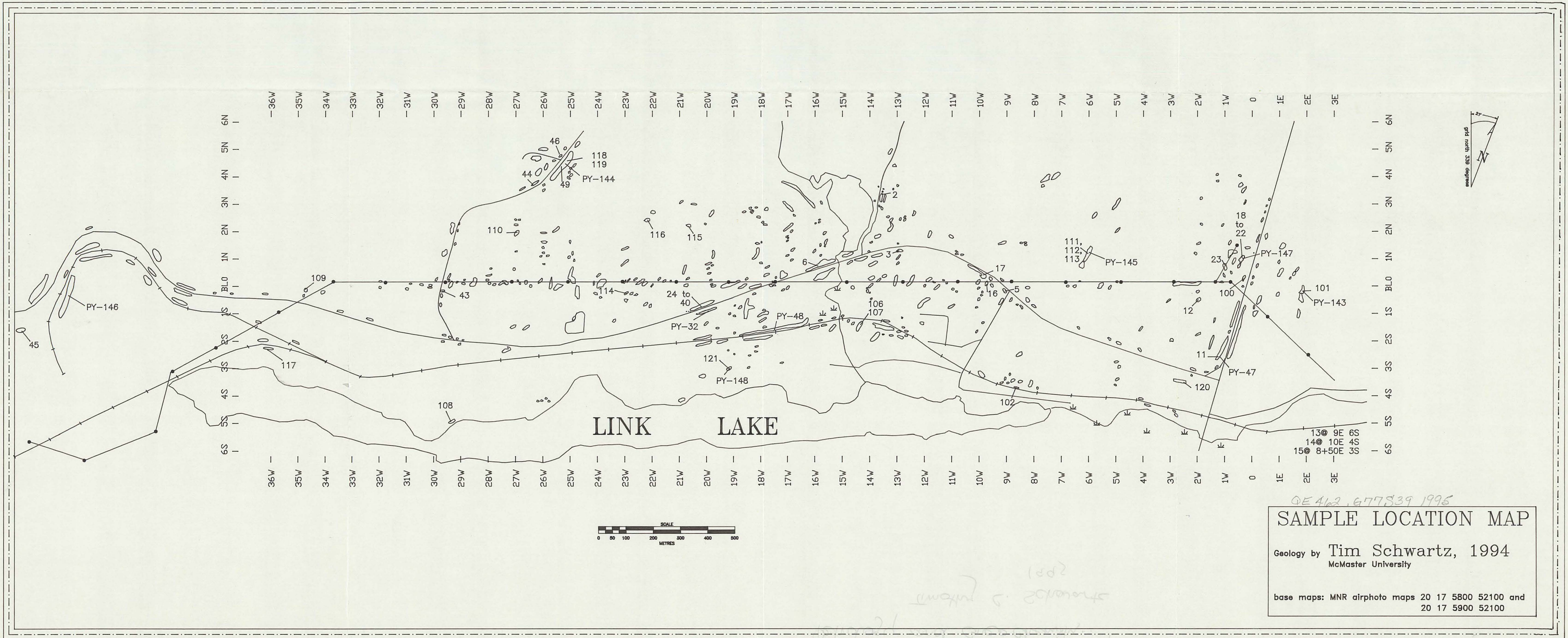
SYMBOLS

- fault, lineament
- geologic contact
- road
- +++ railroad
- power line
- swamp
- foliation strike/dip
- pillow orientation
- bedding strike/dip
- dyke strike/dip
- fault strike/dip
- outcrop mafic, felsic



FIELD MAP
 Geology by **Tim Schwartz, 1994**
 McMaster University
 base maps: MNR airphoto maps 20 17 5800 52100 and
 20 17 5900 52100

Handwritten note: 1994/05/20



QE 462, 677839 1996

SAMPLE LOCATION MAP

Geology by **Tim Schwartz, 1994**
 McMaster University

base maps: MNR airphoto maps 20 17 5800 52100 and
 20 17 5900 52100

Y.M. 9502-32